ABSTRACT

Title of Dissertation:	DETERMINING ELONGATION AT BREAK OF CABLE INSULATIONS USING CONDITION MONITORING PARAMETERS
Author:	Salimeh Gharazi Doctor of Philosophy, 2022
Dissertation directed by:	Professor Mohamad Al-Sheikhly Department of Chemical and Biomolecular Engineering

Many United States nuclear power plants are seeking to renew life licenses to extend the operational life of the plant to an additional 20 or 40 years. Degradation of insulation and jacket of cables, which are originally designed for 40 years in the second round of operation, is a critical issue which can impair the safe and reliable function of cables and ultimately the plant. The main criterion for assessing the end of life of these insulations is defined when the elongation at break reaches 50% of its original value.

However, measuring the elongation at break is done by tensile tests, which are destructive and need large samples; the feasibility of these tests is significantly limited on installed cables at nuclear power plants.

A new model was developed to relate the changes in the activation energy corresponding to EAB in terms of the changes in the activation energies corresponding

to non-destructive condition monitoring, NDE-CM, parameters. The coefficients of the model are obtained by normalizing the calculated activation energy of each CM parameter's changes with the activation energy of EAB changes.

Therefore, it is possible to estimate EAB values, in the present developed equations, from the substitution of activation energy corresponding to EAB changes with the correlated activation energy of the non-destructive condition monitoring parameters.

Cable Polymer Aging database, C-PAD, which is provided by Electric Power Research Institute, and supported by the U.S. Department of Energy, along with experimental results done in the University of Maryland, UMD, laboratory was used as the database. While taking advantage of C-PAD database which contains condition monitoring parameters of insulation cables such as Elongation at break, Modulus and Density provided by many U.S. and international research institutes, extensive aging experimental results on two cables, each with two grades provided us with not only a database but also a better understanding of the aging mechanism.

The published experimental results of cable insulations are used to validate the model. A good fit between the experimental and modeled results confirms the validity of the model.

DETERMINING ELONGATION AT BREAK OF CABLE INSULATIONS
USING CONDITION MONITORING PARAMETERS

by

Salimeh Gharazi

Dissertation submitted to the Faculty of the Graduate School of the
University of Maryland, College Park, in partial fulfillment
of the requirements for the degree of
Doctor of Philosophy
2022

Advisory Committee:
 Professor Mohamad Al-Sheikhly, Chair
 Professor Dongxia Liu
 Professor jeffery B. Klauda
 Professor Lourdes G. Salamanca-Riba
 Professor Srinivasa R. Raghavan
 Professor Patrick McCluskey

Dedication

This thesis is dedicated to

-My mother, who has always encouraged and supported me to move forward and never complained about her own difficulties in my absence.

- Saeed, my great brother who has shed light to my life by his permanent support, inspiration, and guidance.

-Elham, my kind sister who has always supported me in all the tough times.

-Sajad, my younger brother, and my mentor who has generously devoted his time for scientific discussions, without whom getting to this point was not possible.

-The soul of my father, who created a scientific environment in our family and has always inspired me to progress, even after his transition to another world.

-The soul of my grandmother, whose kindness and support are unforgettable.

Acknowledgements

Table of Contents

List of Figures

List of Abbreviations

Elongation At Break	EAB
Nuclear Power Plant	NPP
Cable Polymer Aging Database	C-PAD
Electric Power Research Institute	EPRI
Standard Deviation	SD
Standard Error	SE
Ethylene Propylene Rubber	EPR
Ethylene Propylene Rubber Commercial grade	EPR-Com
Ethylene Propylene Rubber Nuclear grade	EPR-NU
Crosslinked Polyethylene	XLPE
Crosslinked Polyethylene Commercial grade	XLPE-Com
Crosslinked Polyethylene Nuclear grade	XLPE-NU
Dose to Equivalent Damage	DED
Fourier Transform Infrared -Attenuated total Reflectance	FTIR-ATR
Non-Destructive Experiment	NDE
Electron Spin Resonance	ESR
Gray	Gy
Hour	hr
International Atomic Energy Agency	IAEA
Institute of Electrical and Electronics Engineers	IEEE

Condition Monitoring	CM
Conference International des Grands Reseaux Electriques,	CIGRE
Institute for Research in Electronics and Applied Physics	IRIP
Oxidation Index	OI
American Wire Gauge	AWG
Partial Discharge	PD
Strength At Break	SAB

Chapter 1: Introduction

1.1 Motivation and Purpose

In Nuclear power plants, NPPs, 1000 km of Instrumentation, control and power cables are found. Cables' reliability is crucially important for the safety of NPPs particularly to extend the lifetime of the NPPs over their normal designed life which requires to ensure about the cables' safe operation. Cables' insulation suffers from degradation under environmental stresses such as heat, humidity and radiation which affect their integrity. Currently, the EAB values higher than 50 percent is set as the main criteria to evaluate cables' integrity, EPRI 2005. [1] However, EAB values are measured by the tensile test which is destructive and is not possible to be done on installed cables. [2]

Therefore, it has been extensive number of research devoted to correlate EAB values to that of non-destructively measured materials' property. [3], [4], [5] and [6]

However, these correlations are not universally valid over various environmental aging conditions of the insulation cables. The main reason for the invalidity of these correlations is that the EAB values which are correlated to the values of non-destructively condition monitoring, NDE-CM, parameter changes under different environmental conditions.

In this thesis, the activation energy corresponding to EAB changes is correlated to the activation energy corresponding to non-destructively condition monitoring, NDE-CM, parameter.

Therefore, it is possible to estimate EAB values in the present developed equations from the substitution of activation energy corresponding to EAB changes with the correlated activation energy of the non-destructive condition monitoring parameters. [7], [8] and [9]

1.2 Organization of this thesis

Chapter 2 discusses the theory of the model. Chapter 3 presents experimental and characterization methods used to construct the data set. Chapter 4 presents and discusses the results of the experiments. Chapter 5 presents the data set of activation energies calculated from the CPAD and the experiments performed in this thesis. Finally, the summary of research, conclusions, and areas to improve and future research are discussed in Chapter 6.

Chapter 2: Model Theory

2.1 Introduction

The safe operation of NPPs is significantly dependent on the reliable function of cables which are responsible to transmit electricity and control signals to motors and control instruments respectively. [10], [11]

Environmental stresses such as heat, humidity, radiation along with mechanical stresses such as bending can result in cable insulations' aging over time. It is of great importance that cables maintain their integrity over normal and accident conditions of operation at NPPs even when they are aged. [12]

The degradation state assessment of cables is even more important in renewing the license of NPPs after 40 years of operation which requires the lifetime estimation of cables. [13] The end of life of a cable polymeric insulation is defined by reaching its 50% elongation at break, EAB, of the tensile test, which is a destructive test and requires large amounts of insulations. [14] Lifetime estimation of cable insulations performed either by accelerated aging tests or condition monitoring assessments both face challenges as the former method is dependent on EAB measurement of the destructive tensile test and the latter is dependent on a non-invasive control method which is different from the main defined criteria of end of life assessment. [15]

2.2 NPP Cables

Historically, the development of insulation cables refers to 1941 when polyethylene, PE, was employed in cables as insulators. Although the manufacturing process was costly, there were no concerns about as the lifetime of PE cables was expected to be around 100 years. In the early 1970s, it was revealed that "water tree" is a common phenomenon in PE cables which results in the early failure of cables. By 1976, PE cables' early failure was confirmed by the utility reports and EPRI results. On the other hand, crosslinked polyethylene, XLPE, revealed failure rate much lower that of PE cables. By 1980, ethylene propylene rubber, EPR was also introduced to the market. It was discovered that it is possible to reduce the EPR production costs by using the same XLPE manufacturing process for the specific EPR grade. It was found out by 1980 that jackets can protect cables from water treeing by reducing the water penetration to the cable. The progress in the manufacturing process of EPR and XLPE led to removing EP cables from market by 1995. [16]

2.2.1 Cable Constructions

The purpose of employing cables, either control or power, is to transmit current to different spots or instruments. [17] At NPPs, power cables are responsible to transmit high energy levels, 120 V to 15 kV, while control cables are employed to convey low energy levels, millivolts to 120 V. [13]

While power cables require special features to deal with amounts of energy, different layers in control cables are needed to protect them from environmental stresses such as mechanical stress, sunlight and chemical attack. [13], [17]

Figure 1.
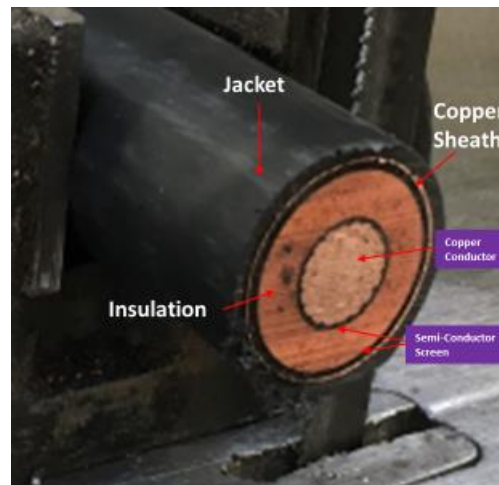
(a)
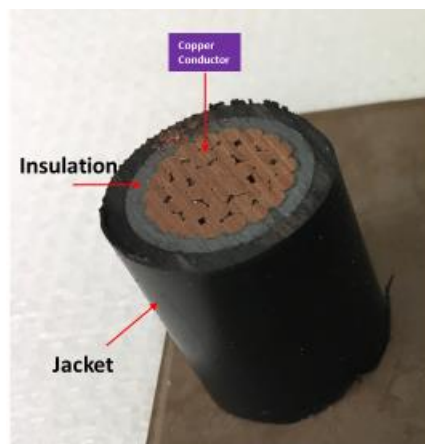
(b)

Figure 1-(a) Typical MV power cable (b) Typical LV power cable

2.2.2 Cable Elements

Cables generally contain elements including conductor, insulation, jackets, and semiconductor screen. These elements will be discussed in more details in the following;

- Conductor

Conductors are used for the purpose of current transmission. Copper is the metallic conductor that is used at NPPs due to several reasons such as low electrical resistivity and high mechanical properties. For instance, Silver's electrical conductivity is higher than that of Copper , however, it is compromised by its softness which makes it an unsuitable choice as cable conductor. [18]

The standard unit for measuring solid conductor sizes in North America and Canada is established as American Wire Gauge (AWG). The conductor #36 AWG has the diameter of 0.005 inches while the conductor #4/0 AWG has the diameter of 0.46 inches. The diameter of stranded conductors over than #4/0 AWG are measured by Circular Mils (cmils or CM). One circular mil is defined by an area of a circle which has the diameter of 1 mil or 0.001 inch. [18], [19]

- Semiconductor Screen

A semiconductor screen is a black , less than 1 mm thickness, layer which keeps the electric field the same by smoothing out the protrusions of the conductor. Any small protrusions increase the electrical field which enhances localized electrical stress over the insulation and ultimately results in insulation failure by exceeding its breakdown strength over time. [16], [20]

Shields mainly serve to decrease electrostatic noise in the cable. The smoothness of shields is significantly important to protect the insulation from high electric stress due to the protrusions in the interface. Shields also protect the insulation from mechanical damages on the jacket such as crack propagation. [21]

Semiconductors are elastomeric copolymers which are compounded with conducting carbon black. They are also crosslinked in the manufacturing process and extruded over the conductor and insulation. The smoothness of the interface between insulation and shield is mostly dependent on the dispersion of carbon black in the compound. [22]

- Insulation

  Before explaining different types of insulations, the concept of energy band structure should be described.

  - Energy Band Structure

Insulators are one of the three categorical solids based on their band structures.

Figure 2 shows three types of solids at 0 K based on their band structures which contain insulators, semiconductors, and metals. There is a large band gap between the conducti
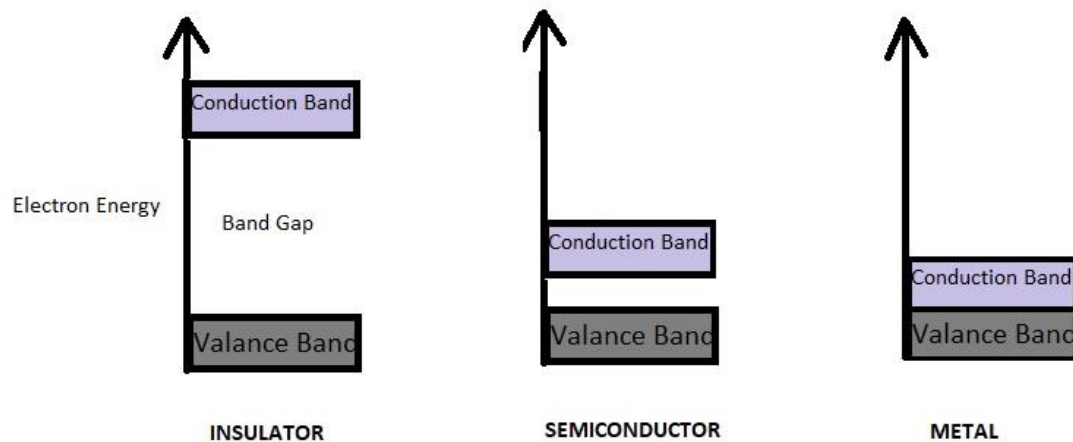
Figure 2- Electron band structures of insulators, semiconductors, and metals

- Crosslinked Polyethylene (XLPE)

  XLPE is produced when polyethylene is crosslinked by undergoing chemical reactions to join different polymeric chains.

  There are three different methods for the crosslinking process;

  1- Incorporating dicumyl peroxide in the extrusion process. After extrusion, the insulation enters a curing tube where the decomposition of dicumyl peroxide happens under high temperature.

  2- Ionizing radiation is used to form free radicals. The reaction of free radicals will produce cross-links.

  3- The polyethylene chains are linked to alkoxysilanes. Siloxane reactions between different chains will produce cross-link the chains.

The XLPE chains in the amorphous regions are coil while they are aligned in the crystalline areas. While crosslinking is mainly responsible in keeping the shape and mechanical properties in insulations, the degree of crystallinity has a significant contribution in this matter. The stressors such as mechanical load, temperature and ionization can reduce the degree of crystallinity.

On the other hand, contaminants, ions, and moisture reside mostly in amorphous areas. As it was stated, under the stressors over the aging period, the amorphous regions extend to crystalline areas which leads to the loss of mechanical properties. [22]

- Ethylene Propylene Rubber (EPR)

Ethylene Propylene Rubber (EPR) is manufactured by polymerization of ethylene and propylene monomers in the extruder. The chemical structure of ethylene and propylene monomers are shown in   Figure 3.

$$-\left(CH_2-CH_2\right)_n\left(CH_2-CH{\overset{\displaystyle |}{\underset{\displaystyle CH_3}{}}}\right)_m$$
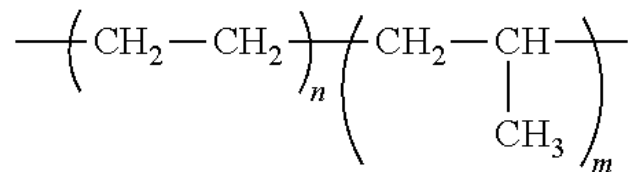
Figure 3- Ethylene Propylene Rubber (EPR) chemical structure

The degree of crystallization depends on the ratio of combining these monomers. Higher ratio of propylene reduces the inherent tendency of ethylene monomers to align and form crystallites. However, it facilitates manufacturing process as higher propylene content increases ductility. EPR and XLPE both are classified as semicrystalline materials because they contain amorphous and crystalline regions in their structure. Before aging, the insulation contains higher content of crystalline areas and therefore higher mechanical properties. However, the crystalline regions will be decomposed to amorphous areas under the stress of heat, electrical and ionization which results to the loss of mechanical properties. Ultimately, the progress of crosslinking reactions in the amorphous areas will result in the brittleness of the cable and electrical failure of the cable due to short curcuit by crack propagation. [23], [22]

The importance of crystalline areas from the cable perspective is that chain motion is limited in these areas which results in less polarization and lower dissipation factor. When the chains are confined in crystalline areas, they have less chance to move towards electrodes with opposite charge which results in lower energy loss in the form of heat, defined as dissipation factor.[22]

Although it was stated that ions and contaminants are mostly found in amorphous areas, the "imperfection" lies also in the crystalline regions from the manufacturing process such as occurrence of oxidation under high temperature in the extruder. That's why a slight polarization happens in crystalline areas too.

EPR insulations also are crosslinked in the manufacturing process. Sometimes a diene monomer is added to the compound to facilitate cross-linking process by high ionizing radiation method, the product of which is called EPDM. [22]

11

- Jacket

Jackets are insulating polymers which are extruded over cable insulation, semiconductor and wire. Jackets' main purpose is to protect cable from water and ions. Some examples are Hypalon (Chlorosulfonated polyethylene (CSPE)), neoprene (Polychloroprene (CR)) and CPE (Chlorinated Polyethylene Elastomer). [22], [24]

Hypalon

$$\left[CH_2 - CH \right]_m \left[CH_2 - CH2 \right]_n \left[CH_2 - CH \right]_k$$
$$\quad\quad\quad\quad | \quad\quad\quad\quad\quad\quad\quad\quad\quad\quad\quad\quad\quad\quad | $$
$$\quad\quad\quad\quad Cl \quad\quad\quad\quad\quad\quad\quad\quad\quad\quad\quad\quad\quad SOCl$$

Neoprene

$$\left[CH_2 - C(Cl) = CH - CH_2 \right]_n$$

CPE

$$\left[CH_2 - CH \right]_m \left[CH_2 - CH_2 \right]_n$$
$$\quad\quad\quad\quad | $$
$$\quad\quad\quad\quad Cl$$
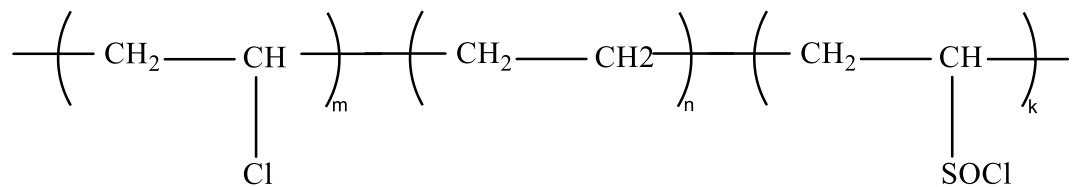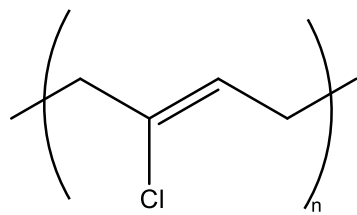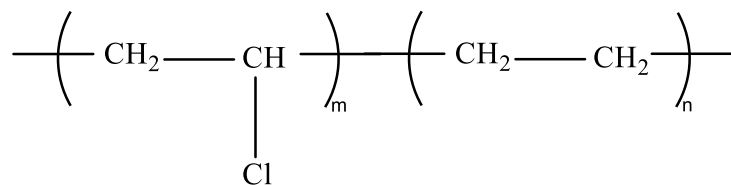
2.3 Degradation

Before classifying different kinds of degradation, the basic forces on cables will be explained.

Electric field, E, is a physical field that exerts force, F, on particles with electrical charge, q. The relationship is shown equation 2.1.

$$F = q.E \qquad\qquad (2.1)$$

$$\varepsilon, \qquad\qquad D = \varepsilon.E \qquad\qquad (2.2)$$

The dielectric permittivity represents the potential of the dielectric to be polarized under the electric field. The relationship between dielectric constant, k, and dielectric permittivity, ε, is shown equation 2.3.

$$k = \varepsilon/\varepsilon_0 \qquad\qquad (2.3)$$

ε_0 represents vacuum dielectric constant in equation 2.3. [25]

Dielectric constant can be visualized as dielectric capability to hold charges. A good cable insulation as low dielectric constant and low dissipation factor, energy lost as heat. When cables are under AC electric field, the charges in the insulation, coming from ions and oxidized groups from manufacturing, move towards the electrodes according to the frequency. The changes in the direction of charged particles' strain and motion produces heat which degrades the insulation, as a result, the dielectric constant and dissipation factor will increase over time.

Dielectric strength is defined as the limiting voltage of insulation electrical beyond which electrical failure happens. [22]

2.3.1 Degradation Mechanisms

There are several electrical failure mechanisms of insulations which will be discussed in the following;

- Partial Discharge (PD)

The presence of voids and cavities in the insulation provides the weakening sites in the insulation. As seen in Figure 4, the electric stress is higher in the air bubble than in the insulator. The dielectric strength of voids is much less than that of insulations, 50 to 100 times. Therefore, when the operation electric field exceeds the voids' breakdown voltage, 3 kV/mm, it results to their decomposition, defined as partial discharges, PD [26].
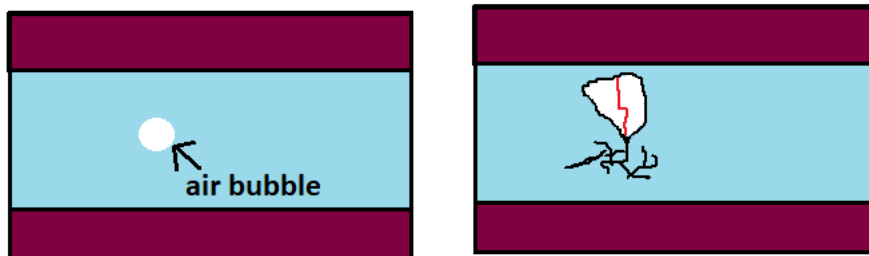
Figure 4- The electrical field in the insulator and air bubble(a) PD propagation in the insulation (b)

After PD, the emitted electrons from gas atoms bombard the insulation in the direction of positive electrode which erodes the insulation by ionization. [25]

The ionization of the insulation after PD, will produce chemical degradation of the insulation which will be extended into the insulation and ultimately lead to a short circuit [25].

2.3.1.1 Free radical formation and oxidation reactions

Oxidation reactions have been known as the most detrimental insulation degradation mechanism. [27], [12], [2], [10]

In these reactions, free radicals initially are formed by partial discharges, ionizing radiation or thermal energy leading to the formation of voids and cracks due the insulation bond breakage. As a result of the thermal, mechanical stress, and ionizing radiation, mainly, ruptures or scissions occur along the backbone of the chain, which lead to the formation of the C-centered free radicals and subsequent decrease in the number average molecular weight (NAMW). Obviously, the decrease in the NAMW leads to the loss of mechanical properties. The scission along the backbone of the chain can take place in both the crystalline and amorphous regions of the polymer chains. Those thermally, mechanochemically, radiolytically produced C-centered radicals react with the dissolved molecular oxygen in the polymer very rapidly to produce the corresponding peroxyl radicals. These reactions are very fast with relatively very low activation energies due to the reductive nature of the C-centered radicals. It is also worth mentioning that the reaction of the C-centered radicals with oxygen occurs

15

mainly in the amorphous region, and at the interfaces between the amorphous and the crystalline region. The C-centered free radicals along the backbone of the chain move to the interface area through H-hoping mechanism. [28], [29], [30], [31], [32]

- Free radical Formation

Reaction (2.4) represents C-H bond of a polymeric chain to break which forms a secondary alkyl free radical, (2.6), and hydrogen atom. Reaction (2.5) represents the breakage on the backbone of the polymer which produces two primary alkyl free radicals.

$$RH \longrightarrow R^{\cdot} + H \qquad\qquad (2.4)$$

$$RR^{\prime} \longrightarrow R^{\cdot} + R^{\prime\cdot} \qquad\qquad (2.5)$$
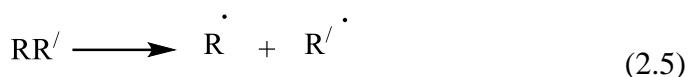
Reaction (2.4) represents C-H bond of a polymeric chain to break which forms a secondary alkyl free radical, (2.6), and hydrogen atom. Reaction (2.5) represents the breakage on the backbone of the polymer which produces two primary alkyl free radicals.

In the case of reaction (2.4), the secondary alkyl free radical can convert to allyl, (2.7), and polyenyl radicals, (2.8) via hydrogen transfer along the chain which are stable radicals due to the presence of the conjugated bonds in the chain. [31]

$$\longrightarrow CH_2 \longrightarrow \overset{\cdot}{CH} \longrightarrow CH_2 \longrightarrow \qquad \text{Secondary Alkyl Free Radical (2.6)}$$

16

$$-CH=CH-\overset{\displaystyle \cdot}{C}H-$$

Allyl Free Radical (2.7)

$$-CH_2\left(\underset{\overset{|}{H}}{\overset{|}{C}}=CH\right)_n\overset{\displaystyle \cdot}{C}H-$$
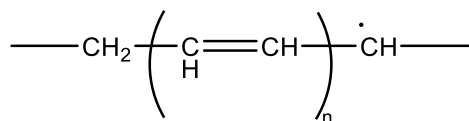
Polyenyl Free Radical (2.8)

Besides, secondary alkyl radicals can undergo termination reactions via crosslinking, Figure 5, where two free radicals are recombined or disproportionation reactions, Figure 6, where a hydrogen atom is abstracted by the acceptor chain and a conjugated bond forms on the donor chain.
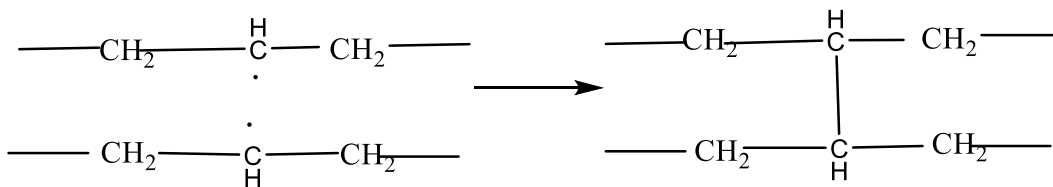
Figure 5- Crosslinking reactions of secondary alkyl radicals
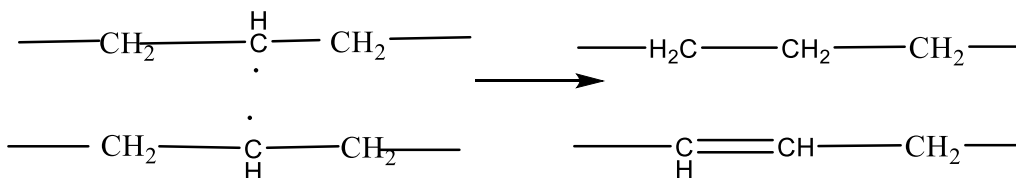
Figure 6- Disproportionation reactions of secondary alkyl radicals

The product of hydrogen atom in reaction (2.4) can be also detrimental to the polymer by forming secondary alkyl free radicals via extracting hydrogen atoms located in both crystalline and amorphous regions. It is attributed to the fact that the hydrogen atom is

very small in size which gives it the possibility to diffuse to crystalline regions too. The exothermal reaction, ΔH=-30 kJ/mol, will produce heat which will be dissipated in the polymer by chain movements, morphology changes and bond breakage which all are detrimental processes. [31], [30]

Finally, the primary free radical formed in reaction (2.5) are short-lived radicals, less than 24 hours, due to the recombination reactions in both amorphous and crystalline regions. However, the primary alkyl radicals in the crystalline region may not recombine due to the confinement and axial chain stress which results in converting to secondary alkyl radicals via hydrogen transfer, Figure 7, or, hydrogen hop, Figure 8.

Hydrogen-transfer mechanism happens along a polymer chain, Figure 7, whereas a hydrogen atom is abstracted from adjacent polymer chains in hydrogen-hopping mechanism, Figure 8. [32], [30], [31]
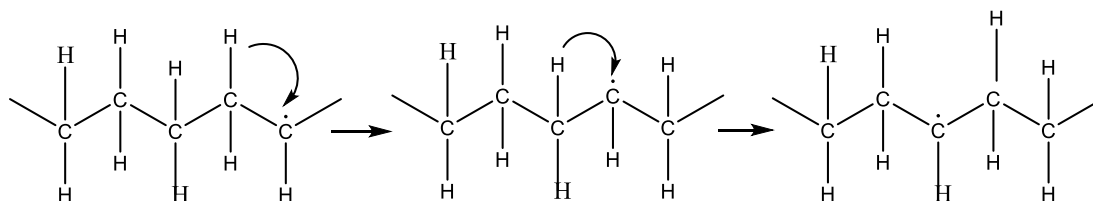
Figure 7- Hydrogen-transfer mechanism
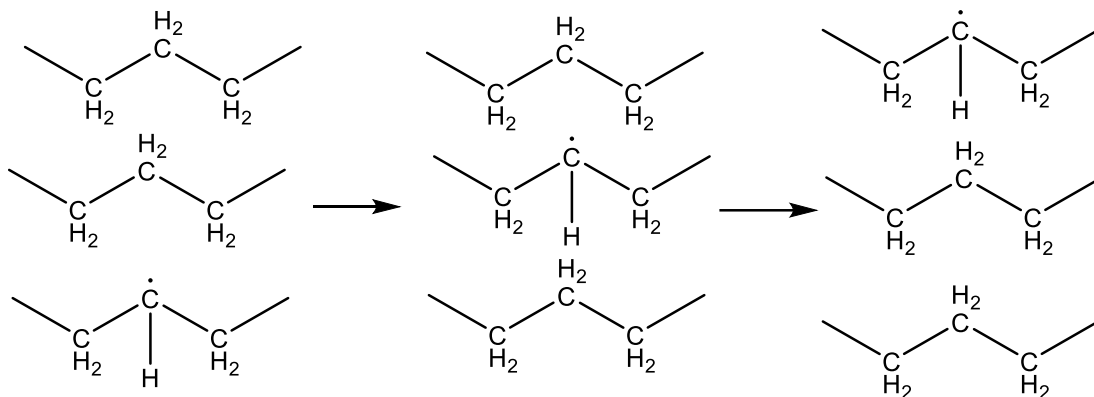
Figure 8- Hydrogen-hopping mechanism

The secondary alkyl radicals may migrate to amorphous regions where oxygen is more available or, as discussed above, may form stable polyenyl and allyl radicals.

- Oxidation reactions

The presence of oxygen along with alkyl radicals will produce a series of reactions that leads to the formation of hydrophilic products such as carboxylic acids, ketones and alcohols which drop the dielectric property of the insulation. Besides, the increase of water penetration along with loss of mechanical properties and crack propagation will deteriorate insulation cables. [22], [31]

Oxygen is initially introduced to polymers in the manufacturing process, while later the diffusion of oxygen to the amorphous region enhances the oxygen concentration.

Alkyl radicals will combine with oxygen through thermodynamically favorable peroxidation reactions, (2.9), which produce peroxyl radicals, $RO_2^\bullet$. [31], [30]

$^{\bullet}RH + O_2 \rightarrow RHO_2^{\bullet}$ Peroxidation   (2.9)
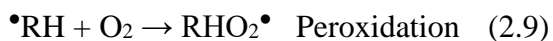
There are three important reactions of peroxyl radicals with polymeric chain, (2.10), which proceeds propagation reactions as well as with alkyl radical, (2.18) and another peroxyl radical, (2.19), which are termination reactions.

- Peroxyl radical reaction with polymeric chain

Peroxyl radicals, $RHO_2^{\bullet}$ can initiate chain reactions by abstracting H, which results in the formation of new C-centered radicals and hydroperoxides.

$HRO_2^{\bullet} + RH \rightarrow RO_2H + {}^{\bullet}R$ (2.10)
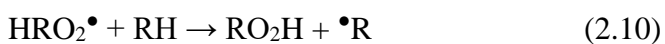
The abstraction reaction is by far much slower than the peroxidation reaction, and with much higher activation energy.

Hydroperoxides decompose to hydroxyl, $\overset{\bullet}{O}H$, alkoxyl, $\overset{\bullet}{R}O$, radicals as well as ketone, R_2CO, and water in reactions (2.11)   and (2.12)   respectively.

$ROOH \longrightarrow \overset{\bullet}{R}O + \overset{\bullet}{H}O$ (2.11)

(2.12)
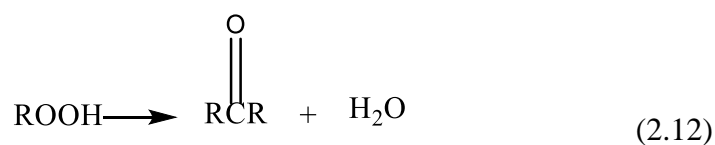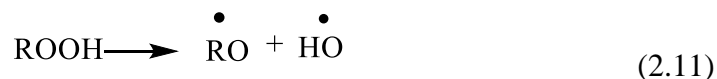
The hydroxyl, $\overset{\bullet}{O}H$,alkoxyl, $\overset{\bullet}{R}O$, radicals are highly reactive products and are considered as important propagation reactions.

(2.13)

20

$$\text{—CH}_2\text{—}\overset{\text{O}}{\overset{\|}{\text{C}}}{}^\bullet \longrightarrow \text{—}\overset{\bullet}{\text{CH}}_2 + \text{CO}$$ (2.14)
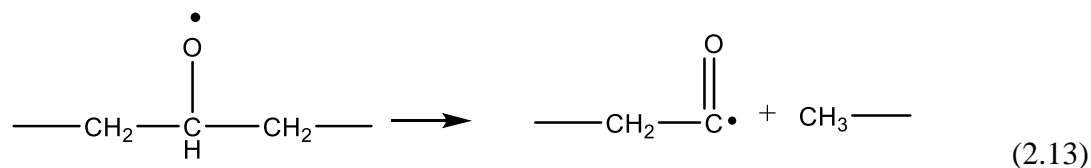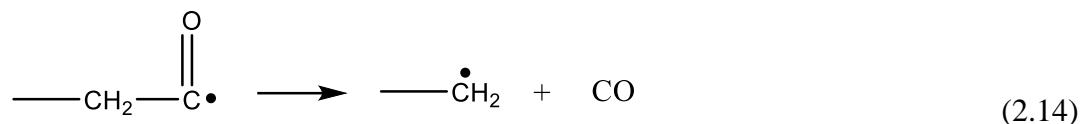
Alkoxyl, $\overset{\bullet}{R}O$, radicals will produce alkyl and carbon monoxide in reactions (2.13) and (2.14) which have a very low activation energy.

The other possible reaction of alkoxy radicals is abstraction of hydrogen from polymeric chains which forms new alkyl radicals and alcohol products, (2.15). [31], [32], [28]

$$RO^\bullet + R'H \rightarrow ROH + {}^\bullet R'$$ (2.16)
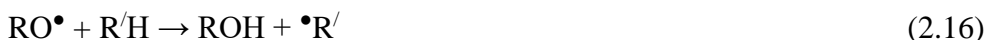
The other highly reactive product of reaction (2.11) is hydroxyl radicals, $\overset{\bullet}{O}H$, which can abstract a hydrogen atom from a polymeric chain to produce a new alkyl radical and water, (2.17).

$$HO^\bullet + R'H \rightarrow H_2O + {}^\bullet R'$$ (2.17)

- Peroxyl radical reaction with alkyl radical

The reaction of peroxyl radicals with alkyl radicals produces peroxides, (2.18).

$$ROO^\bullet + {}^\bullet R' \rightarrow ROOR'$$ (2.18)

These reactions are one of the terminations reactions and thermodynamically feasible due to the migration of alkyl radicals along the polymeric chain and ultimate reaction with peroxyl radicals. [31], [28]

- Peroxyl radical reaction with Peroxyl radical

The other termination reaction of peroxyl radicals is their reaction with peroxyl radicals, (2.19), which produces tetraoxide.

$$HRO_2^\bullet + HRO_2^\bullet \rightarrow HROOOORH \hspace{3cm} (2.19)$$

This bimolecular termination reaction, (2.19), is not a favored reaction and will decompose to hydrophilic products, i.e. aldehyde and alcohol, which increases polarity, the likelihood of moisture ingress and insulation failure;

$$HROOOORH \rightarrow R^{/} OH + R^{//} OH + O_2 \hspace{2.5cm} (2.20)$$
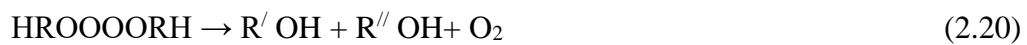
In the absence or at low concentration of oxygen, and increase in the number of free radicals over aging , C-centered radicals can undergo crosslinking reactions. [29], [33], [34]

The oxidation reactions are summarized in Figure 9.
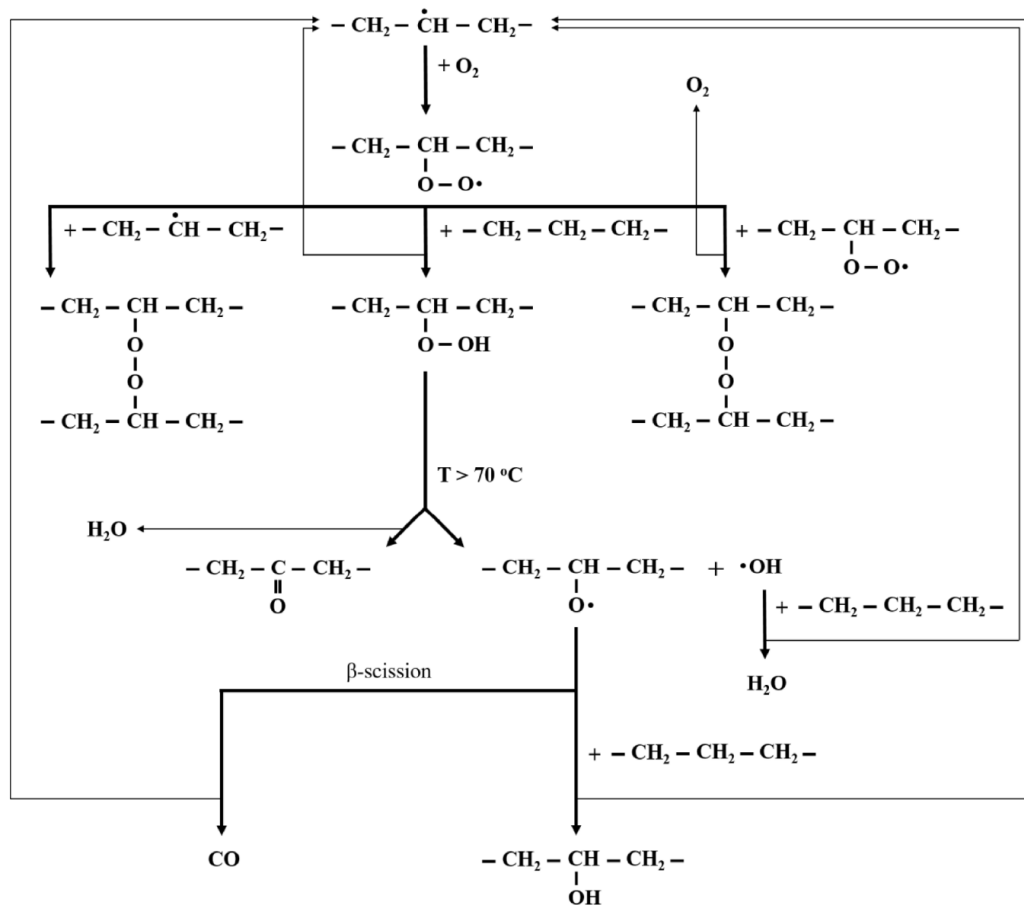
Figure 9- Oxidation reactions of polymeric chains in the amorphous region, Copied from Figure 25 of [31].

2.4 End of life criterion

The end of the life is defined as reaching elongation at break in tensile test, EAB, parameter to 50% of its original value. [35] This criterion has been chosen based on the importance of mechanical integrity in electrical failure of cable insulations. Indeed, aging promotes loss of flexibility, crack propagation and ultimately electrical failure. Measuring EAB is performed by tensile tests for which large samples of cable insulations must be cut and taken to laboratory for tensile test measurements.

- Ductility

One of the important parameters that is evaluated in tensile test is ductility. Ductility represents the level of plastic deformation in materials. As shown in Figure 10, the degree of ductility is very low in brittle materials. From atomistic perspective, plastic deformation corresponds to the lack of freedom of atoms and molecules to return to the original place after the removal of stress. Indeed, atoms form new bonds with their adjacent atoms after breaking bonds between original atoms under stress. Elongation at Break, EAB, in equation (2.9), is a quantitative expression of ductility. [36]
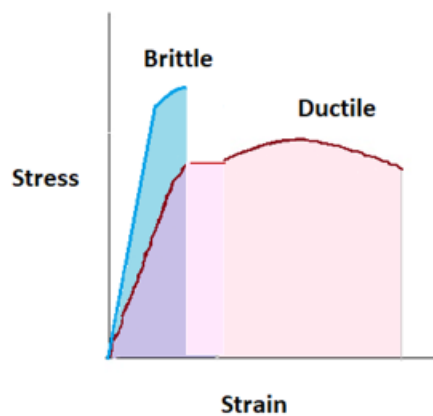
Figure 10- Typical stress-strain plot of brittle and ductile materials

24

$$\%EAB = \left(\frac{l_f - l_0}{l_0}\right) \times 100 \qquad (2.21)$$

where $\%EAB$ is percent plastic elongation, l_f is fracture length (m) and l_0 is the original length (m).

Two other parameters of mechanical properties are Ultimate Tensile Strength, UTS, and Elastic Modulus. UTS is the maximum stress and EM is the slope of the linear region of the stress-strain plot.

2.5 Conventional approaches for lifetime estimation

NPPs still maintain their attractiveness as a sustainable and secure energy resources, which do not produce greenhouse gas emission effect. [37] In order to make NPPs more affordable energy production resource, Nuclear Regulatory Commission (NRC) renews life licenses of plants. [38], [39]

This involves continued operation of plant's structures, components, and systems beyond their originally designed life. Therefore, extra attention should be dedicated towards maintaining the safe and reliable function of aged assets among which the integrity loss of cable insulation and jackets can pose a significant threat to the safety system of the plant. Since the total replacement of cables is both time consuming and expensive, the useful lifetime of cables has been verified by several approaches and models.

- Accelerated aging tests

Accelerated aging tests are widely used to estimate the conservative lifetime of in-service cables by aging tests at accelerated conditions. [40] The first accelerated aging methodology, IEEE Standard 323, was developed in 1974. Accelerated tests were used to reach the end of life of cables faster than the operational in-service conditions. However, there are limitations where the morphology, volatility and solubility of the stabilizers are fundamentally different from below to higher the transition temperature range. [2]

The main assumption is that the degradation behavior remains the same in accelerated and in-service conditions. The results of accelerated aging were used to estimate the end of life by the Arrhenius method. While since then international groups such as Conference International des Grands Reseaux Electriques, CIGRE, International Atomic Energy Agency, IAEA, etc. were extensively devoted a lot of research to establish a reliable methodology to estimate the degradation behavior of ambiently aged cables, deviations from the expected lifetime of naturally aged cables proved more research must be done. It was found out that the in-service cables' degradation behavior is different from that of accelerated aged cables. [41] Several reasons may account for the observed non-Arrhenius behavior. First, degradation mechanisms which are assumed in aging models do not match those happen at field. For instance, Arrhenius model which is widely used to extrapolate accelerated aging test results to ambient temperature is based on identical activation energy of degradation reactions at different temperature zones. [42] However, the observation of non-Arrhenius behavior at lower temperatures brings about a curvature in Arrhenius plot which invalidates linear

26

extrapolation assumptions. While the details of non-Arrhenius behavior are still unknown due to the complexity of degradation processes, physical changes such as morphology, diffusion limited oxidation, and the stabilizer solubility may be accounted as reasons. In addition, chemical changes such as variations in the dominant degradation reaction have been known to significantly affect the curvature of the Arrhenius plot. [43]

Moreover, the variations in cable processing which are not disclosed by manufacturers, adds to the complexity of the system and therefore making the degradation mechanism of cables as a black box. [41]

- Condition Assessment

The other method for lifetime estimation of cables is based on determining current state of degradation of installed cables by assessing mechanical and electrical properties of cables, with non-destructive experiments. Currently, 50% elongation-at-break, EAB, is defined as the end of life. However, EAB values are measured with destructive tensile tests which needs large samples of cable insulations to be cut and taken to laboratory for the test. Indentation modulus, on the other hand, is a non-destructive test that displayed a good correlation with EAB and can be used as an alternative experiment to assess mechanical properties of cables. However, the applicability of indentation method is limited only to easily accessible parts. While there are limitations on mechanical property assessment experiments, there are several aging key indicators corresponding to physical and chemical property changes that can be employed to nondestructively assess the health state of cables without spatial limitations. Chemical and physical properties of cables change as a result of degradation reactions. Detecting

27

gradual changes of these properties can provide early warnings of aging status which over time leads to embrittlement and ultimately mechanical and electrical failure. [39] Condition monitoring, CM, is an approach that several key age indicators are assessed by Non-Destructive Experiments, NDE, on installed cables in periodic plant inspections. The CM parameters are used to monitor degradation processes by comparing with the analytical results obtained from correlating changes of the CM parameters under accelerated aging conditions with elongation-at-break, EAB values. While the definition of end of life is corresponding to 50% EAB, correlating CM parameter changes to EAB variations can result in carrying out non-destructive experiments to obtain the relationship between CM parameter changes and end of life instead of performing destructive tensile tests to directly estimate end of life from EAB data. Condition monitoring is used for the life assessment of ambiently aged cables under the assumption that the correlation between CM parameters and EAB data under accelerated aging conditions remains valid under operational conditions. Therefore, the time variation of CM parameters can be used to estimate the remaining useful life, RUL, of installed cables. However, instances such as irregular variations of CM parameters with time or "induction-time behavior" cases where a sharp decay of material property happens without early warning, makes RUL estimations less applicable. [15]

Under many ambient-condition-assessment investigations, the condition indicators which can detect significant aging mechanisms are found and graded to several classifications to provide guidance on the level of severity of ambiently aged cables. [44], [45], [46], [47], [48]

However, there is a crucial need to develop quantitative requirements based on scientific principles to reduce the probability of subjective assessments of degradation state of cables. While there are several empirical models developed to address this issue by correlating CM parameter changes and that of EAB under accelerated conditions, the practical use in operational conditions is very limited due to the arbitrary nature of the model which is not based of physico-chemical scientific principles of the degradation. [49], [50], [51], [52]

2.6 Insulator Aging Models

Models corresponding to insulator aging are classified into three categories: thermal, electrical, ionizing radiation and combined models.

2.6.1 Thermal Models

The most used models in the thermal aging of the insulators are based on Arrhenius and time-temperature superposition principles.

- Arrhenius model

Thomas Dakin proposed a method for estimating lifetime of insulations based on Arrhenius equation which has been the basis of lots of models developed so far. [53], [54], [55], [56],[57]

Dakin used Arrhenius equation to determine the rate of physical property changes under the assumption that changes of physical properties of insulation are proportional to the changes of the concentration of the most important chemical component. In other

words, he assumed that the concentration changes of one chemical component, which is involved in one reaction, is proportional to the variations of physical properties. Based on this assumption, he suggested a life model, so called "Arrhenius model", AM;

$$lnt = \frac{E_a}{RT} + const \qquad (2.22)$$

where t represents lifetime of insulation (h), i.e. the time it takes for the insulation to reach 50% EAB, E_a activation energy $(\frac{J}{mol})$, T absolute temperature (K) and R gas constant $(\frac{J}{mol\ K})$.

From equation (2.22), it is concluded that lifetime is linearly dependent on temperature when it is plotted in logarithmic scale versus inverse of temperature. The Activation energy can then be calculated from the slope of this plot. [53]

- Time-Temperature Superposition

In 1941, H. Leaderman suggested a method for extrapolation of viscoelastic properties at a given temperature. He based his suggestion on the observation that horizontal shifting of creep recovery values obtained at various temperatures along the logarithmic scale of time axis produced a superposed master curve. The master curve covers a wide range of time axis on logarithmic scale which can overcome the practical issues of long time requirement by experiments at ambient temperatures. [58]

This observation was the basis of Time-Temperature Superposition, TTS, which is explained in the following equations.

$$E_T(a(T).t) = E_{T_0}(t) \qquad (2.23)$$

30

$$E_{T_0}\left(\frac{t}{a(T)}\right) = E_T(t) \qquad\qquad (2.24)$$

where $a(T)$ is the shift factor at temperature T, E_T (Pa) modulus at temperature T, T (K), E_{T_0} modulus (Pa) at temperature T_0 (K).

To obtain $a(T)$, modulus data plotted versus log time will be shifted horizontally until they are superposed. The amount of shift is expressed as $a(T)$. Equations (2.23) and (2.24) assert that the effect of temperature on viscoelastic properties, in linear viscoelastic region, can be found by multiplication or division of a constant shift factor by time. [58]

In insulator aging, TTS is combined with Arrhenius model to employ all the data rather than a few data points. [59]

The data obtained at accelerated conditions is shifted horizontally along the log time axis to superpose and then obtain shift factor. The experimentally found shift factors are plotted against reciprocal of temperature to calculate the activation energy as the slope of the plot according to the following equation; [32]

$$\ln a_T = \frac{-E_a}{RT}\left(\frac{1}{T_r} - \frac{1}{T}\right) \qquad\qquad (2.25)$$

where a_T is shifting factor to the lowest accelerated temperature, E_a is activation energy, R gas constant, T absolute temperature, T_r reference temperature, i.e. lowest accelerated temperature

After calculating activation energy, lifetime of insulation at operational temperature will be calculated from the following equation;

$$\ln a_T = \ln\frac{t}{t_r} = \frac{-E_a}{RT}\left(\frac{1}{T_r} - \frac{1}{T}\right) \qquad (2.26)$$

where t is the lifetime at an accelerated temperature, t_r lifetime at reference temperature, i.e. operational temperature, and T_r reference temperature, i.e. operational temperature.

2.6.2 Radiation Models

Gillen et al extended the time-temperature superposition, TTS, concept to the field of radiation in the name of Time-Temperature Dose Rate Superposition. [60]
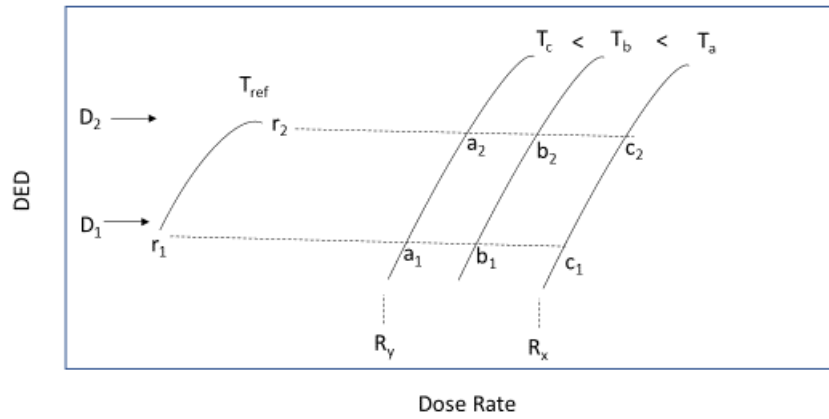
Figure 11- DED versus dose-rate plot in an idealized diagram. [60]

In Figure 11, it is shown that datapoints lie on isotherms, T_a, T_b and T_c, on Dose Equivalent to Damage, DED, versus dose-rate diagram. The datapoints a_1, b_1 and c_1 have the same total dose, D_1. In fact, the isodose line D_1 intersects the isotherms T_a, T_b and T_c with the intersections of a_1, b_1 and c_1. Equation (2.27) is used to extrapolate the a_1, b_1 and c_1 on the T_{ref} isotherm.

according to the following equation;

$$r = \frac{R_x}{R_y} = \exp \frac{E_a}{R}\left[\frac{1}{T_c} - \frac{1}{T_a}\right] \qquad (2.27)$$

where r represents ratio of dose rates, R_x high dose rate (Gy/h) at T_a (K), R_y low dose rate (Gy/h) at T_c (K).

This relationship models combined environments containing temperature and dose rate as stressors.
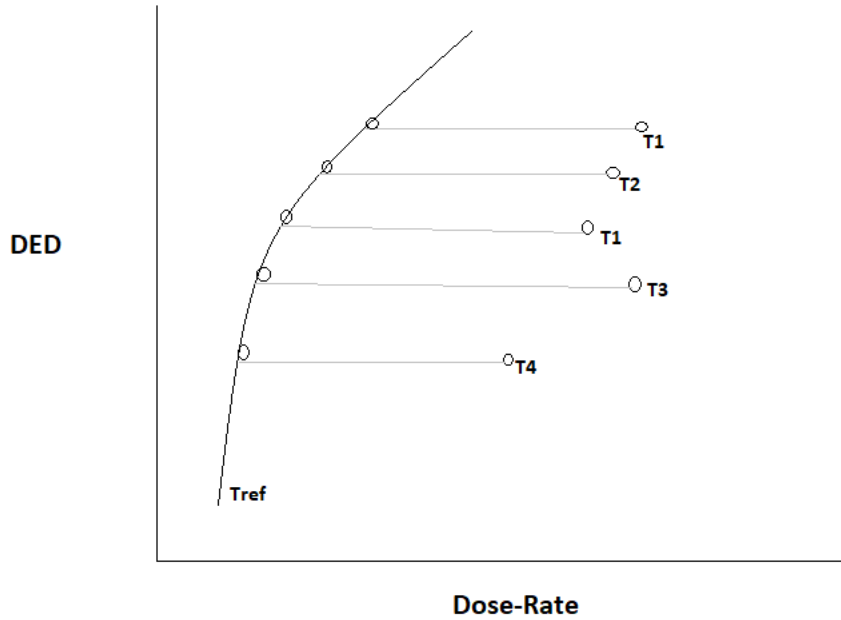
Figure 12-Hypothetical diagram of DED versus dose-rate. [60]

The datapoints lying on isodose lines in Figure 11 is an ideal representation. Figure 12, on the other hand, shows the real hypothetical representation of datapoints in a DED versus dose-rate plot with different total dose values. It is possible to shift the data

33

points on Figure 12 to the reference temperature, T_{ref}, by the activation energy which gives the best superposed curve. In fact, iteration of activation energy values to obtain the best superposed curve is due to the assumption that only one single activation energy holds.

2.6.3 EAB estimating models

Models estimated EAB with time will be explained as follows;

- Buslik et.al. developed a probabilistic model to estimate the probability of failure time of low voltage control cables inside containment, considering that the stressors degrading these cables are mainly temperature and radiation.[8] Lifetime assessment was evaluated by embrittlement criterion which is 50% EAB. He based his model on this assumption that cable insulations have an initial capacity, resistance to degradation, h_0, which will decrease by exposure to stressors, Temperature and Radiation, according to the following equation;

$$h = h_0 - tR(T, D) \qquad (2.28)$$

where h is the capacity of insulation at time t (h), h_0 initial capacity, R (T,D) rate of degradation (h^{-1}) as a function of Temperature T and dose rate D.

The rate is assumed constant at constant T and D which leads to expressing degradation, f(t,T,D), as a product of time and rate. He obtained R(T,D) from the following equation;

$$R(T, D) = e^{-\beta E}(1 + dD^n e^{n\beta E}) \qquad (2.29)$$

34

where $\beta = \frac{1}{RT}\left(\frac{mol}{J}\right)$, E activation energy $\left(\frac{J}{mol\ K}\right)$ n and d are parameters of the model.

The first part of the above equation is related to the thermal-induced degradation, while the second part is related to radiation-induced degradation. On the other hand, when high dose rates are used, radiation degradation dominates, and the rate equation will approach time-temperature dose rate superposition.

In order to determine the relationship between EAB and the change in resource, h_0, the data corresponding to each parameter were plotted. An exponential curve fitting was shown to be the best fit with experimental data which was used to derive the equation below;

$$\ln EAB = A + Bh_0 \qquad\qquad (2.30)$$

He concluded that the change in resource can be found from equation (2.29) which can be substituted in equation (2.30) to estimate EAB.

- The most widely used approach to empirically model EAB with time is based on determining a polynomial or exponential function which best fits EAB versus time curve. [49], [9]

  Kemari et al used an exponential function to describe the relationship between EAB and time. [9]

$$EAB = E_0 - Ae^{t/\tau} \qquad\qquad (2.31)$$

where E₀, A and τ are the parameters of the model.

- A mechanistic model which estimated EAB with time was developed by Chang et al in 2018. [7]

Chang based his model on the assumption that EAB of cable insulations will slightly change for specific amount of time which subsequently will be dropped sharply to reach end of life. He hypothesized that the sharp decay is due to the complete depletion of insulation out antioxidants via evaporation and consumption. He assumed the degradation mechanism by considering that degradation which is represented by EAB decay is initially constant over specific time interval but will be progressed significantly in the next step. He assigned the "incubation time" to the time coordinate of the first step and "drop off rate" to the rate of the second step. [7]

Normalized EAB is defined as the ratio of EAB corresponding to an aged specimen to that of unaged specimen.[61][62]

Then, he assumed that a tensile specimen is divided into unit cubes while each unit cube can be divided into m subunits. He assumed that n subunits out of m sub units of a unit cube are degraded. He then derived the following equation for modeling the variations of normalized EAB with time;

$$\delta = 1 - (1 - e^{-\vartheta t})^{\frac{1}{3}} \qquad\qquad (2.32)$$

36

where ϑ is drop of rate (1/s) , δ is normalized EAB which is EAB at time t divided by EAB at time 0, t time (s).

Then, he subtracted incubation time from time t because drop off rate is negligible at times smaller than incubation time.

$$\boldsymbol{\delta = 1 - (1 - e^{-\vartheta(t-\tau)})^{\frac{1}{3}}} \qquad (2.21)$$

where τ(s) is incubation time.

2.7 This dissertation Model Theory

The model of this PhD dissertation is based on the correlation of activation energies corresponding to physical property changes and that of EAB. The correlation is based on Dakin's theory which stated that the activation energy of chemical reactions is correlated with that of physical properties. [53]

Figure 13 schematically shows the correlation between the activation energy of degradation and crosslinking reactions in the insulation and the activation energy corresponding to physical property changes.
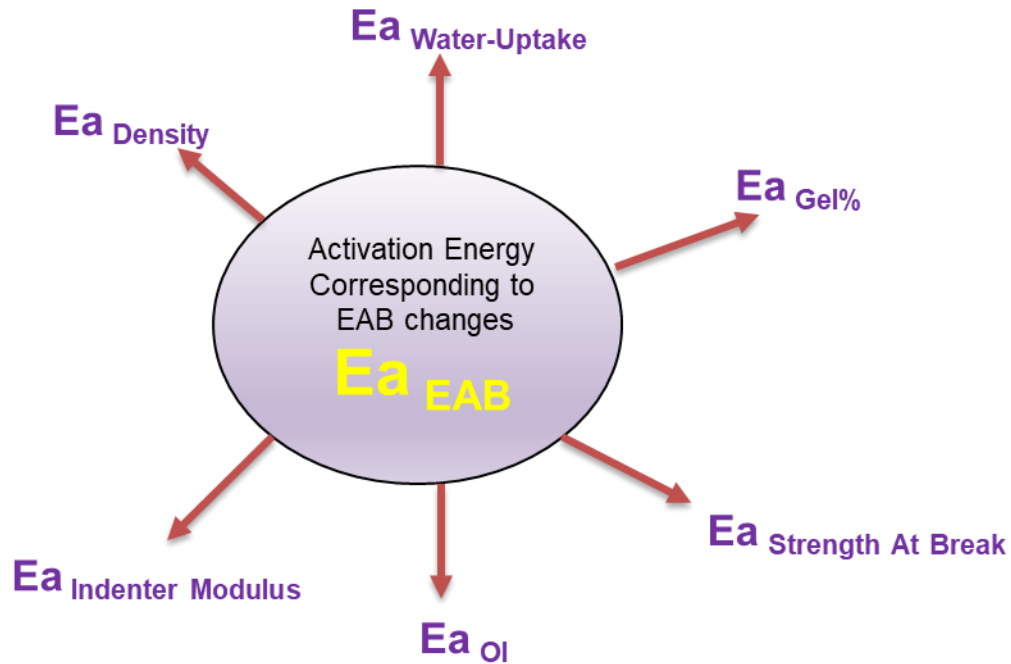
Figure 13- Schematic diagram of correlation of activation energy of different properties.

It can be concluded that the activation energy of NDE-CM parameters' changes is equal to the activation energy of EAB changes. However, the equality has not always been observed due to the experimental conditions and the accuracy of calculation methods. A coefficient multiplication to each activation energy of NDE-CM parameters' changes can make them equal to the activation energy of EAB changes. This coefficient is obtained by the average of normalizing activation energy of each NDE-CM parameter's changes with the activation energy of EAB changes.

Therefore, it is possible to find a mathematical relationship between activation energy of EAB variations and that of other physical properties.

The practical use of this finding is to substitute the correlated activation energy in any of EAB models discussed above to estimate EAB based on variation of CM parameters.

38

Chapter 3:

Experimental and Characterization Methods

3.1 Introduction

In this chapter, the experimental methodologies along with characterization methods and parameters are explained and discussed. Fourier transform infrared spectroscopy – attenuated total reflectance (FTIR–ATR) spectroscopy was used to measure Oxidation Index (OI). Electron paramagnetic resonance (EPR) spectroscopy was used to measure free radical concentration. To measure the mechanical properties in order to relate the changes in the chemical structure to physical properties as a function of aging process, tensile test was used. For each data point, three samples were used and the standard error was calculated.

 In addition, the physical properties of indenter modulus, density, gel%, SAB and water-uptake along with their corresponding EAB data from published literature were included in the data source.

It should be noted that although brand new cables are used in the experiments of this thesis, the results can be useful for NPPs. The reason is attributed to the fact that at NPPs, the aged cables are replaced with newer cables before the end-of-life. [14]

3.2 Experimental method

The cable materials and experimental methods are explained in this section.

3.2.1 Materials Selection and Acquisition

We are donated commercial grade XLPE cables by General Cables and purchased EPR commercial grade cables from Platt supply company. Nuclear-grade cables were purchased from RSCC World Class Nuclear Cable Company which are commonly used

in the nuclear industry. The characteristics of each nuclear-grade cable are summarized

in Table 1.

Table 1- Cable Characteristics

Material	Grade	Insulation Thickness (mm)	Abbreviation
EPR	Nuclear	4.95	EPR-NU
XLPE	Nuclear	2.25	XLPE-NU
EPR	Commercial	7.50	EPR-Com
XLPE	Commercial	2.77	XLPE-Com

3.2.2 Specimen Preparation and Treatment Methods

Samples were prepared by cutting the cables into 6-inch-long sections using a

bandsaw. The cables cut into 6 inches are shown in Figure 14.

Figure 14- The 6-inch-cut cables

The EPR and XLPE cables were then placed in ovens at temperatures of 90 °C, 120 °C as well as 90 °C, 120 °C and 140 °C respectively which were extracted monthly up to 6 months. However, the samples aged at 90 °C did not reach the end of life after 6 months. Therefore, they were let to be aged for 3 years and 9 months at 90 °C oven and then extracted.

The reason of selecting the temperatures of 90 °C and 120 °C for both XLPE and EPR cables was attributed to the fact that melting temperatures of XLPE and EPR lies in the range of 110-125 °C and 120-130 °C. [2] Therefore, both of these temperatures are lower or close to the melting temperature of XLPE and EPR cables.

After extraction, the 6-inch-cut cables were again cut with bandsaw machines at the Institute for Research in Electronics and Applied Physics (IRIP) of University of Maryland to strip the cable which will be explained in more details in the following.

43

First, the 6-in-cut cable was placed in a bandsaw guide to get more protection while working the bandsaw machine. Then, the length of the cable was cut in half from the cross section which made it 3 in, shown in Figure 15. Then, the 3-in-cut cable was placed in the bandsaw guide again and adjusted accordingly. The length of the 3-in-cut cable was cut with the bandsaw until the blade touches the metal. Then, the guide was flipped to cut the other side of the cable. The copper strands and jacket were then removed from the insulation.
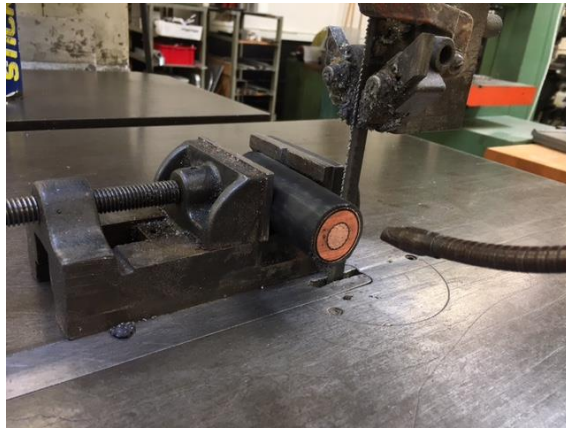
Figure 15- The cable inserted in the guide

3.3 Characterization Techniques

As it was explained above, the characterization techniques are based on the experimental data source.

3.3.1 Tensile Test

Tinius Olsen Universal Testing Machine was used for tensile strength testing of our samples, Figure 16.   The samples were tested at a strain rate of 13mm/min. The RAY-RAN test equipment dog-bone press, shown in Figure 17, was used for cutting dog bones which uses dog-bone cutting die dimension according to TSC-ASTM D638-5 Dog Bone. [63]

The dimensions of the dog-bone cutting die are demonstrated in Figure 18.

It should be noted that the dog bones were cut from the same or different parts of the cables which can explain the high or low error bars which will be observed in the following chapters.

Figure 16- Tinius Olsen Universal Testing Machine

Figure 17- RAY-RAN test equipment Dog-Bone press
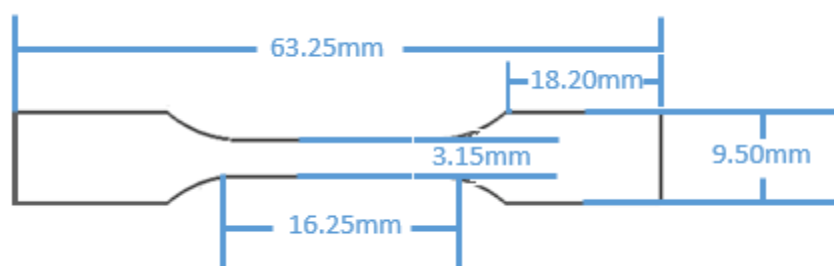
Figure 18-Dog-bone cutting die dimension

3.3.2 Fourier Transform Infrared -Attenuated total Reflectance (FTIR-ATR)

Thermo Nicolet iS50 FTIR equipped with ATR module, was used to analyze the structural changes of the insulations.

The number of 128 scans from 650 cm^{-1} to 4000 cm^{-1} wavenumbers with a resolution of 2 cm^{-1} were averaged to make the ultimate FTIR-ATR spectrum after subtracting from the collected background.

The normalization of the absorption values was performed to enable the comparison of different spectra. The relative absorbance was found by dividing the absorption values to the independent absorption peaks of aging for XLPE and EPR which are assigned to the bands at 720 cm^{-1} and 1155 cm^{-1} respectively. [64]

Oxidation index, OI, of samples was calculated as the area under the relative absorbance spectra versus wavenumbers between 1700 cm^{-1} to 1750 cm^{-1} which are assigned to carbonyl oxidation products.

3.3.3 Electron Spin Resonance (ESR)

Electron Spin resonance, ESR or Electron Paramagnetic resonance, EPR, is a powerful technique to detect free radicals.

In the ESR spectroscopy the magnetic moment changes of unpaired electrons is exploited. When unpaired electrons are placed in a magnetic field, the level of their energy splits to two levels. The higher energy level corresponds to those electrons whose magnetic moment is antiparallel to the magnetic field, while the lower energy level corresponds to the electrons with magnetic moment parallel to the magnetic field. The equation 3.1 represents electron energy, E.

$$E = -\mu H \text{ (erg)} \tag{3.1}$$

Where μ corresponds to the electron magnetic moment (erg/G) and H corresponds to the external magnetic field (G).

$$\mu = -g \beta M_s \tag{3.2}$$

Where g represents g factor, a proportionality constant (~2), β represents Bohr magneton, which expresses the unit of magnetic moment of electron (($9.274096 \pm 0.000010) \times 10^{-21}$ erg G^{-1}), M_s represents Spin quantum number ($\pm 1/2$).

Substituting equation (3.2) in (3.1) ;

$$E = \pm \tfrac{1}{2} g \beta H \text{ (erg)} \tag{3.3}$$

$$\Delta E = g \beta H \quad \text{(erg)} \tag{3.4}$$

The split of energy levels of unpaired electrons under magnetic field is called Zeeman splitting effect.

As it is seen in equation (3.4), the energy difference between the two states is equal to $g\beta H$. We know from Planck's law that the electromagnetic radiation will be absorbed only if the energy difference between two states is $(h\nu)$ where h represents the Plank's constant and represents the frequency of the microwave radiation.

Figure 19 shows the absorbed energy required for a transition between the two energy states.
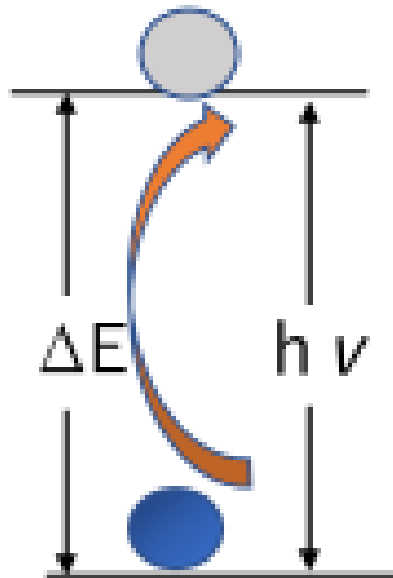
Figure 19- absorbed energy corresponding to transition between two energy states,

Therefore, only microwave radiation can be absorbed which has the same energy difference as the spin energy states.

$$\Delta E = g\beta H = h\nu \qquad\qquad\qquad (3.5)$$

According to equation (3.5), there are two methods that can be applied in ESR for a microwave absorption. In the first method, the magnetic field is constant while the frequency is swept, which will be reversed in the second method. These methods along with the absorption diagram are illustrated in Figure 20. The second method is more commonly used in ESR instruments.
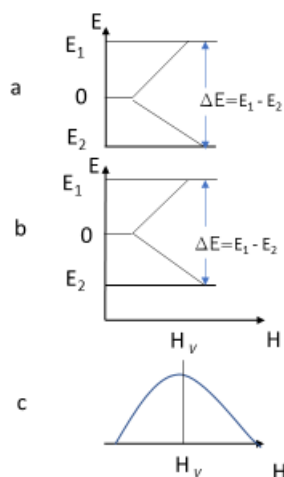
Figure 20- Absorption of microwave radiation in a magnetic field at (a) constant magnetic field and varying frequency, (b) at constant frequency and varying magnetic field (c) microwave absorption diagram

It should be noted that the ESR signal is displayed as a first derivative of the absorption which is due to the employment of phase detection technique which elevates the sensitivity of the spectrum[65].

In this thesis, ESR spectra were recorded on a EMX EPR spectrometer (Bruker corporation, USA) located at UMD lab. The working parameters of the instrument are as follows; Conversion time of 40.96 ms, time constant of 20.48 ms, modulation amplitude of 3.12 G, receiver gain of 6.32E3, MW power of 5 mW, MW attenuation of 16 dB and sweep width of 1000.

Figure 21- EMX EPR spectrometer

Figure 21. show EMX EPR spectrometer with all of the components and with detailed display of radiation source, magnet and cavity components respectively.

To have a better understanding of different components of EMX EPR, a schematic of the instrument along with labeled components is presented in Figure 22.

The microwave source is placed along with the detector in a box called the microwave bridge. The magnet is responsible for generating magnetic field. The sample is placed in a cavity surrounded by a metallic box which is called resonator. The metal box amplifies the weak signals. Console contains the control elements and signal processing electronics. The computer is used for analyzing data and synchronizing all the spectrum unites. [66]
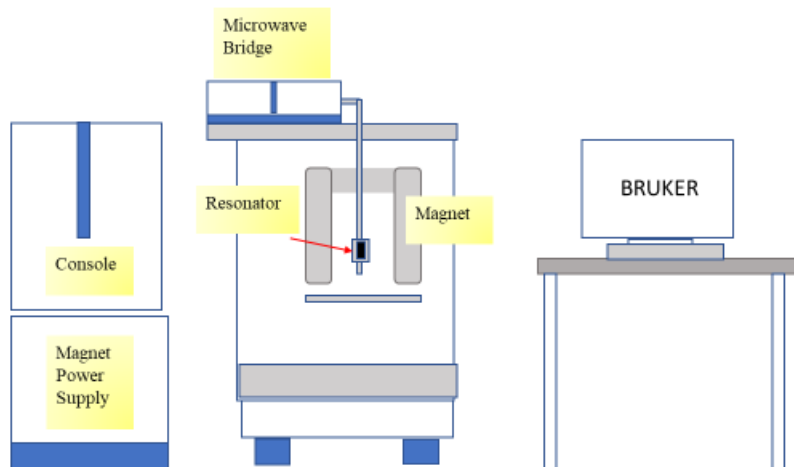
Figure 22- A general layout of EMX spectrometer

To have a better understanding of the signal processing, a schematic of microwave bridge is presented in Figure 23. As it is seen, one part of the radiation from source, A,

goes to the attenuator, B, which controls the intensity of the radiation. Then, it travels

to the circulator, C, which ultimately will be sent to cavity, D. If the sample absorbs

the radiation, no signal will be sent to the detector. On the other hand, one part of the

radiation was sent to the reference arm which will be compared to the reflected

radiation coming from cavity. The signals will be converted into electric current in the

detector, G. [66]
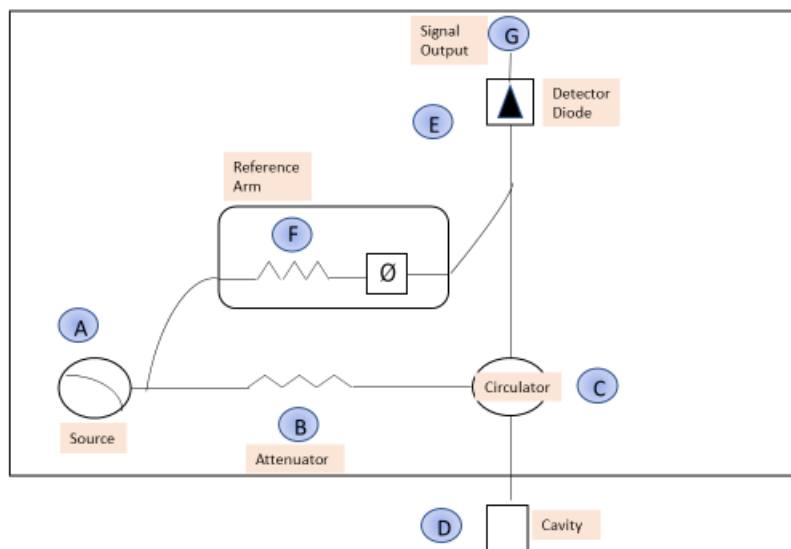
Figure 23- microwave bridge schematic

3.4 Characterization parameters

As it was explained above, the characterization parameters are based on the literature data source.

3.4.1 Density

Density is a physical parameter that is mostly measured in CM methods which is usually measured by density gradient column methods. In these methods, the column is filled with two miscible liquids which can measure the density of samples after calibration. [67]

3.4.2 Indenter Modulus

Indenter modulus is a compressive modulus which measures the ratio of the applied force versus deformation. A conceptual diagram of indenter modulus is illustrated in Figure 24. [6]
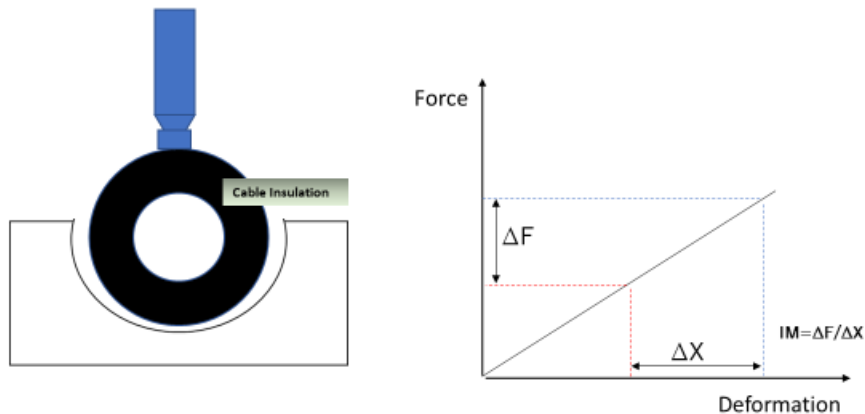
Figure 24- indenter modulus schematic

3.4.3 Gel%

Gel% or gel fraction is a relative measurement of crosslinking content which is determined by immersing insulation specimens in Xylene solvent at 110 °C to 140 °C to extract the sol. The ratio of the dried residue weight to the initial weight of the specimens will determine the gel % or gel fraction. [68], [69], [70]

3.4.4 Strength At Break , SAB

Strength At Break (SAB) is simply the stress coordinate of fracture point on the stress-strain plot, Figure 10, which is measured by tensile test. [36]

3.4.5 Water Uptake

Water uptake measurement is a method of determining hydrophilicity of insulation cables. The specimens are immersed in water for a specific time. Water uptake is equal to the ratio of the weight difference before and after immersion to the initial weight. [71]

Chapter 4:

Experimental Results Analysis

4.1 Introduction

The results on FTIR-ATR experiments and tensile tests on EPR and XLPE cables in both commercial and nuclear grades will be discussed in this chapter.

4.2 EPR Cables

In this section, the results of EAB measurements of EPR-NU and EPR-Com cables aged at 90°C and 120°C will be discussed.

4.2.1 EAB measurements

In this section, the results of EAB measurements of EPR cables, will be discussed.

4.2.1.1 EAB measurements on EPR-NU
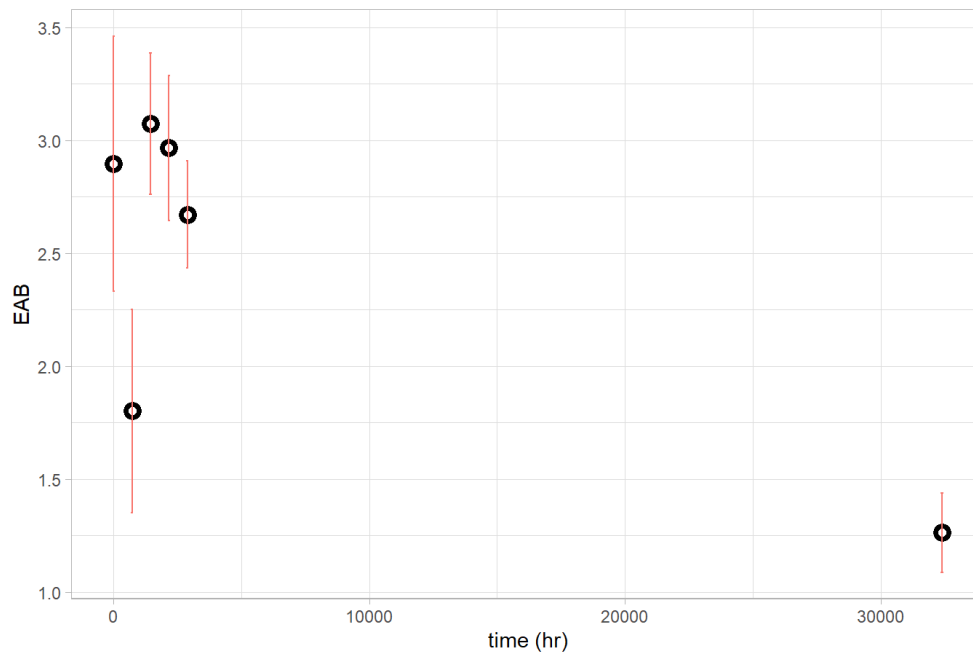
Figure 25- EAB versus time at 90 °C, error bars represent SE
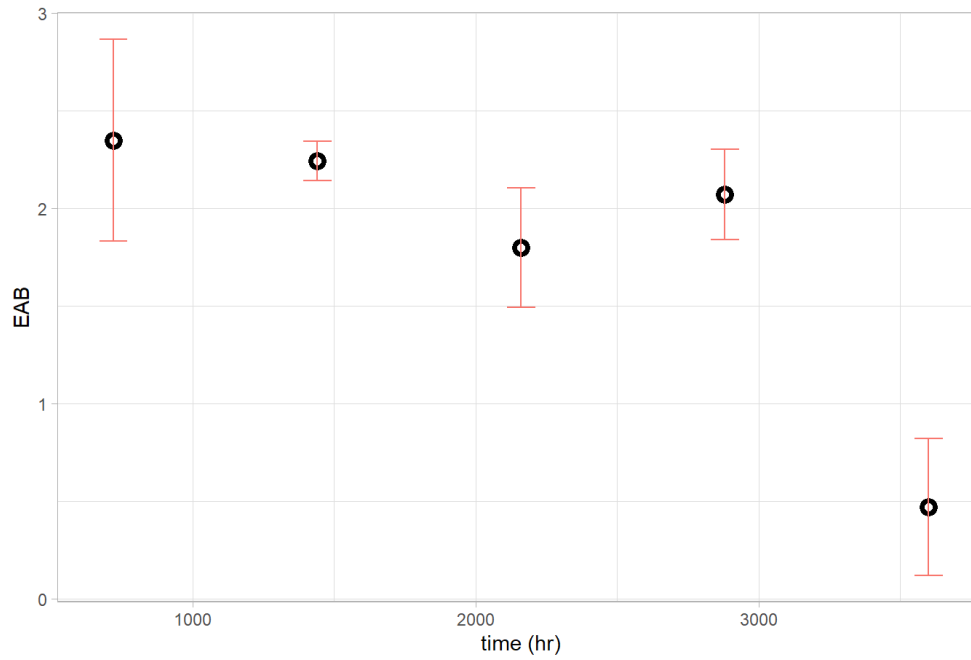
Figure 26- EAB versus time at 120 °C, error bars represent SE

The EAB values at 90 °C and 120 °C are shown in Figure 25 and Figure 26 respectively.

Figure 27 shows the EAB versus time (hr) of EPR-NU cable aged at 90°C and 120 °C.
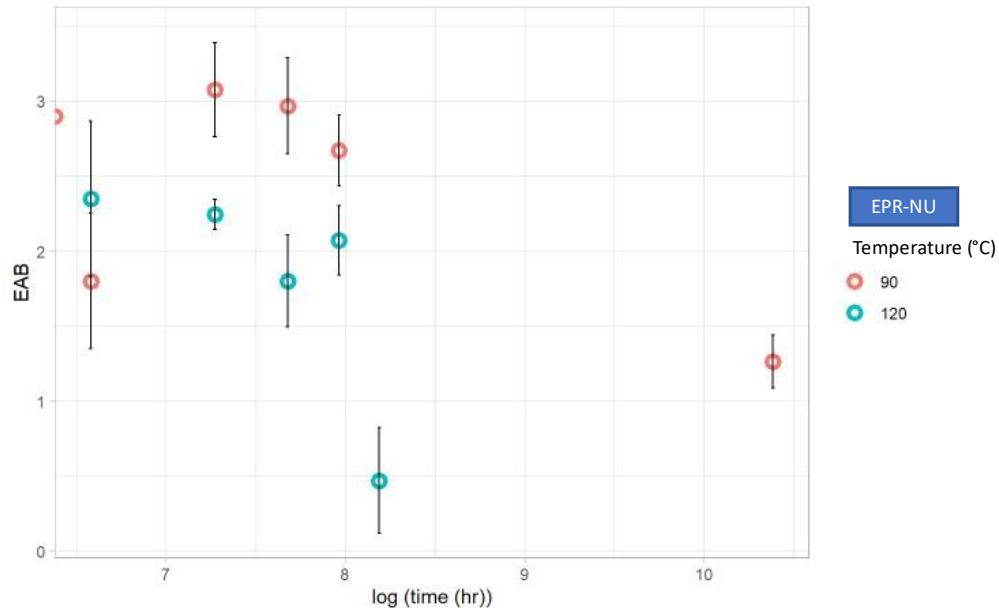
Figure 27- EAB versus time of EPR-NU cable aged at 90°C and 120°C, error bars represent SE

The reduction of EAB with time is seen in Figure 27.

Using time-temperature superposition method, the plots of relative EAB at 120 °C were shifted to the reference temperature, 90 °C. The results are shown in Figure 28Figure 28. As seen, the two plots are nicely superposed at the reference temperature.

It is very important to note that the nice superposition of the plots occurred while there is a broad range of temperature difference in the plots. This can be assuring that the accelerated assumption is valid in this material. [59]
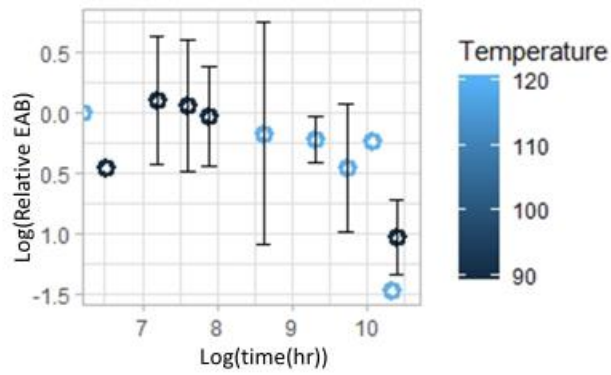
Figure 28-Time-temperature superposed EAB results at the reference temperature of 90°C, error bars represent SE

The shift factors corresponding to different temperatures are given in the Table 2.

Table 2- Shift factors for the thermally aged EPR-NU cable

Temperature (°C)	a_T	$Ln(a_T)$
90	1	0
120	8.27	2.11

In the next step, the activation energy will be calculated from the slope of the Arrhenius plot of shift factor versus temperature, shown in Figure 29.
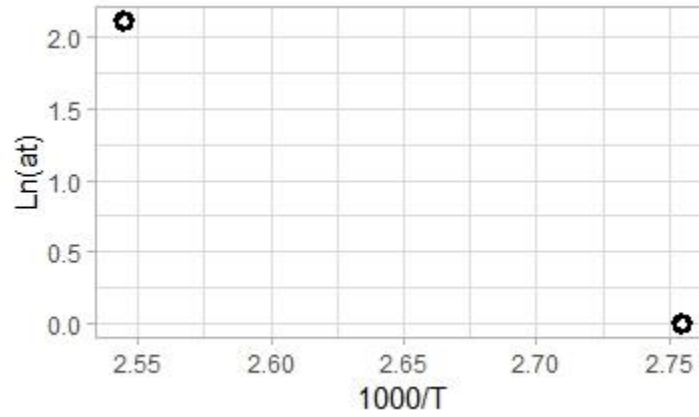
Figure 29-Shift factor versus temperature in the Arrhenius plot

The activation energy was calculated according to equation (2.14) to be 83.47 kJ/mol.

4.2.1.2 EAB measurements on EPR-Com

In this section, the results of EAB measurements of EPR nuclear grade cables, will be discussed. The EAB values versus time at 90 °C and 120 °C are shown in Figure 30 and Figure 31.
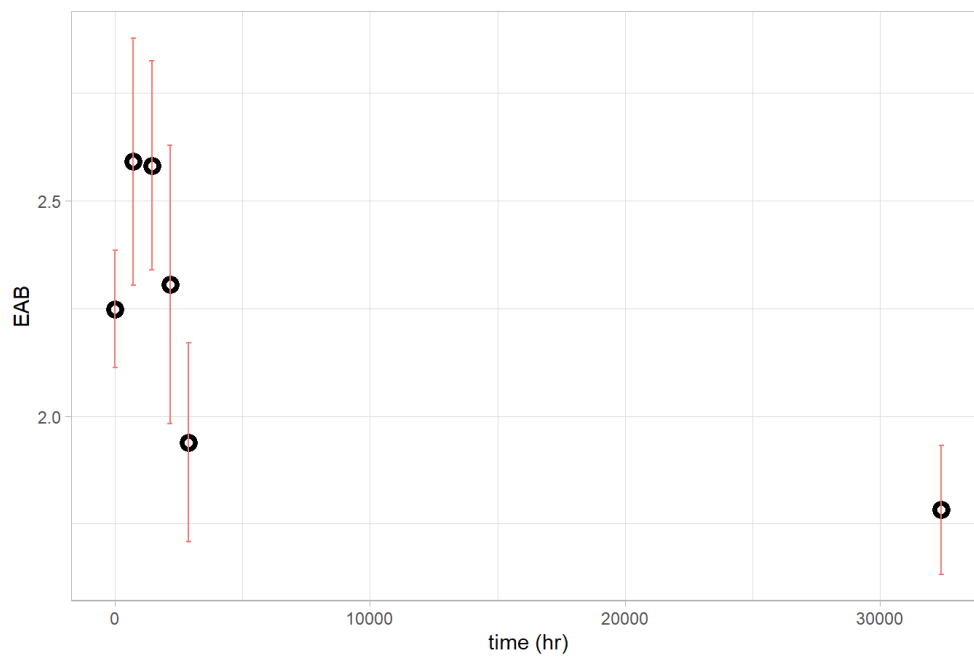
Figure 30- EAB versus time at 90 °C, error bars represent SE
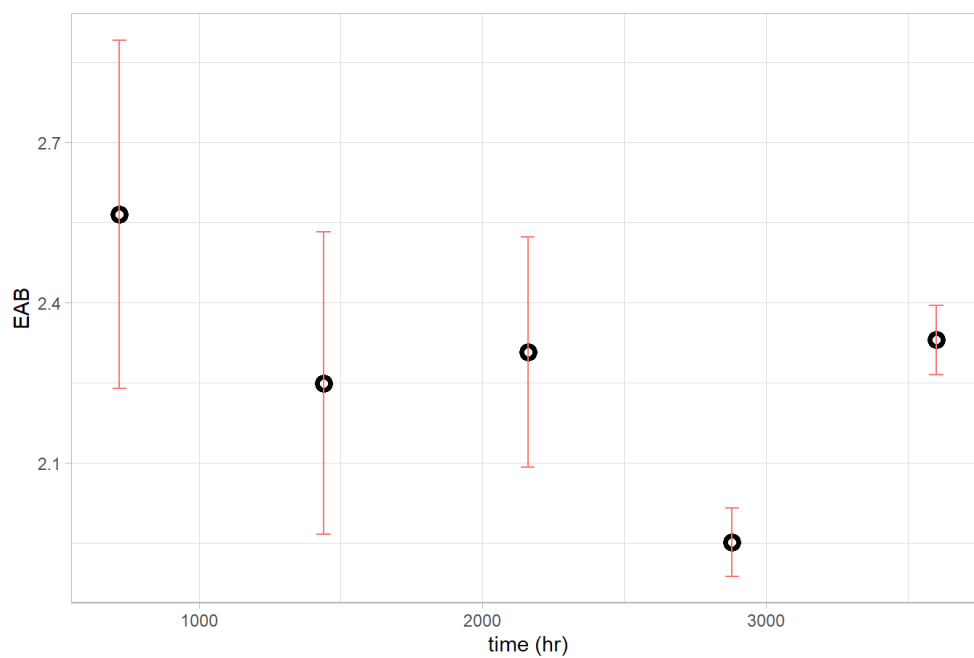
Figure 31- EAB versus time at 120 °C, error bars represent SE
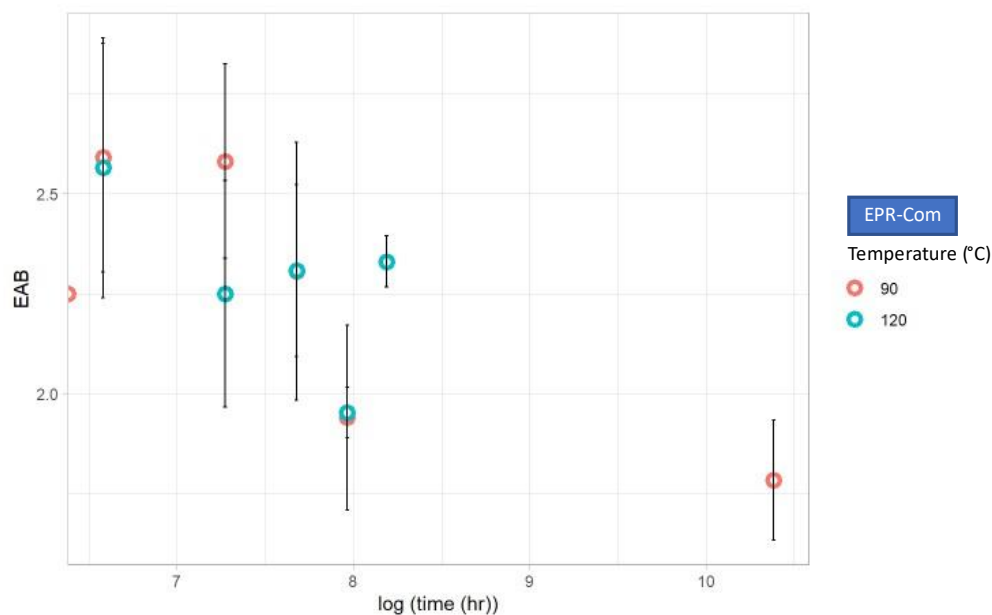
Figure 32-EAB versus time of EPR-Com cable aged at 90°C and 120°C, error bars represent SE

The EAB versus time plots at 90°C and 120 °C temperatures are shown in Figure 32.

It is seen in Figure 32that the EAB values of EPR-Com cables aged at 90 °C and 120 °C are almost the same. Therefore, it is impossible to shift the EAB values of EPR-Com cables aged at 120 °C to the reference temperature of 90 °C.

4.2.3 FTIR-ATR results

In this section the results of FTIR-ATR on EPR cables aged at 90°C and 120 °C will be discussed.

4.2.3.1 FTIR-ATR results on EPR-Com

In   Figure 33 and Figure 34, the ATR spectrum of an un-aged EPR-Com specimen and enlarged scale of FTIR spectrum in the oxidation region of un-aged EPR-Com are seen. The wide peaks at 1710 cm^{-1} and 3356 cm^{-1} are assigned to carbonyl and hydroxy groups respectively while the peaks at 2850 cm^{-1} and 2916 cm^{-1} are assigned to the vibration of -CH$_2$- groups. [72], [73], [74]
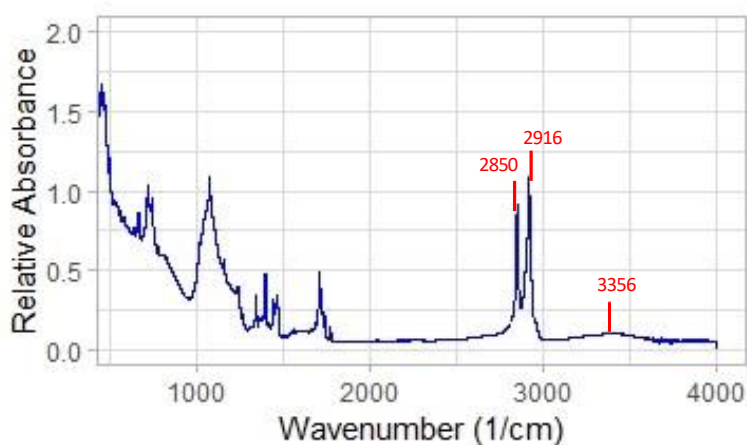
Figure 33-FTIR spectrum of un-aged EPR-Com
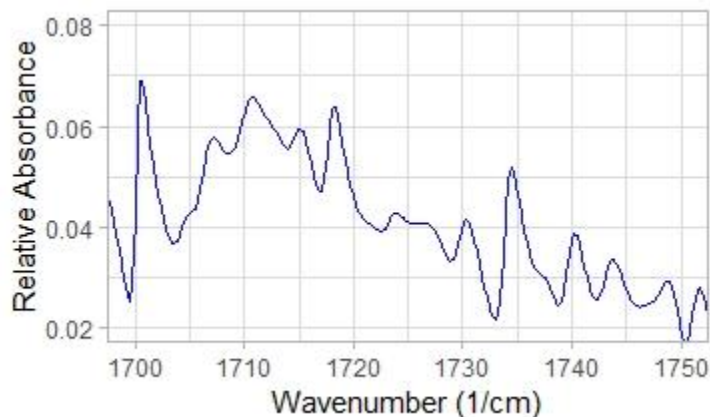
Figure 34- enlarged scale of FTIR spectrum in the oxidation region of un-aged EPR-Com

It is interesting to note that the un-aged specimen contains oxidized groups which are most likely introduced to the insulation through the manufacturing process. [75]

In Figure 35 to Figure 40, the ATR spectra of aged EPR-Com specimens after one month to three months at 90 °C specimen long with their corresponding enlarged scale of FTIR spectrum in the oxidation region are shown. It is observed that the oxidation peaks are dropping in intensity while the peak intensity at 2850 cm^{-1} and 2916 cm^{-1} are growing larger due to the progression of crosslinking or crystallinity region. [76], [34]

Figure 35- FTIR spectrum of EPR-Com insulation after one month at 90°C
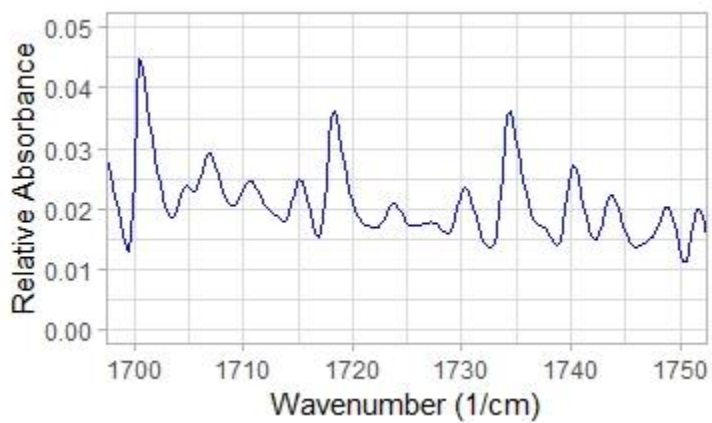
Figure 36- enlarged scale of FTIR spectrum in the oxidation region of EPR-Com insulation after one month at 90°C

67

Figure 37- FTIR spectrum of EPR-Com insulation after two months at 90°C
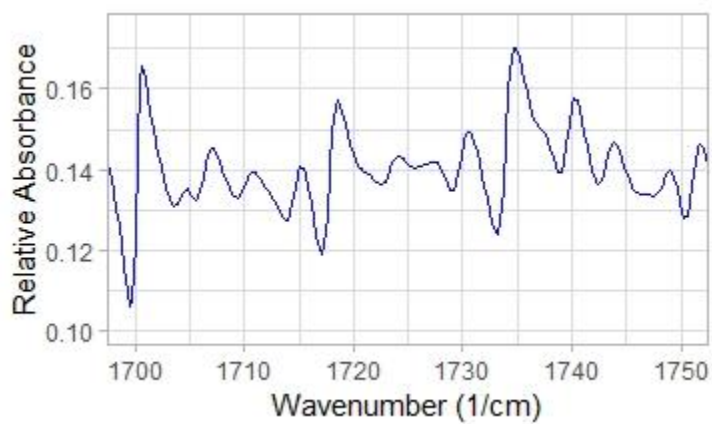
Figure 38- enlarged scale of FTIR spectrum in the oxidation region of EPR-Com insulation after two months at 90°C

Figure 39- FTIR spectrum of EPR-Com insulation after three months at 90°C

Figure 40- enlarged scale of FTIR spectrum in the oxidation region of EPR-Com insulation after three months at 90°C

In Figure 41 and Figure 42, the ATR spectrum of an aged EPR-Com specimen after

four months at 90 °C and the corresponding enlarged scale of FTIR spectrum in the

oxidation region are shown. The peak at 3356 cm^{-1} is disappeared while the wide peak at 1672 cm^{-1} shifted to a small peak at 1714 cm^{-1}. It is also observed that the peak at 2850 cm^{-1} and 2916 cm^{-1} are grown more than two times in intensity. The rise of peak intensity at 2850 cm^{-1} and 2916 cm^{-1} is attributed to the progression of crosslinking or crystallinity region. [76], [34]

On the other hand, the drop in the oxidation group peak area shows that chain scission reactions were mostly due to the thermal stressor than thermo-oxidative reactions.

The aging at 90 °C continued to 3 years and 9 months. In Figure 43 and Figure 44, the ATR spectrum of an aged EPR-Com specimen after four months at 90 °C along with the corresponding enlarged scale of FTIR spectrum in the oxidation region are shown. it is observed that the carbonyl peak at 1714 cm^{-1} grows larger than our observation in Figure 41 .while the double peaks at 3356 cm^{-1} and 3533 cm^{-1} assigned to hydroxyl groups emerge.

In addition, the peak intensity at 2850 cm^{-1} and 2916 cm^{-1} is almost the same in Figure 41 and Figure 43. This observation shows the progression of oxidation reactions after 3 years and 9months which resulted in scission reactions. However, the competence between scission reactions and either crosslinking reactions or crystallinity area did not

let the intensity of peaks at 2850 cm^{-1} and 2916 cm^{-1} drop which ultimately increases

brittleness.

Figure 41- FTIR spectrum of EPR-Com insulation after four months at 90°C

Figure 42- enlarged scale of FTIR spectrum in the oxidation region of EPR-Com insulation after four months at 90°C

Figure 43-FTIR spectrum of EPR-Com insulation after 3 years and 9 months at 90°C

Figure 44- enlarged scale of FTIR spectrum in the oxidation region of EPR-Com insulation after 3 years and 9 months at 90°C

In Figure 45 and Figure 46 , the ATR spectrum of an aged EPR-Com specimen after

one month at 120 °C along with the corresponding enlarged scale of FTIR spectrum in

the oxidation region are shown. Comparing with the spectrum of an un-aged specimen

in Figure 33, the peak at 3356 cm^{-1} is disappeared while the wide peak at 1672 cm^{-1}

shifted to a small peak at 1714 cm^{-1}. It is also observed that the peak intensity at 2850

cm^{-1} and 2916 cm^{-1} are almost the same. Therefore, there is not that much of change in

the microstructure after one month in 120°C.

Figure 45- FTIR spectrum of EPR-Com insulation after one month at 120°C

Figure 46- enlarged scale of FTIR spectrum in the oxidation region of EPR-Com insulation after one month at 120°C

Figure 47- FTIR spectrum of EPR-Com insulation after two months at 120°C

74

Figure 48- enlarged scale of FTIR spectrum in the oxidation region of EPR-Com insulation after two months at 120°C

In Figure 47 and Figure 48, the ATR spectrum of an aged EPR-Com specimen after two months at 120 °C is shown. Comparing with the spectrum of the aged specimen in Figure 45, the peak intensity at 2850 cm^{-1} and 2916 cm^{-1} grew more than two times.

The rise of peak intensity at 2850 cm^{-1} and 2916 cm^{-1} is attributed to the progression

of crosslinking or crystallinity region. [76], [34]

On the other hand, the drop in the oxidation group peaks at 1714 cm^{-1} and 3500 cm^{-1}

area shows that chain scission reactions were mostly due to the thermal stressor than

thermo-oxidative reactions.

Figure 49- FTIR spectrum of EPR-Com insulation after three months at 120°C

Figure 50- enlarged scale of FTIR spectrum in the oxidation region of EPR-Com insulation after three months at 120°C

In Figure 49 and Figure 50, the ATR spectrum of an aged EPR-Com specimen after three months at 120 °C along with the corresponding enlarged scale of FTIR spectrum in the oxidation region are shown. It is observed that the carbonyl peak at 1714 cm^{-1} grows larger and the peak intensity at 2850 cm^{-1} and 2916 cm^{-1} drops to half of its value in Figure 47. This observation shows the progression of oxidation reactions which resulted in scission reactions which resulted in the intensity drop of peaks at 2850 cm^{-1} and 2916 cm^{-1}.
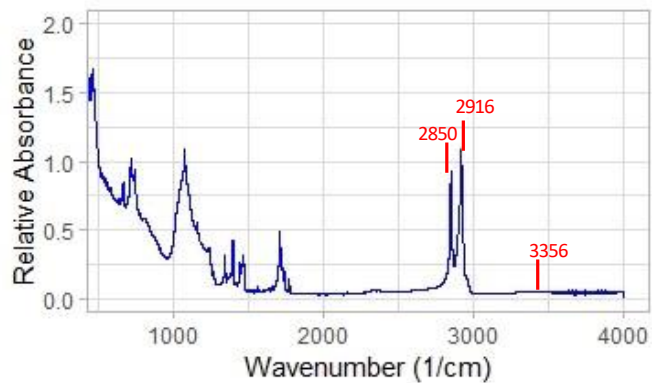
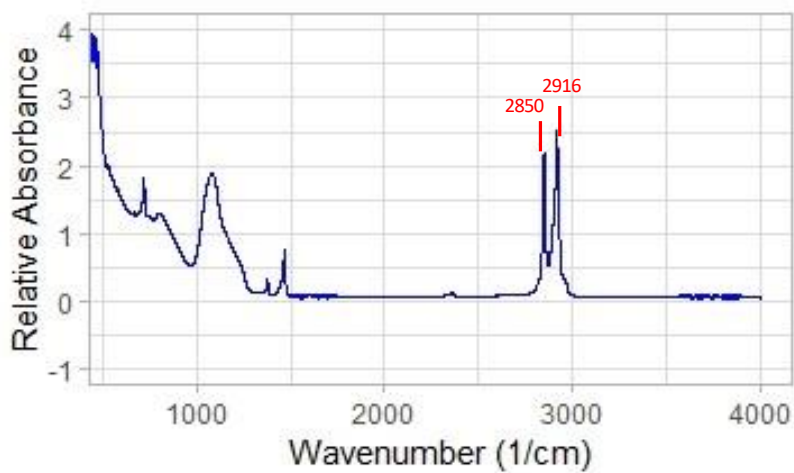*Figure 51-FTIR spectrum of EPR-Com insulation after four months at 120°C*

Figure 52- enlarged scale of FTIR spectrum in the oxidation region of EPR-Com insulation after four months at 120°C

In Figure 51 and Figure 52, the ATR spectrum of an aged EPR-Com specimen after four months at 120 °C along with the corresponding enlarged scale of FTIR spectrum in the oxidation region are shown. It is observed that the carbonyl peak at 1714 cm^{-1}

grows smaller and the peak intensity at 2850 cm^{-1} and 2916 cm^{-1} increases to more than

double times of its value in Figure 49. This observation shows that the scission

reactions are mostly due to thermal stressors and not thermo-oxidative reactions.
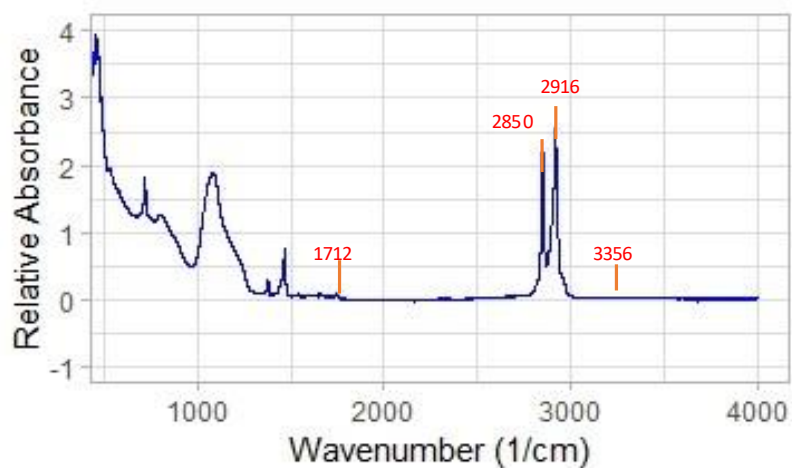

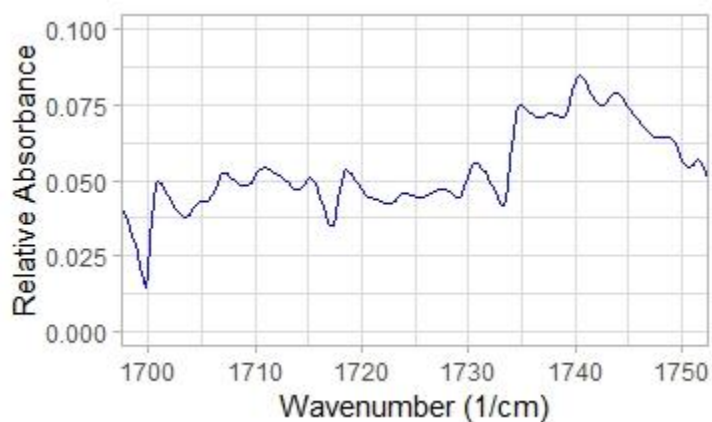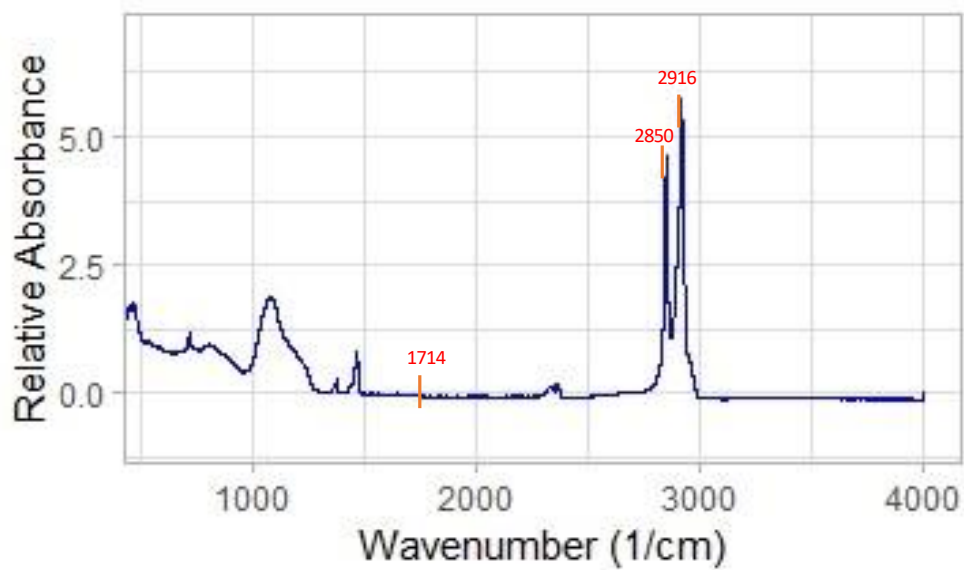*Figure 53- FTIR spectrum of EPR-Com insulation after five months at 120°C*

Figure 54- enlarged scale of FTIR spectrum in the oxidation region of EPR-Com insulation after five months at 120°C

79

In Figure 53 and Figure 54, the ATR spectrum of an aged EPR-Com specimen after five months at 120 °C along with the corresponding enlarged scale of FTIR spectrum in the oxidation region are shown. It is observed that the carbonyl peak at 1714 cm^{-1} grows larger and hydroxy wide peak at 3480 cm^{-1} emerges. The peak intensity at 2850 cm^{-1} and 2916 cm^{-1} increases to the highest value. This observation shows that the progression of oxidation reactions while the progression of crosslinking reactions or crystalline area dominate the chain scission reaction caused by oxidation reactions which results to the peak intensity increase at 2850 cm^{-1} and 2916 cm^{-1}. [77], [70]

4.2.3.2 FTIR-ATR results on EPR-NU

In this section the results of FTIR-ATR on EPR-NU cables aged at 90°C and 120 °C will be discussed.

In Figure 55 and Figure 56, the ATR spectrum of an un-aged EPR-NU specimen along with the corresponding enlarged scale of FTIR spectrum in the oxidation region are shown.

There a small peak 1714 cm^{-1} assigned to carbonyl as well as the peaks at 2850 cm^{-1} and 2916 cm^{-1} assigned to the vibration of -CH$_2$- groups. [72], [73], [74]

It is interesting to note that the un-aged specimen contains oxidized groups which are most likely introduced to the insulation through the manufacturing process. [75]
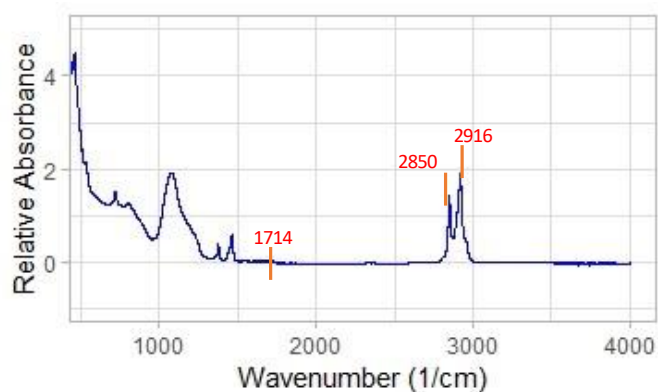
Figure 55- FTIR spectrum of un-aged EPR-NU
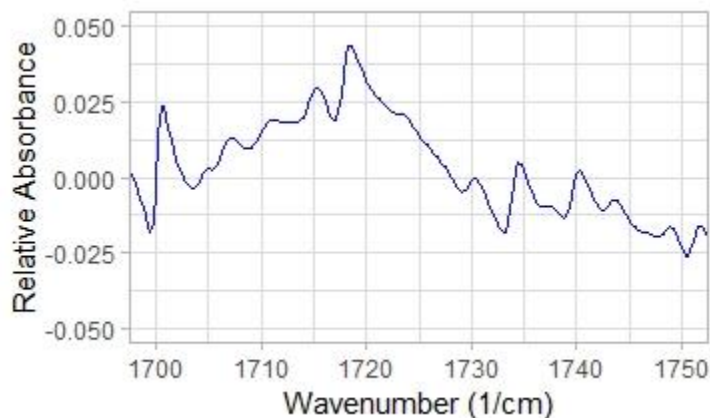
Figure 56- enlarged scale of FTIR spectrum in the oxidation region of un-aged EPR-NU

In Figure 57 and Figure 58, the ATR spectrum of an aged EPR-NU specimen after one months at 90 °C along with the corresponding enlarged scale of FTIR spectrum in the oxidation region are shown. The small peak at 1714 cm^{-1} grew larger while the peaks at 2850 cm^{-1} and 2916 cm^{-1} are in the same intensity. This evidence shows that chain scission reactions caused by oxidation reactions were in competence with the

progression of crosslinking reactions or crystallinity area which kept the intensity of

the peaks at 2850 cm^{-1} and 2916 cm^{-1} the same.

Figure 57- FTIR spectrum of EPR-NU insulation after one month at 90°C

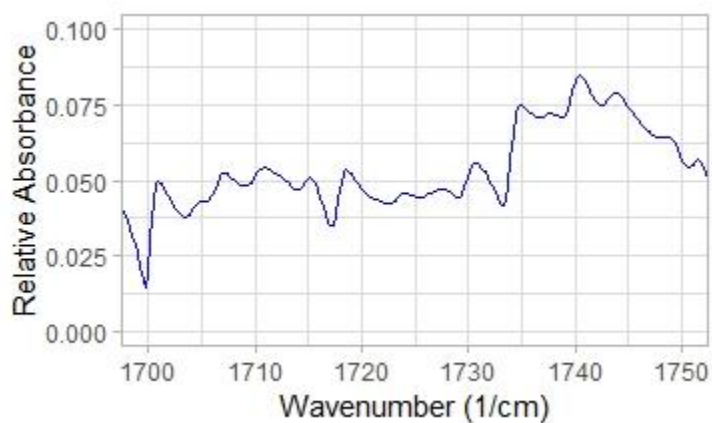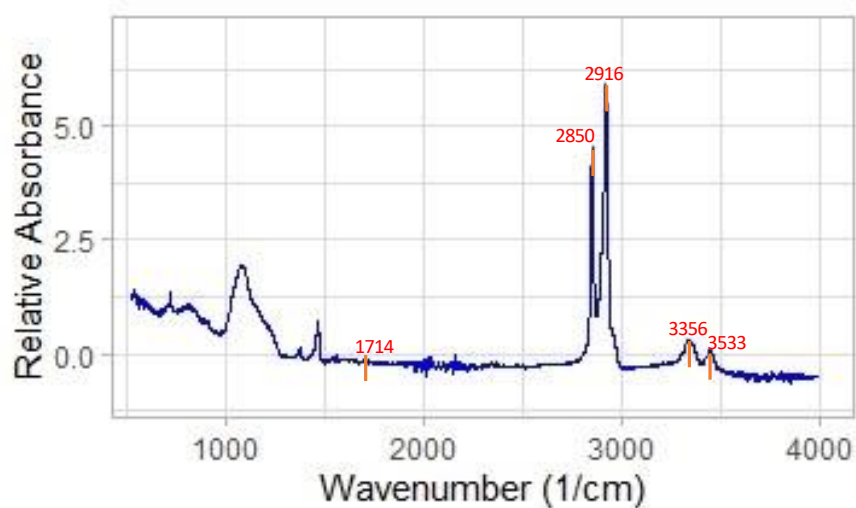*Figure 58- enlarged scale of FTIR spectrum in the oxidation region of EPR-NU insulation after one month at 90°C*

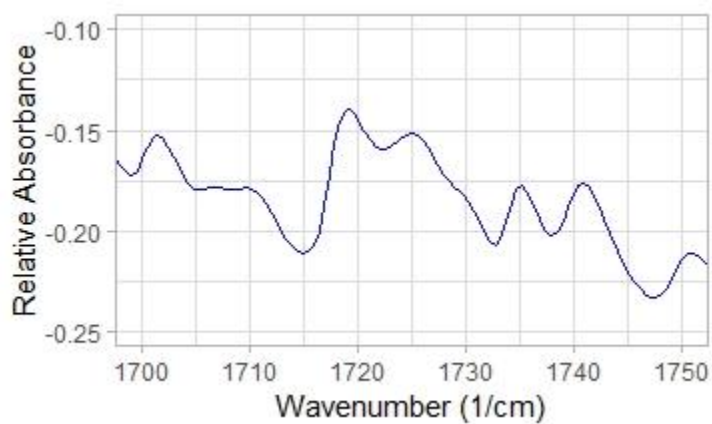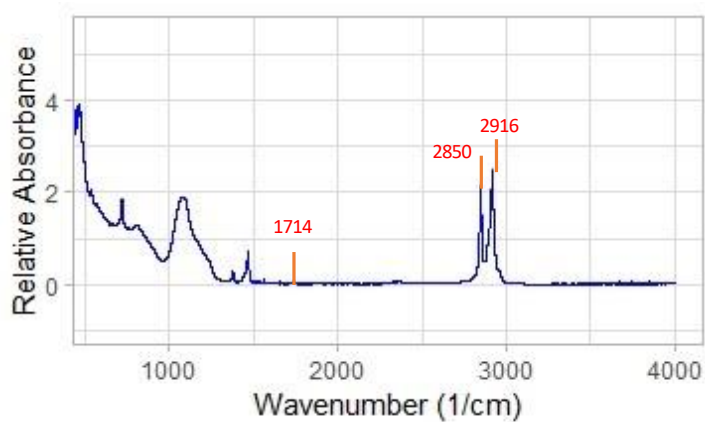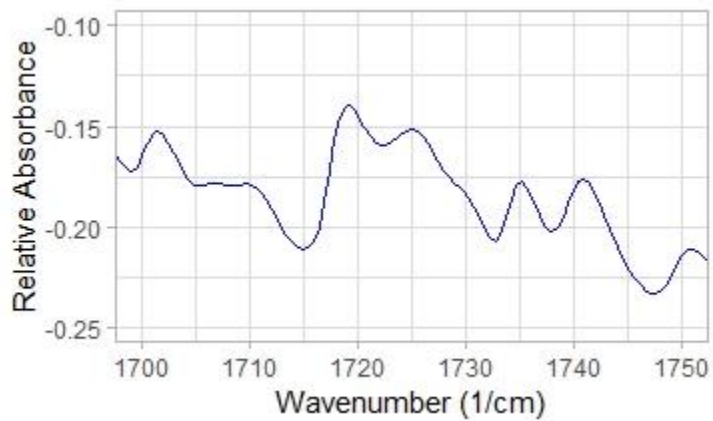*Figure 59- FTIR spectrum of EPR-NU insulation after two months at 90°C*
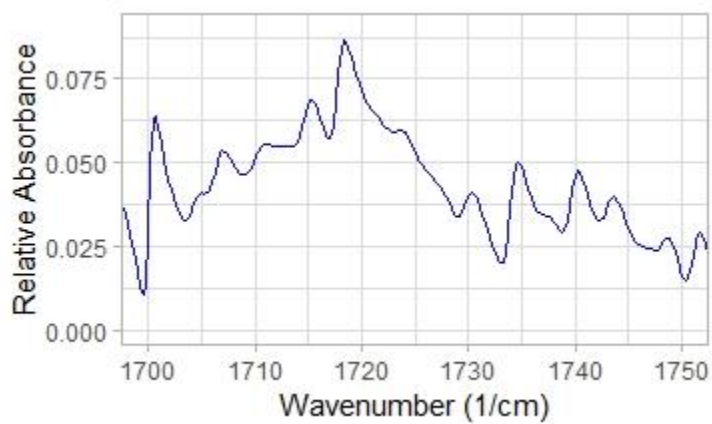
Figure 60- enlarged scale of FTIR spectrum in the oxidation region of EPR-NU insulation after two months at 90°C

Figure 61- FTIR spectrum of EPR-NU insulation after three months at 90°C

Figure 62- enlarged scale of FTIR spectrum in the oxidation region of EPR-NU insulation after three months at 90°C

Figure 59 to Figure 62 show the ATR spectra of aged EPR-NU specimens after two to three months along with the corresponding enlarged scale of FTIR spectrum in the oxidation region respectively. There are not that much of difference in the characterizing peak intensity from the first month of aging to the third month which can constitute the induction time interval.
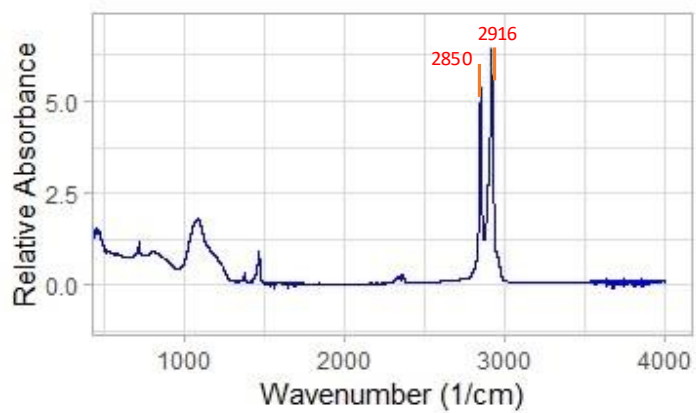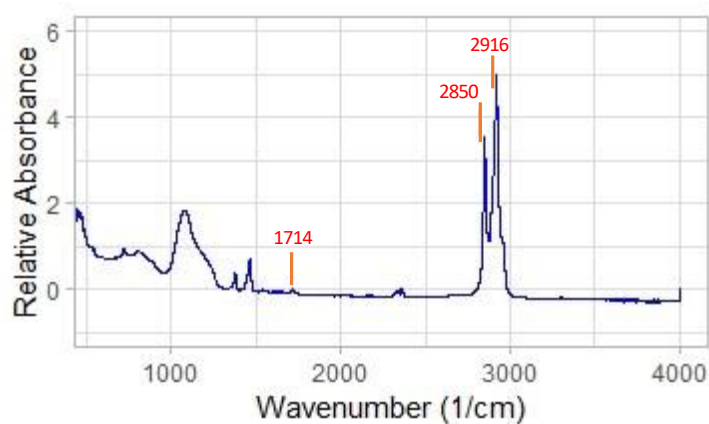
Figure 63- FTIR spectrum of EPR-NU insulation after four months at 90°C

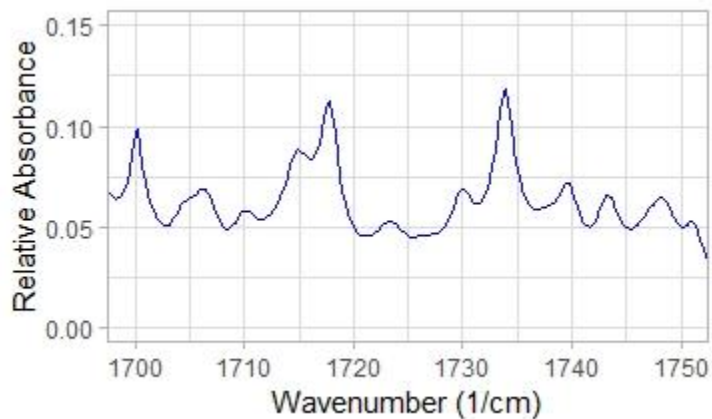*Figure 64- enlarged scale of FTIR spectrum in the oxidation region of EPR-NU insulation after four months at 90°C*

Figure 63 and Figure 64 show ATR spectrum of EPR-NU insulation after four months at 90°C along with the corresponding enlarged scale of FTIR spectrum in the oxidation region . It is seen that the carbonyl peak at 1714 cm^{-1} grew larger and the peaks at 2850 cm^{-1} and 2916 cm^{-1} also grew more than two times in their intensity. This evidence shows that the progression of crosslinking reactions or crystallinity area dominated the

chain scission reactions caused by oxidation reactions which grew the intensity of the
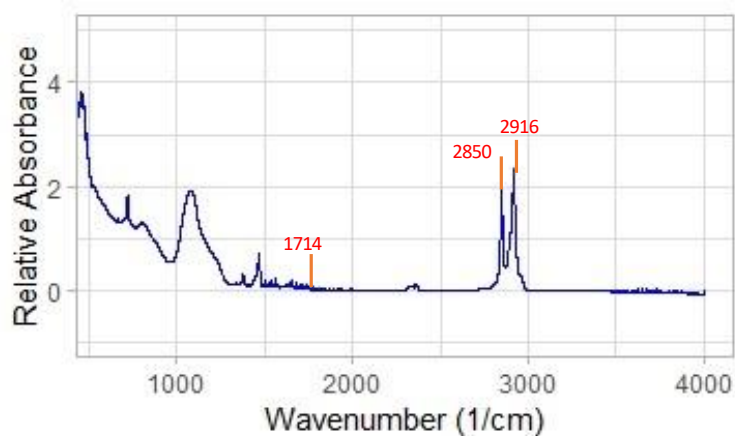
peaks at 2850 cm^{-1} and 2916 cm^{-1}.
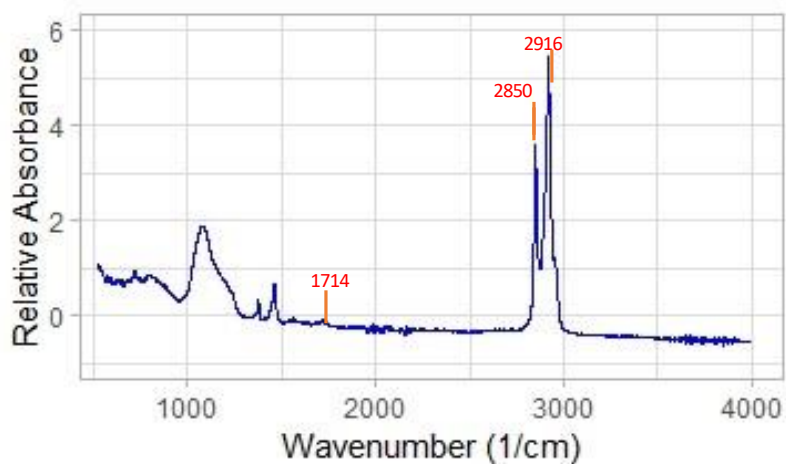
Figure 65- FTIR spectrum of EPR-NU insulation after 3 years and 9 months at 90°C
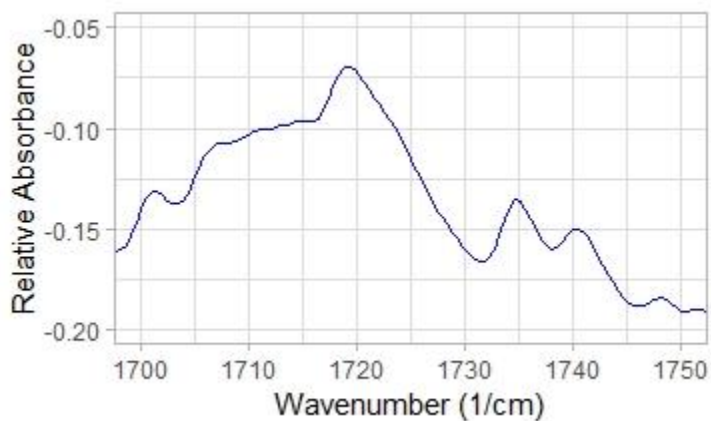
Figure 66- enlarged scale of FTIR spectrum in the oxidation region of EPR-NU insulation after 3 years and 9 months at 90°C

Figure 65 and Figure 66 show ATR spectrum of EPR-NU insulation after 3 years and 9 months at 90°C along with the corresponding enlarged scale of FTIR spectrum in the oxidation region. It is seen that the carbonyl peak at 1714 cm^{-1} grew larger in intensity comparing with the spectrum in Figure 63 while the peaks at 2850 cm^{-1} and 2916 cm^{-1} are in the same intensity. This evidence shows that chain scission reactions caused by oxidation reactions were in competence with the progression of crosslinking reactions or crystallinity area which kept the intensity of the peaks at 2850 cm^{-1} and 2916 cm^{-1} the same. [77], [70]
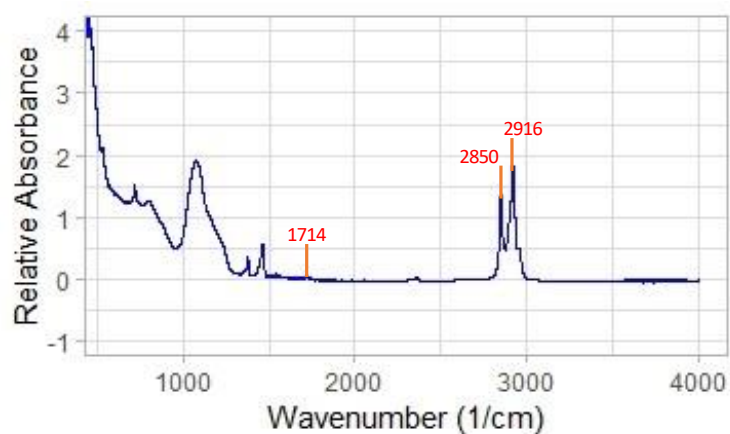
Figure 67- FTIR spectrum of EPR-NU insulation after one month at 120°C
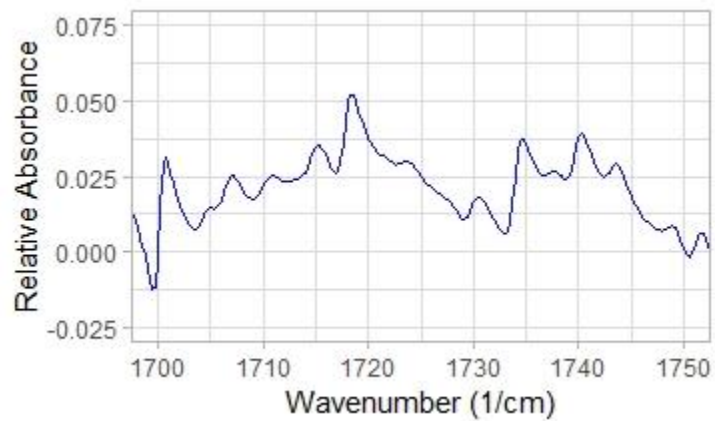
Figure 68- enlarged scale of FTIR spectrum in the oxidation region of EPR-NU insulation after one month at 120°C
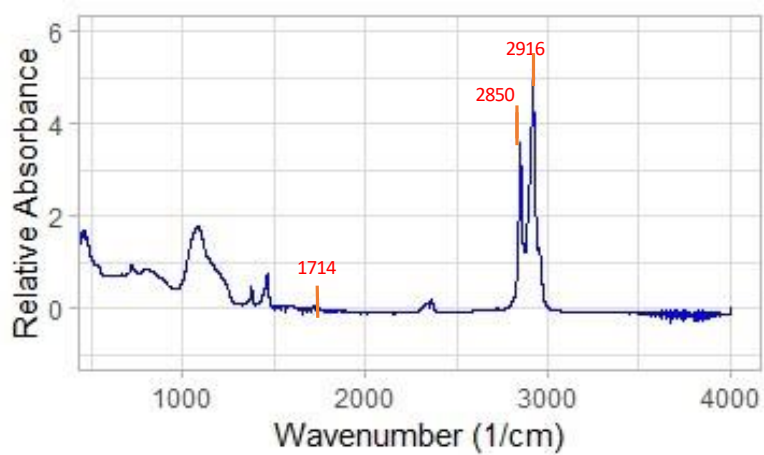
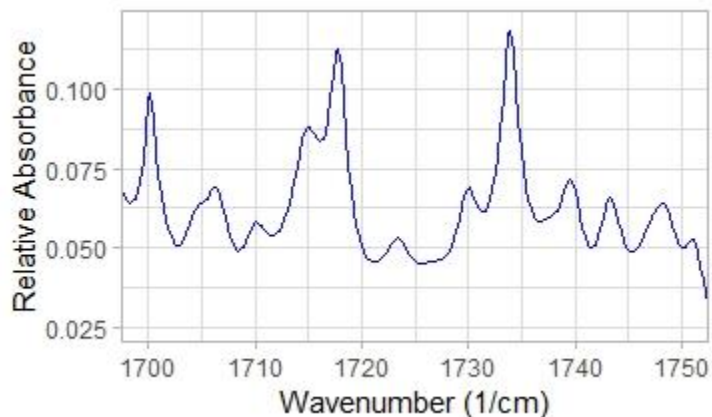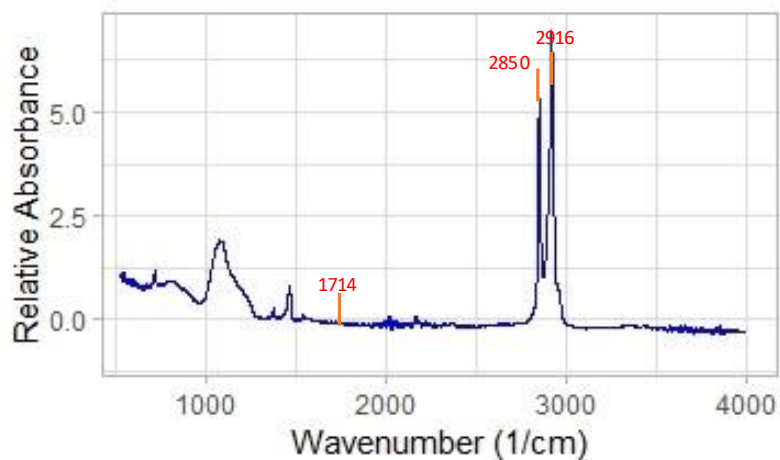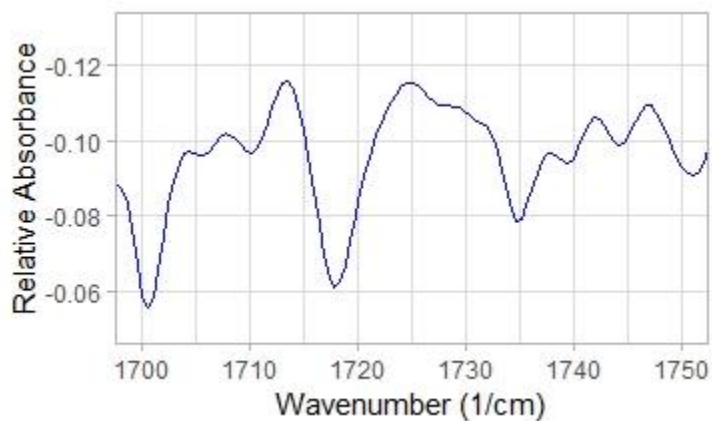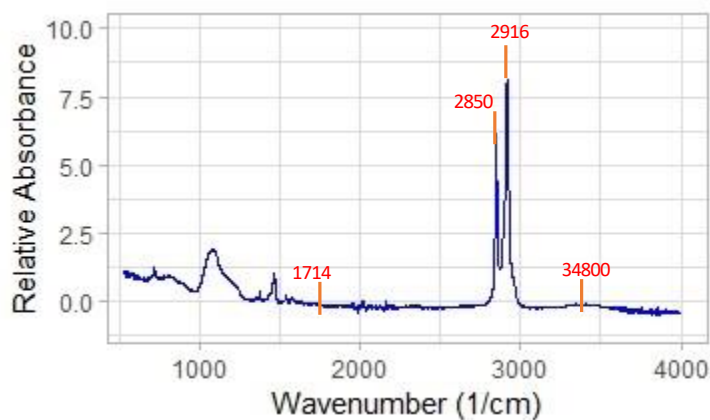*Figure 69- FTIR spectrum of EPR-NU insulation after two months at 120°C*
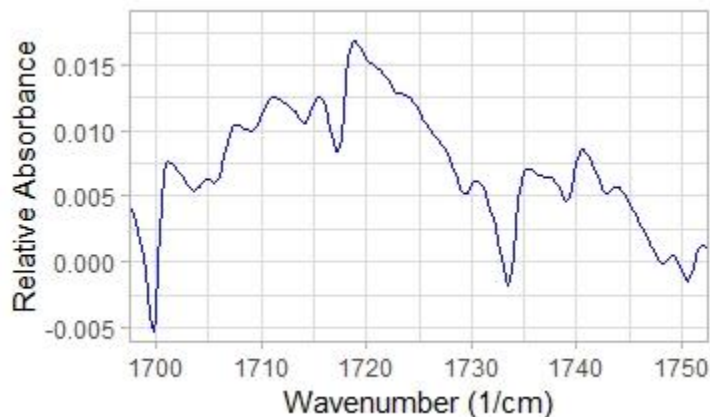
Figure 70- enlarged scale of FTIR spectrum in the oxidation region of EPR-NU insulation after two months at 120°C

Figure 67 and Figure 68 show the ATR spectrum of EPR-NU insulation after one month at 120°C. The characterizing peaks 2850 cm^{-1} and 2916 cm^{-1} did not change compared to the ATR spectrum of the un-aged EPR-NU specimen in Figure 55. However, the at 1714 cm^{-1} grew slightly larger which evidence the progression of chain scission reactions due to oxidation reactions. The same intensity of the 2850 cm^{-1} and 2916 cm^{-1} in Figure 55 and Figure 67 shows that crosslinking reactions or the progression of crystallinity areas were competing with chain scission reactions resulting in keeping the intensity of these peaks the same.

Figure 69 and Figure 70 show the FTIR-ATR spectrum of EPR-NU insulation after two months at 120°C along with the corresponding enlarged scale of FTIR spectrum in the oxidation region. [72]

It is observed that the carbonyl peak at 1714 cm^{-1} grew larger and the peaks at 2850 cm^{-1} and 2916 cm^{-1} also grew more than two times in their intensity. This evidence shows that the progression of crosslinking reactions or crystallinity area dominated the

chain scission reactions caused by oxidation reactions which increased the intensity of the peaks at 2850 cm^{-1} and 2916 cm^{-1}.
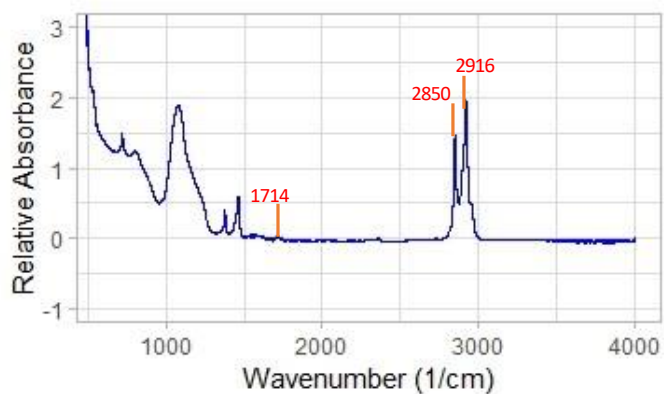
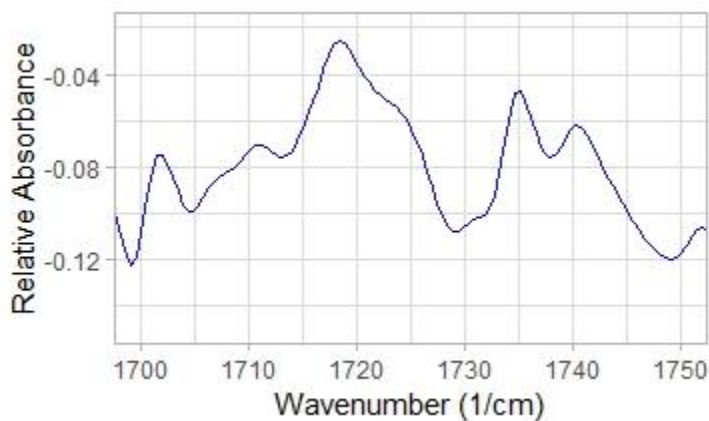*Figure 71- FTIR spectrum of EPR-NU insulation after three months at 120°C*
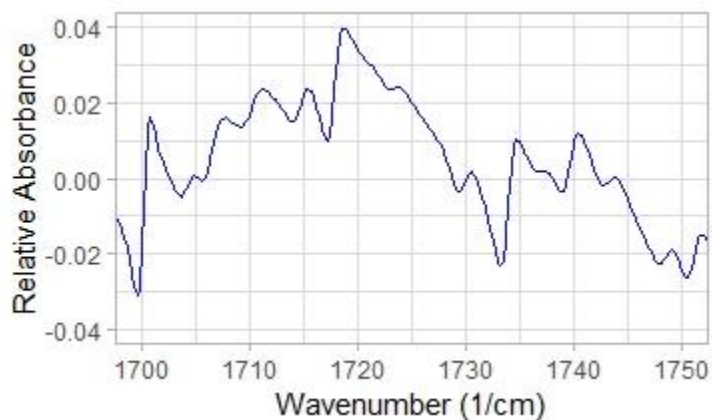
Figure 72- enlarged scale of FTIR spectrum in the oxidation region of EPR-NU insulation after three months at 120°C

Figure 71 and Figure 72 show the FTIR-ATR spectrum of EPR-NU insulation after three months at 120°C along with the corresponding enlarged scale of FTIR spectrum in the oxidation region.

It is observed that the carbonyl peak at 1714 cm^{-1} grew larger and the peaks at 2850 cm^{-1} and 2916 cm^{-1} decreased to half of their intensity in Figure 69. This evidence shows that the progression of chain scission reactions caused by oxidation reactions dominated crosslinking reactions or crystallinity area which decreased the intensity of the peaks at 2850 cm^{-1} and 2916 cm^{-1}.
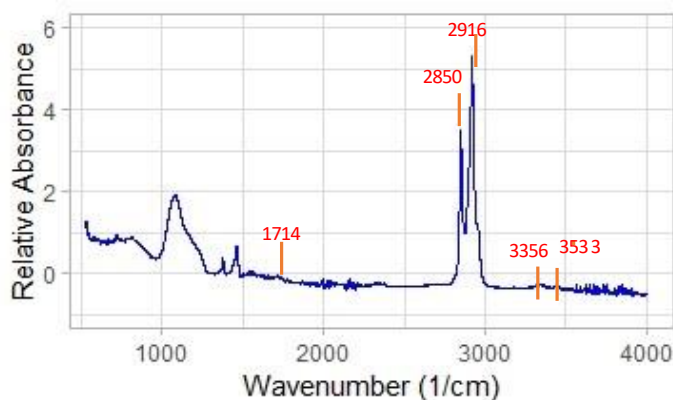
Figure 73- FTIR spectrum of EPR-NU insulation after four months at 120°C
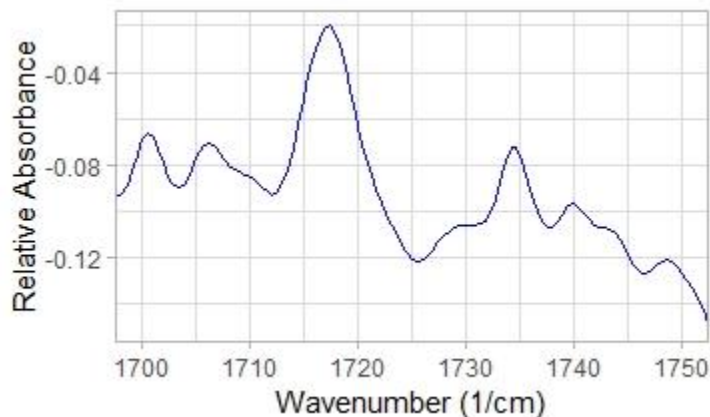
Figure 74- enlarged scale of FTIR spectrum in the oxidation region of EPR-NU insulation after four months at 120°C

Figure 73 and Figure 74 show the FTIR-ATR spectrum of EPR-NU insulation after four months at 120°C along with the corresponding enlarged scale of FTIR spectrum in the oxidation region.

It is observed that the carbonyl peak at 1714 cm^{-1} grew larger and hydroxyl peaks at 3356 cm^{-1} and 3533 cm^{-1} emerge. The peaks at 2850 cm^{-1} and 2916 cm^{-1} also grew more than two times in their intensity.

This evidence shows that the progression of crosslinking reactions or crystallinity area dominated the chain scission reactions caused by oxidation reactions which increased the intensity of the peaks at 2850 cm^{-1} and 2916 cm^{-1}. [70], [72]
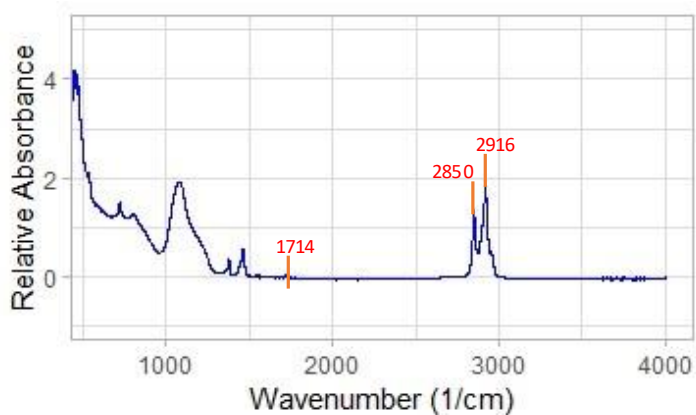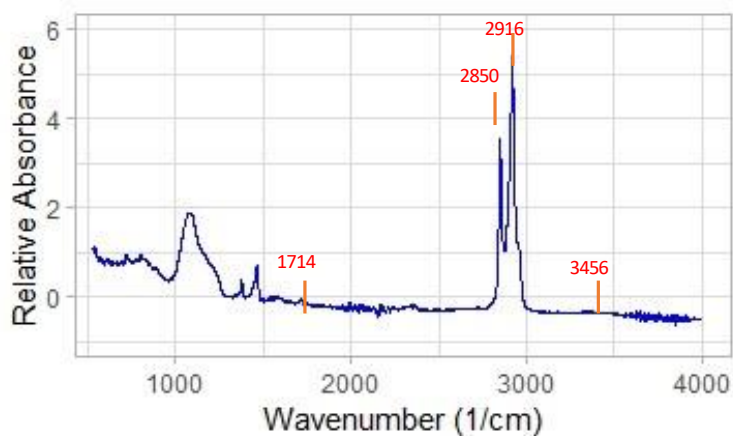
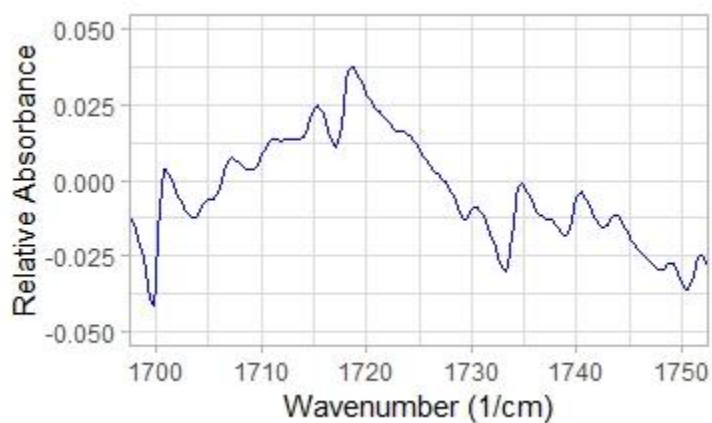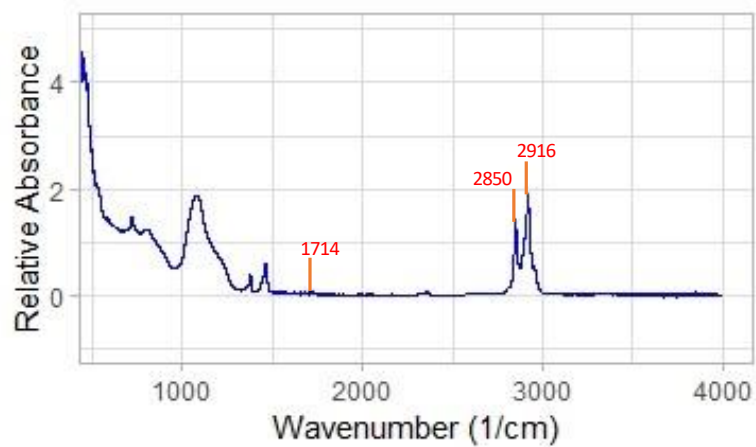*Figure 75- FTIR spectrum of EPR-NU insulation after five months at 120°C*
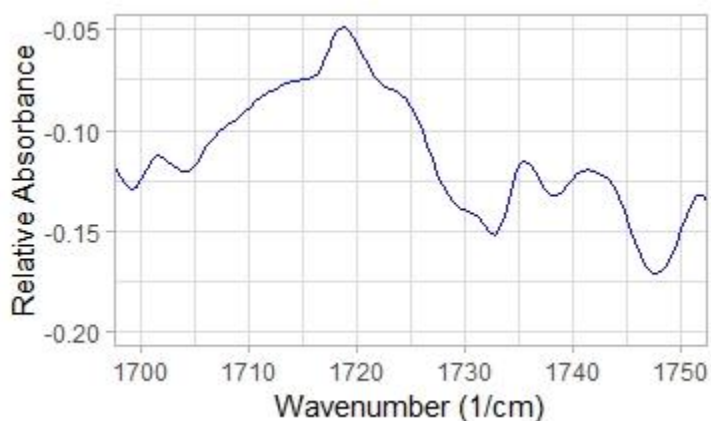
Figure 76- enlarged scale of FTIR spectrum in the oxidation region of EPR-NU insulation after five months at 120°C

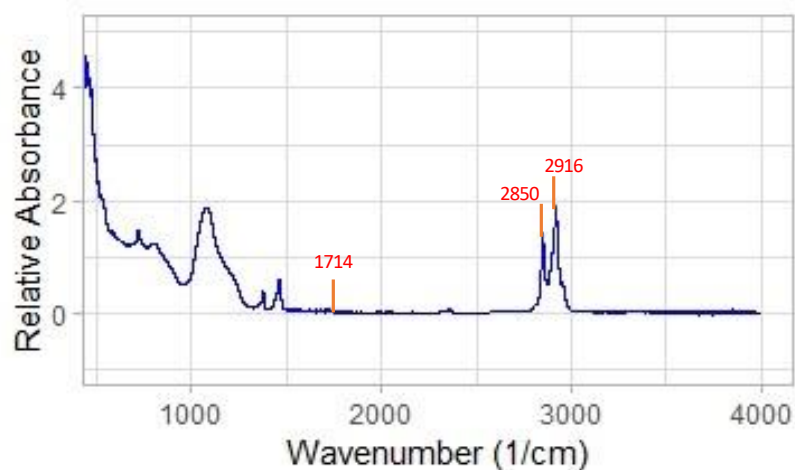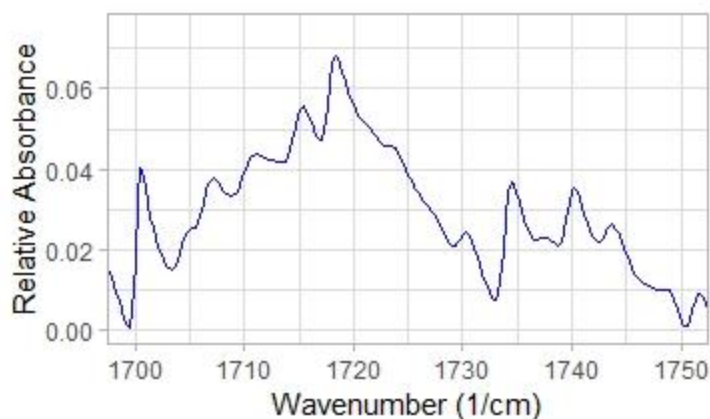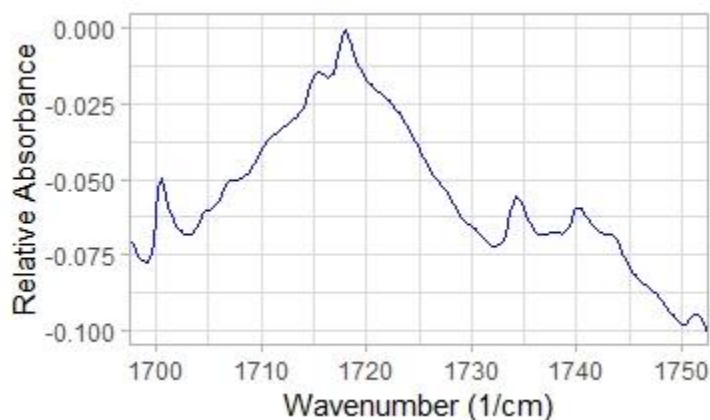Figure 75 and Figure 76 shows the FTIR-ATR spectrum of EPR-NU insulation after five months at 120°C along with the corresponding enlarged scale of FTIR spectrum in the oxidation region. The characterizing peaks at 1714 cm^{-1}, hydroxyl peaks at 3456

cm^{-1} as well as the peaks at 2850 cm^{-1} and 2916 cm^{-1} did not change in their intensity compared to the spectrum in Figure 73.

As it was discussed in Figure 73, this evidence shows that the progression of crosslinking reactions or crystallinity area dominated the chain scission reactions caused by oxidation reactions which increased the intensity of the peaks at 2850 cm^{-1} and 2916 cm^{-1}. [72]

4.2.4 ESR results

In this section, ESR spectroscopy results on EPR cable insulations will be explained. Over the 50 years of the advent of ESR spectroscopy, a very limited number of research have been done an ESR spectroscopy analysis of cable insulations. In fact, these investigations briefly mentioned the existence of peroxyl radicals associated with the ESR spectra and did not employed ESR spectra changes at different aging conditions for the insulation aging investigation. [78], [79], [80] and [81]

To our knowledge, this is the first time, a thorough investigation on ESR spectra analysis on aged EPR cable insulations has been done. It should be noted that the ESR spectra were recorded after four years of aging of EPR cable insulations, with an exception for that recorded on 45 months of aging EPR cable insulations after three months, which evidences the stability of the studied free radicals.[82]

4.2.4.1 ESR results on EPR-Com

As it was explained in 2.3.1.1, in oxidation reactions, $RO_2^{\cdot}$ undergo bimolecular reactions to produce the intermediate tetroxide.

The intermediates ROOOOR undergo various decomposition processes leading to degradation of the polymers. Other proposed R1OOOOR2 decay mechanisms are suggested which involve the production of the aldehyde and ketone. [28]

The ESR results on EPR-Com specimens aged for 1 month, 4 months and 45 months at 90 °C are illustrated in Figure 77.
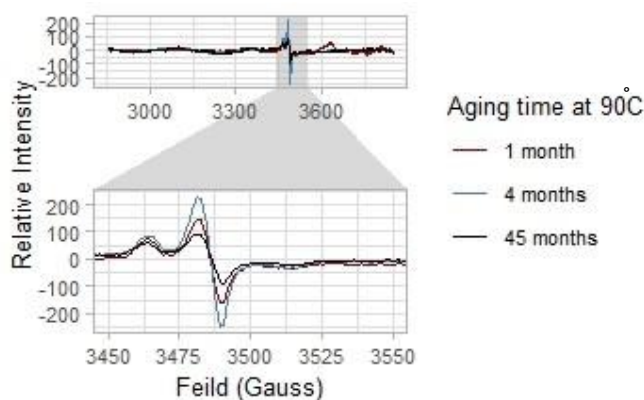
Figure 77- The ESR spectra on EPR-Com specimens aged at 90 °C for 1 month, 4 months and 45 months.

As it is seen in Figure 77, all the ESR spectra are similarly asymmetric which represents the existence of the polyenyl C-centered radicals and small contribution from peroxyl radicals. [82] and [83]

As it is shown, the peak amplitude increases from one month to four months of aging at 90 °C. However, it goes down after 45 months of aging at 90 °C. It is attributed to the stable polyenyl free radicals and peroxyl radicals. During the aging processes, the captured alky radicals in the crystalline structures convert to polyenyl. Due to their

highly conjugated structure, their reactions with oxygen are very small. So, it is expected to see both are present in the aged samples. It should also be mentioned that the concentration from oxidation reactions over the first four months of aging which are consumed in the crosslinking reactions after 45 months of aging. [82]

The ESR results on EPR-Com specimens aged for 3 month, 4 months and 5 months at 120 °C are illustrated in Figure 78.
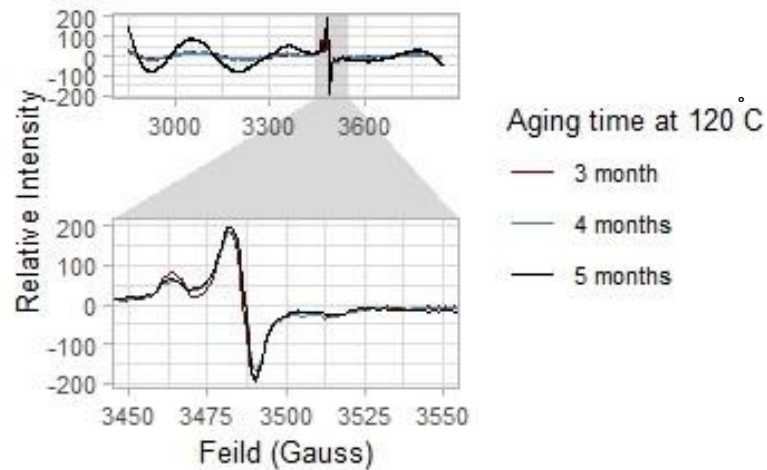
Figure 78- The ESR spectra on EPR-Com specimens aged at 120 °C for 3 months, 4 months and 5 months.

As it is shown from Figure 78, all the ESR spectra exhibit singlet and other small peak, representing the polyenyl C-centered radicals and peroxyl radicals, respectively. [82] [30]

As it is shown, the peak amplitude of the sample aged for three months in the shoulder peak is the highest with respect to that of samples aged for 4 and 5 months at 120 °C.

This is attributed to more scissions have occurred to produce C-centered radicals as well as more peroxyl radicals are also produced. The higher peroxyl radical concentration in the sample aged for 3 months which is reduced by crosslinking reactions in the samples aged for 4 and 5 months at 120 °C.

It is seen in Figure 77 and Figure 78, the main peak and shoulder peak amplitude displays changes respectively. It can be attributed to the peroxyl radical location on the backbone or side chain. [82]
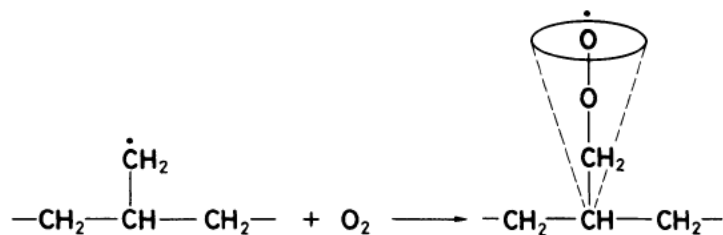
Figure 79- The schematic of peroxy radical formation on the side chain of polypropylene, obtained from schematic (7.2) of [82]
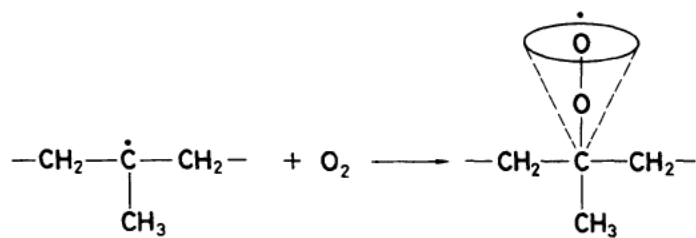
Figure 80- The schematic of peroxyl radical formation on the side chain of polypropylene, obtained from schematic (7.3) of [82]

The schematic of peroxyl radical formation on the side chain and backbone of polypropylene is seen in Figure 79and Figure 80 respectively. The presence of peroxyl radical on the side chain gives the peroxyl radical more freedom to move with respect to that on the backbone. [82]

Therefore, depending on the concentration of peroxyl radicals and the polyenyl radicals, the combined ESR signals have become more complicated.

Figure 81 shows the ESR spectra of four months aged cable insulations at 120 °C and 90 °C.

As it is seen, the peak amplitude of the aged cable insulation at 90 °C is higher than that at 120 °C which is attributed to the higher peroxy radical concentration in the former due to the progression of oxidation reactions.[64]
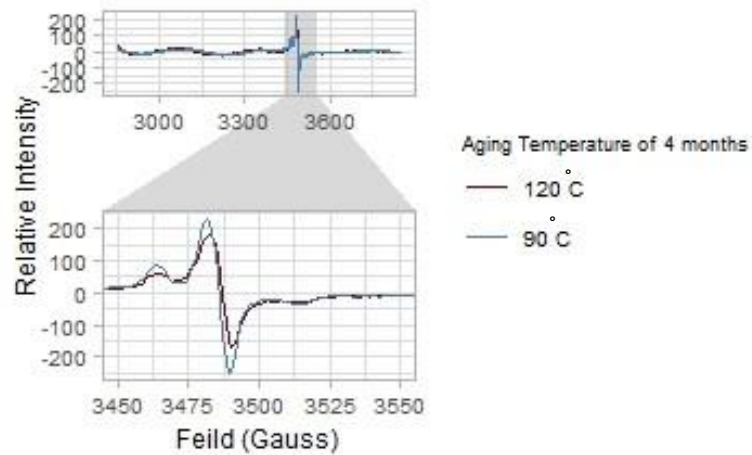
Figure 81- The ESR spectra of four months aged EPR-Com cable insulations at 120 °C and 90 °C

4.2.4.2 ESR results on EPR-NU

The ESR results on EPR-NU specimens of unaged and aged for 1 month, 4 months and 45 months at 90 °C are illustrated in Figure 82.
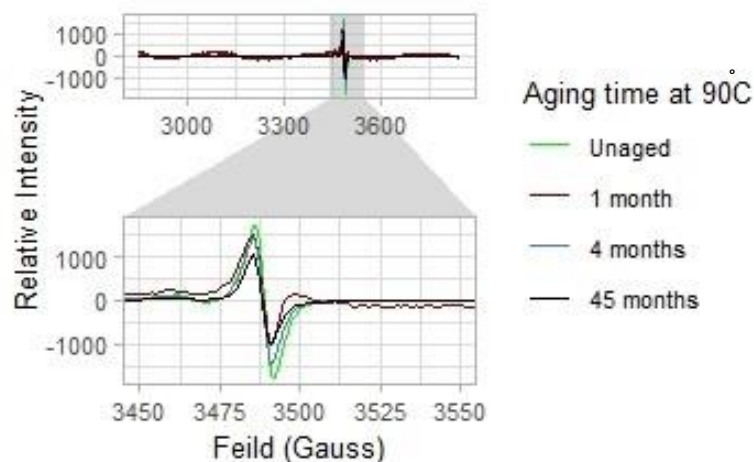
Figure 82-The ESR spectra on EPR-NU specimens of unaged and aged at 90 °C for 1 month, 4 months and 45 months.

As it is seen in Figure 82, the presence of a singlet in all the ESR spectra represents the existence of polyenyl and peroxyl radicals. [82] The highest peak amplitude belongs to the unaged specimen which is attributed to the presence of peroxyl radicals over the manufacturing process. [75] However, after one month of aging the amplitude is reduced which is due to the progression of crosslinking reactions. [28]

As it is shown, the peak amplitude of one-month-aged samples increases to that of four-month-aged samples at 90 °C.

However, it goes down after 45 months of aging at 90 °C. The decrease in the concentration may be attributed to the radical-radical reactions at higher temperatures. The ESR spectra on EPR-NU specimens of unaged and aged for 3 months, 4 months and 5 months at 120 °C are illustrated in Figure 83.
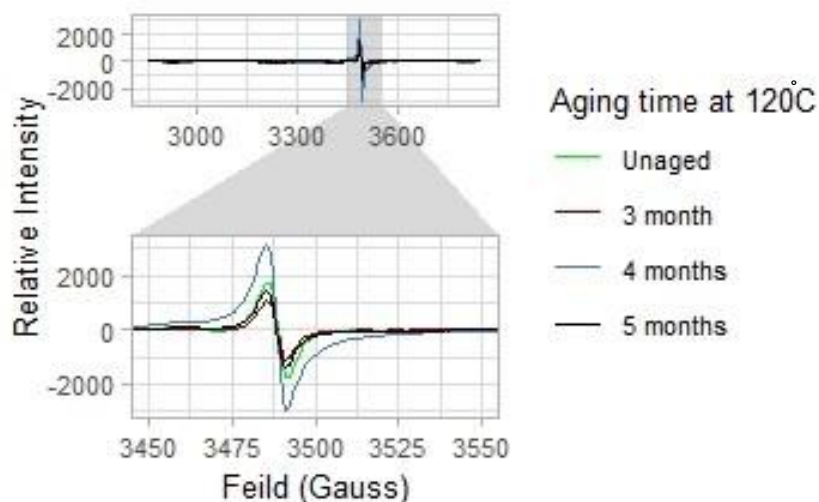
Figure 83-The ESR spectra on EPR-NU specimens of unaged and aged at 120 °C for 3 months, 4 months and 5 months.

As with previous ESR spectra, the singlet in Figure 83, shows the presence of the polyenyl and the peroxyl radicals.[82]

The peak corresponding to the unaged specimen is assigned to the C-centered radicals and their corresponding peroxyl radicals which were formed over the manufacturing process.[75] After three months of aging the amplitude is reduced which is due to the progression of crosslinking reactions. [28], [64]

A sudden remarkable increase in the peak amplitude of specimens aged for 4 months is observed which may be due to the oxidation of lower molecular weight species formed by the fragmentation of polymeric chains after four months of aging at 120 °C. [28]

However, the reduction of the peak amplitude after five months is observed which is due to the dominance of crosslinking reactions.

Figure 84 shows the ESR spectra of four months aged EPR-NU cable insulations at 120 °C and 90 °C. This may be related to more scissions are taking place.

As it is seen, the peak amplitude of the aged cable insulation at 120 °C is higher than that at 90 °C which is attributed to the higher radical concentration due the oxidation induced scissions at higher temperatures and longer period, after four months of aging at 120 °C. [31]
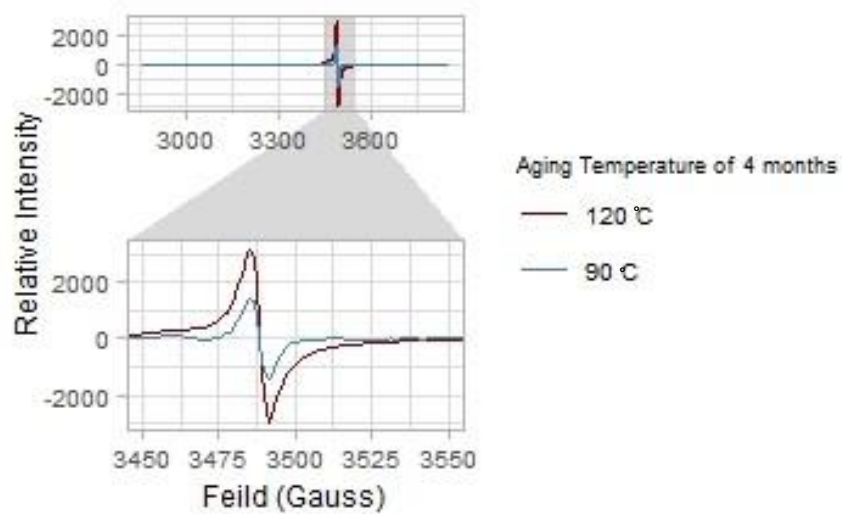
Figure 84- The ESR spectra of four months aged EPR-NU cable insulations at 120 °C and 90 °C

4.3 XLPE cables

In this section, the results of EAB measurements of XLPE-NU and XLPE-Com cables aged at 90°C, 120 and 140°C will be discussed.

4.3.1.1 EAB measurements on XLPE-Com

In this section, the results of EAB measurements of XLPE nuclear grade cables aged at 90 °C, 120 °C and 140 °C, will be discussed.

The EAB changes with time at 90 °C, 120 °C and 140 °C are shown in Figure 85, Figure 86 and Figure 87 respectively.
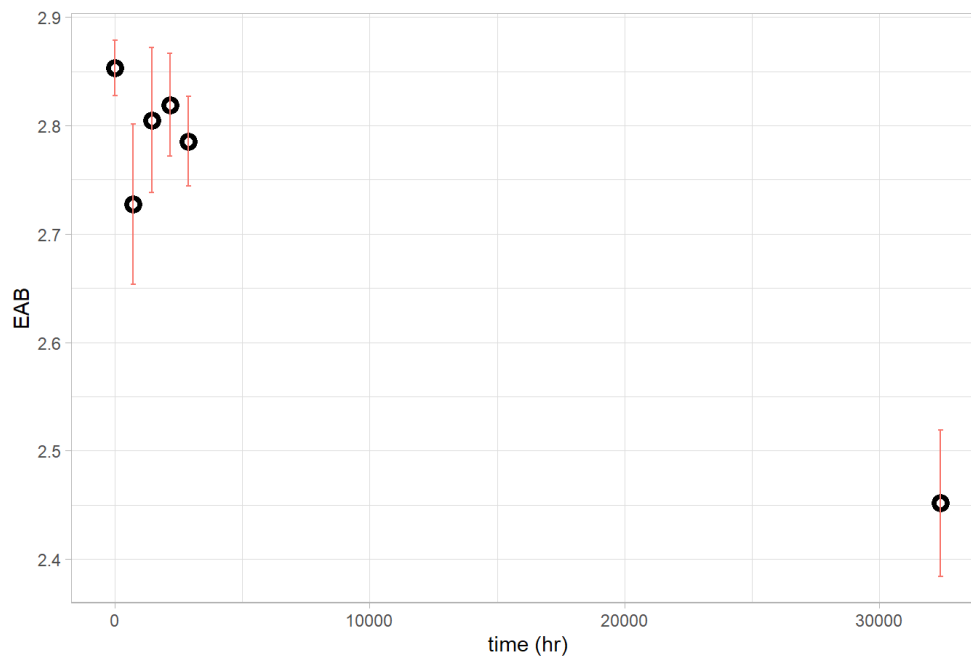
Figure 85- EAB versus time at 90°C, error bars represent SE
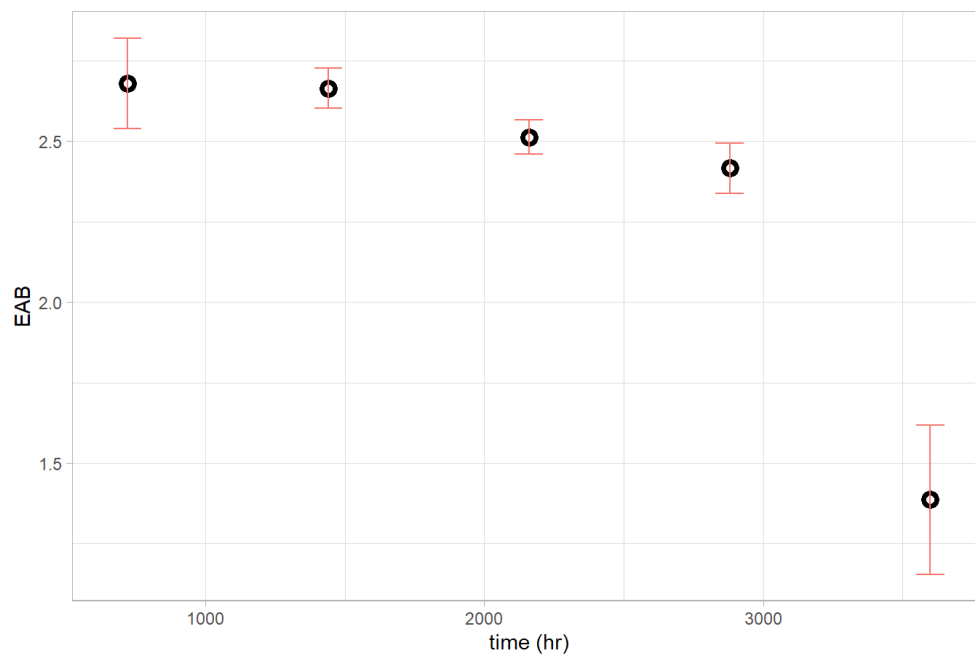
Figure 86- EAB versus time at 120 °C, error bars represent SE
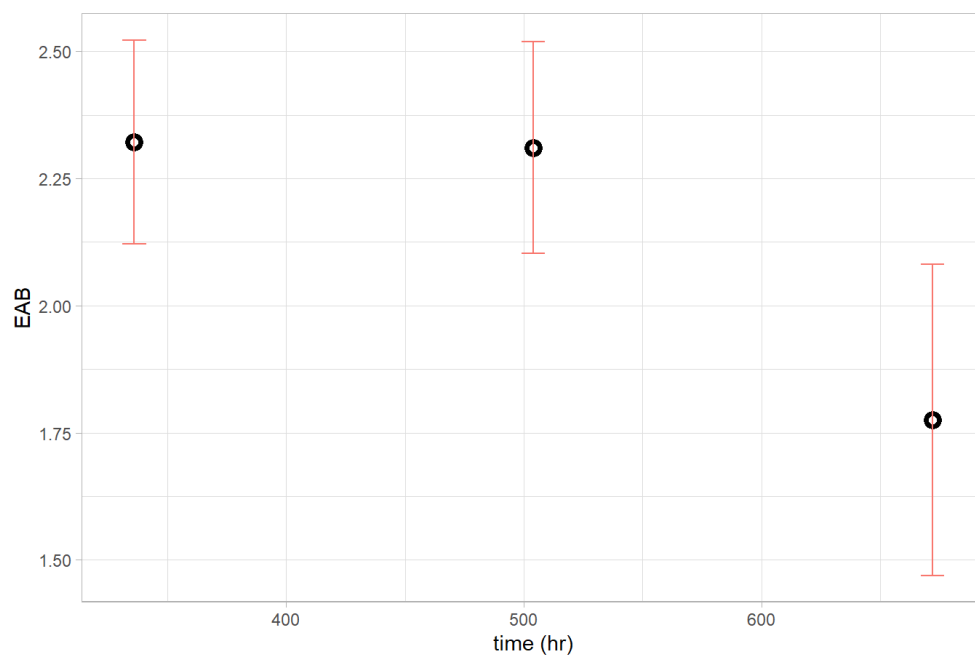
Figure 87- EAB versus time at 140 °C, error bars represent SE

Figure 88 shows the EAB values versus time (hr) of XLPE-Com cable aged at 90 °C, 120°C and 140 °C.
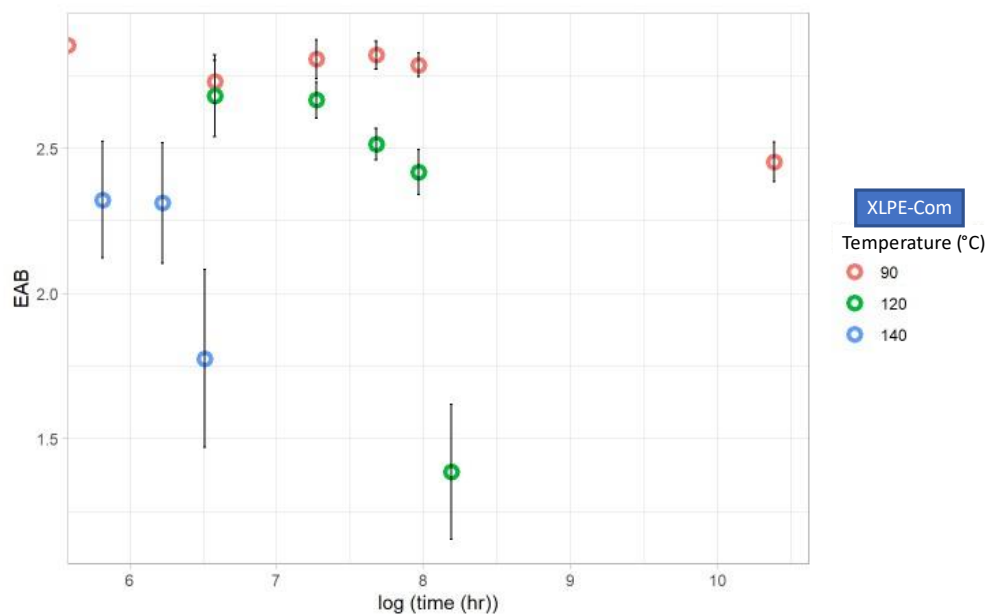
Figure 88- EAB versus time of XLPE-Com cable aged at 90 °C, 120 °C and 140°C, error bars represent SE

 Using time-temperature superposition method, the plots of relative EAB at 140 °C were shifted to the reference temperature, 120 °C. The EAB decay at 90 °C needs more time to get to the end of life. Therefore, the EAB plots at 120 °C and 140 °C were considered for superposition.

The results are shown in Figure 89. As seen, the two plots in log scale are nicely superposed at the reference temperature.
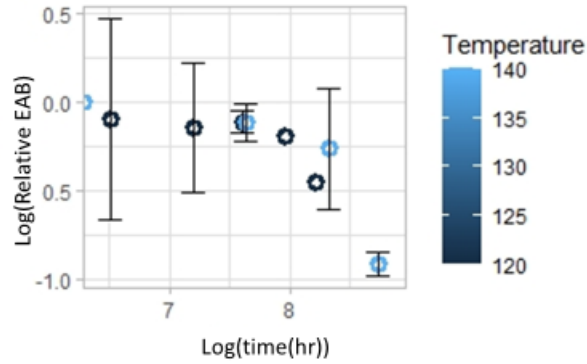
Figure 89-Time-temperature superposed EAB results at the reference temperature of 120°C, error bars represent SE

The shift factors corresponding to different temperatures are given in the Table 3.

Table 3- Shift factors for the thermally aged XLPE-Com cable

Temperature (°C)	a_T	$Ln(a_T)$
120	1	0
140	12.37	2.5

In the next step, the activation energy will be calculated from the slope of the Arrhenius plot of shift factor versus temperature, shown in Figure 90.
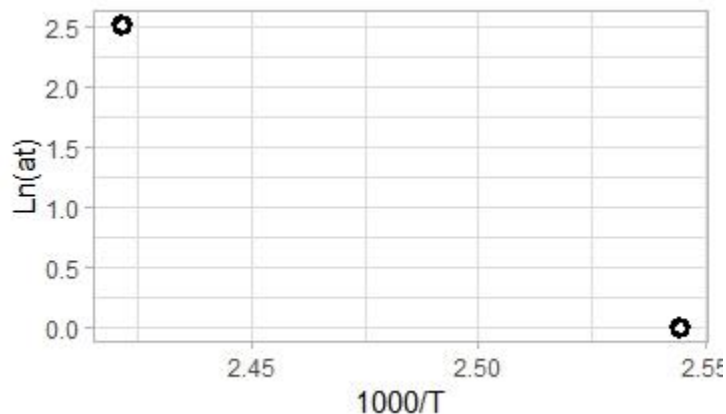
Figure 90-Shift factor versus temperature in the Arrhenius plot

Activation energy was calculated according to equation (2.14) to be 169.6 kJ/mol.

From literature review, we noticed that the range of activation energy in thermal

degradation is 60-130 kJ/mol. [59]

Therefore, the results were excluded from model.

4.3.1.2 EAB measurements on XLPE-NU

In this section, the results of EAB measurements of XLPE nuclear grade cables aged

at 90 °C, 120 °C and 140 °C, will be discussed.

The EAB changes with time at 90 °C, 120 °C and 140 °C are shown in Figure 91,

Figure 92 and Figure 93, respectively.
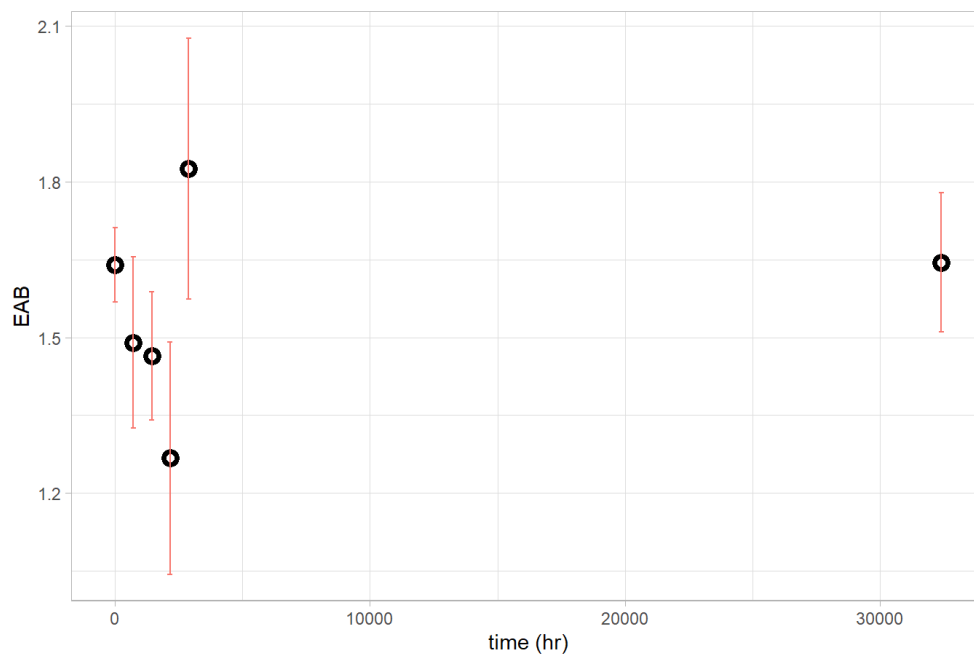
Figure 91- EAB versus time at 90 °C, error bars represent SE
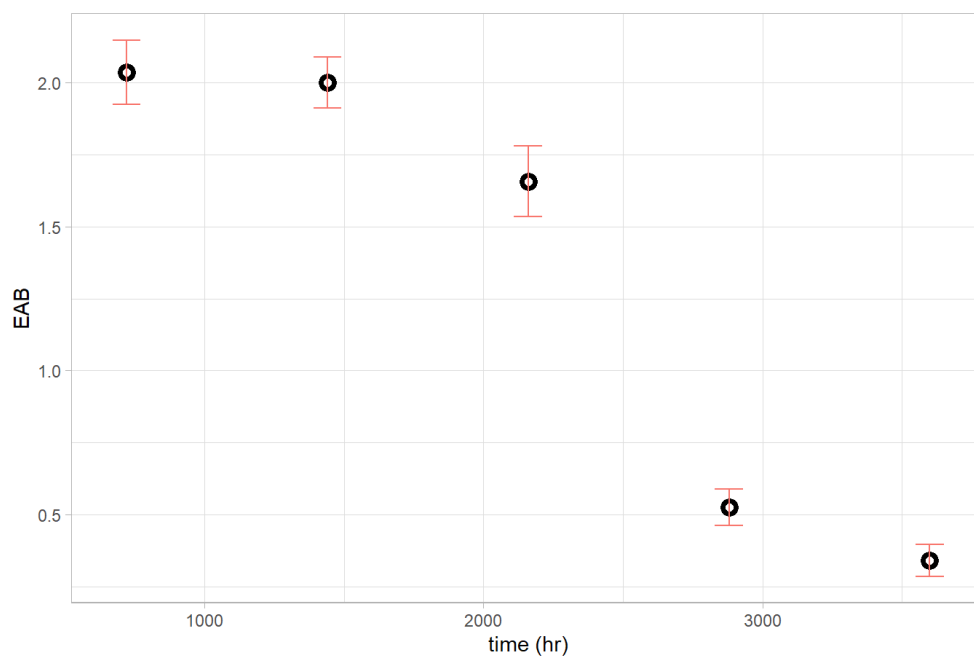
Figure 92- EAB versus time at 120 °C, error bars represent SE

107
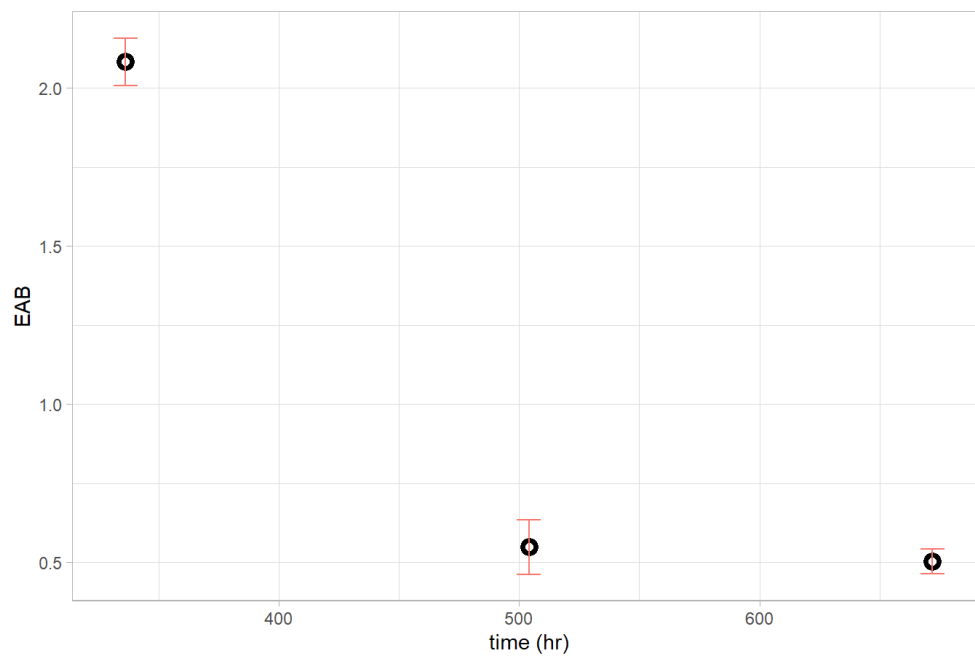
Figure 93- EAB versus time at 140 °C, error bars represent SE
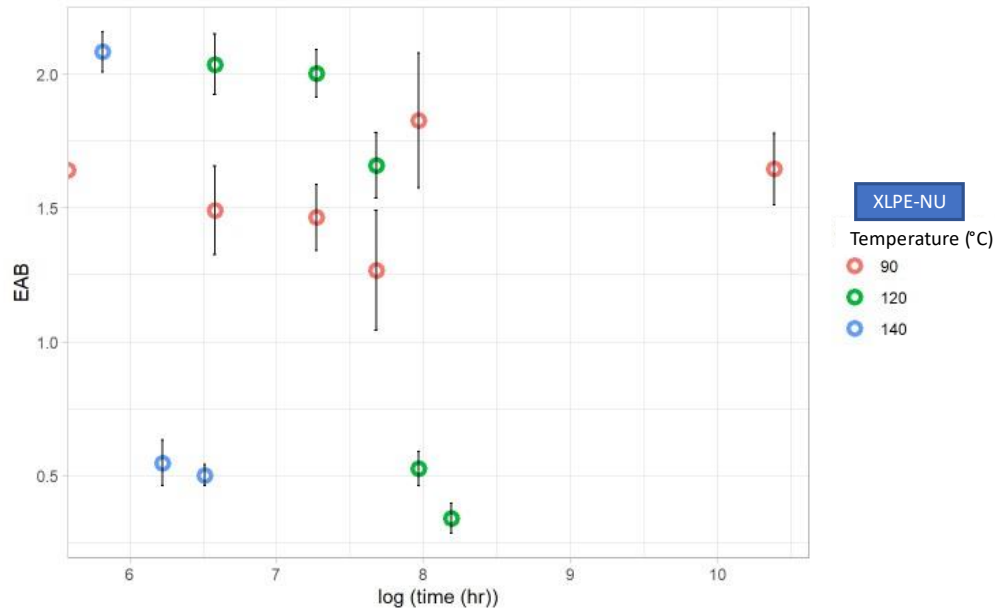
Figure 94- EAB versus time of XLPE-NU cable aged at 90 °C, 120 °C and 140°C, error bars represent SE

The EAB versus time plots at 90 °C, 120°C and 140 °C temperatures are shown in Figure 94- EAB versus time of XLPE-NU cable aged at 90 °C, 120 °C and 140°C. Because the EAB decay at 90 °C needed longer time to reach the end of life, it was eliminated from the results for superposition.

Using time-temperature superposition method, the plots of relative EAB in log scale at 140 °C were shifted to the reference temperature, 120 °C. The results are shown in Figure 95. As seen, the two plots are nicely superposed at the reference temperature.
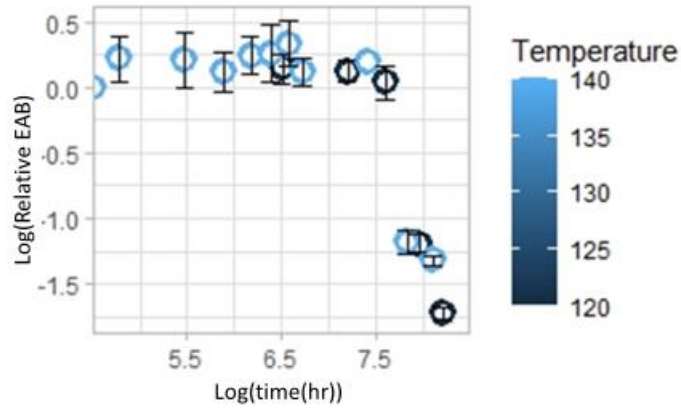
Figure 95-Time-temperature superposed EAB results at the reference temperature of 120°C, error bars represent SE

The shift factors corresponding to different temperatures are given in the Table 4.

Table 4- Shift factors for the thermally aged XLPE-NU cable

Temperature (°C)	a_T	$Ln(a_T)$
120	1	0
140	4.99	1.61

In the next step, the activation energy will be calculated from the slope of the Arrhenius plot of shift factor versus temperature, shown in Figure 96.
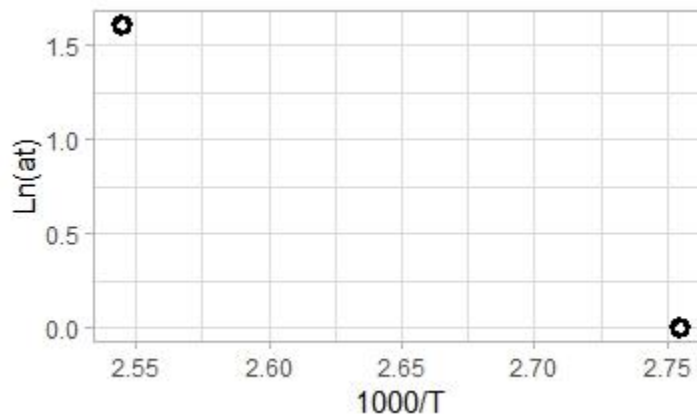
Figure 96-Shift factor versus temperature in the Arrhenius plot

Activation energy was calculated according to equation (2.14) to be 63.5 kJ/mol.

4.3.2.1 FTIR-ATR results on XLPE-Com

In this section the results of FTIR-ATR on XLPE-Com cables aged at 90°C and 120 °C will be discussed.

In Figure 97, the ATR spectrum of an un-aged XLPE-Com specimen is shown. The peaks at 1710 cm^{-1} and 3454 cm^{-1} are assigned to carbonyl and hydroxy groups respectively while the peaks at 2850 cm^{-1} and 2916 cm^{-1} are assigned to the vibration of -CH$_2$- groups. [72], [73], [74]

111
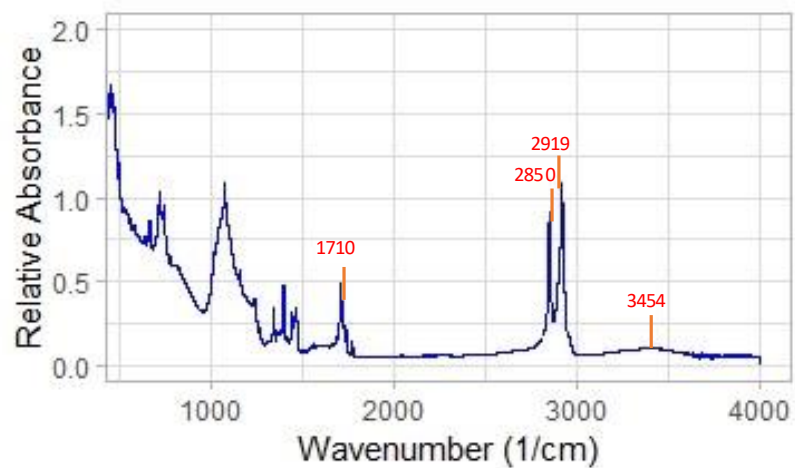
Figure 97- FTIR spectrum of un-aged XLPE-Com
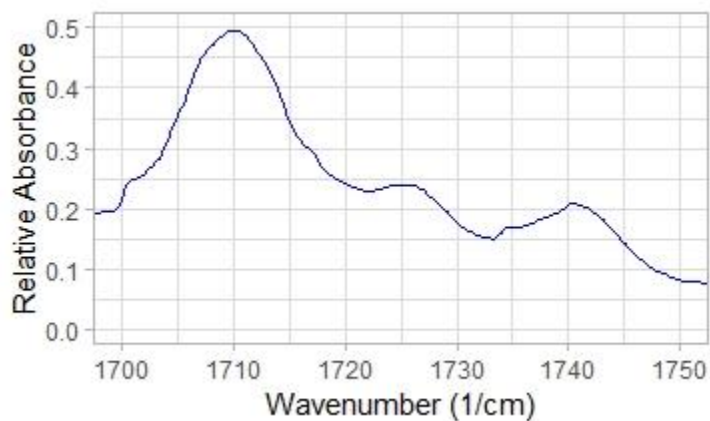
Figure 98- enlarged scale of FTIR spectrum in the oxidation region of un-aged

XLPE-Com

It is interesting to note that the un-aged specimen contains oxidized groups which are most likely introduced to the insulation through the manufacturing process. [75]

In Figure 98, the enlarged scale of FTIR-ATR spectrum in the oxidation region of un-aged XLPE-Com specimen is shown. The peaks at 1710 cm^{-1}, 1725 cm^{-1} and 1740 cm^{-1} are assigned to carboxylic acid, ketones and esters respectively. [70]

The OI , which is the area under the relative absorbance versus wavenumber in Figure 98, was calculated to be 9.5.
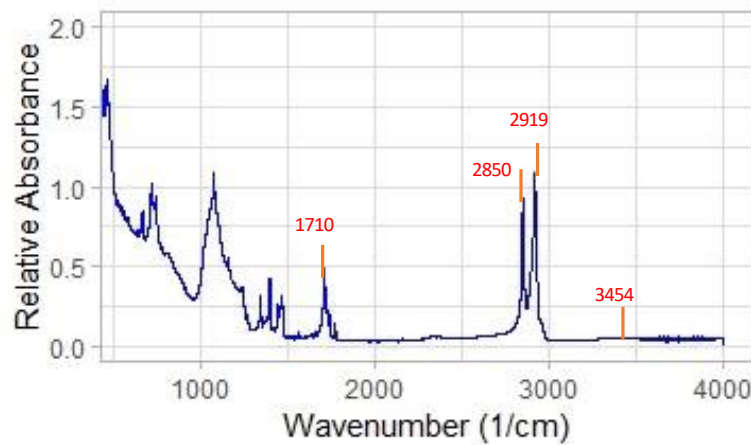
Figure 99- FTIR spectrum of XLPE-Com insulation after one month at 90°C
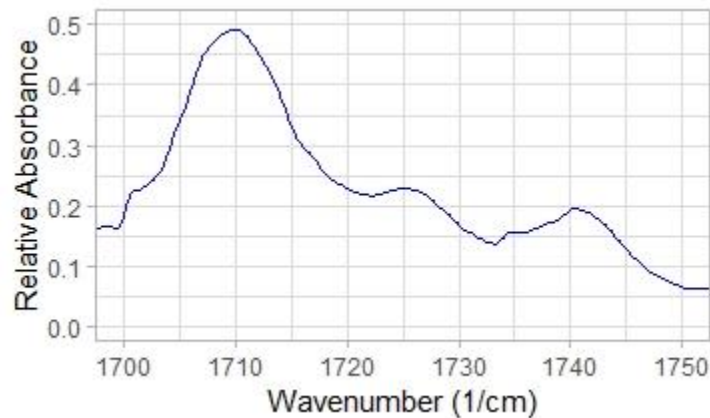
Figure 100- enlarged scale of FTIR spectrum in the oxidation region of XLPE-Com insulation after one month at 90°C

113

Figure 101- FTIR spectrum of XLPE-Com insulation after three months at 90°C

Figure 102- enlarged scale of FTIR spectrum in the oxidation region of XLPE-Com insulation after three months at 90°C

114

In Figure 99 and Figure 101, the ATR spectra of aged XLPE-Com specimens after one month and three months at 90 °C specimen are shown. The characterizing peaks at 1710 cm^{-1} and 3454 cm^{-1} as well as the peaks at 2850 cm^{-1} and 2916 cm^{-1} did not change in their intensity compering to the spectrum in Figure 97. The enlarged scale of FTIR-ATR spectrum in the oxidation region of XLPE-Com insulation after one month and three months at 90°C in Figure 100 and Figure 102 shows that the intensity of the peaks at 1710 cm^{-1}, 1725 cm^{-1} and 1740 cm^{-1} did not change comparing with that in Figure 98.

The OI , which is the area under the relative absorbance versus wavenumber in Figure 100 and Figure 102 was calculated to be 9.75.

Figure 103- FTIR spectrum of XLPE-Com insulation after four months at 90°C

Figure 104- enlarged scale of FTIR spectrum in the oxidation region of XLPE-Com insulation after four months at 90°C

In Figure 103, the ATR spectrum of an aged XLPE-Com specimen after four months at 90 °C is shown. The peak at 1710 cm^{-1} shifted to 1711 cm^{-1} and doubled in the intensity and the peak at 3454 cm^{-1} shifted to 3301 cm^{-1} and became sharper. The peaks at 2850 cm^{-1} and 2916 cm^{-1} doubled in their intensity.

In Figure 104, the enlarged scale of FTIR-ATR spectrum in the oxidation region of aged XLPE-Com specimen after four months at 90 °C is shown. The peaks at 1710 cm^{-1}, 1725 cm^{-1} and 1740 cm^{-1} doubled up in their intensity. the ATR results shows that the chain scission reactions due to oxidation reactions proceeded after four months at 90 °C while the peak intensity at 2850 cm^{-1} and 2916 cm^{-1} grew more than two times. The rise of peak intensity at 2850 cm^{-1} and 2916 cm^{-1} is attributed to the progression of crosslinking or crystallinity region. [76], [34]

The OI, which is the area under the relative absorbance versus wavenumber in Figure 104, was calculated to be 11.2.
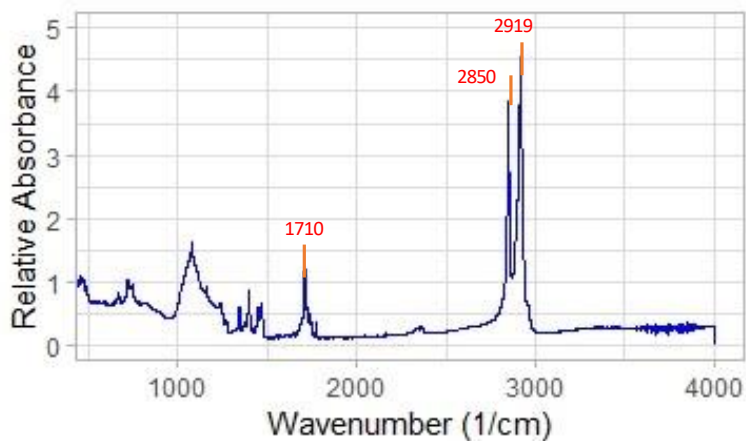
Figure 105- FTIR spectrum of XLPE-Com insulation after 3 years and 9 months at 90°C
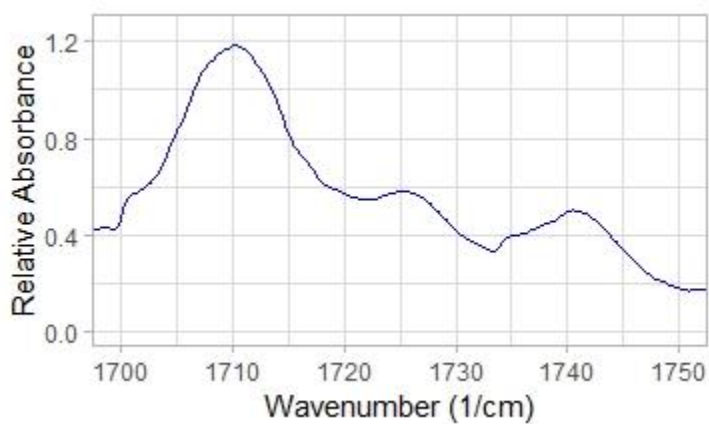
Figure 106- enlarged scale of FTIR spectrum in the oxidation region of XLPE-Com insulation after 3 years and 9 months at 90°C

In Figure 105, the ATR spectra of aged XLPE-Com specimens after 3 years and 9 months at 90°C is shown. The characterizing peaks at 1711 cm^{-1} and 3301 cm^{-1} as well

as the peaks at 2850 cm^{-1} and 2916 cm^{-1} did not change in their intensity compering to the spectrum in Figure 103. The enlarged scale of FTIR-ATR spectrum in the oxidation region of XLPE-Com insulation after 3 years and 9 months at 90°C is shown in Figure 106. It is seen that the intensity of the peaks at 1710 cm^{-1}, 1725 cm^{-1} and 1740 cm^{-1} did not change comparing with that in Figure 104.

The OI value, which is the area under the relative absorbance versus wavenumber in Figure 106, was calculated to be 20.

The OI values change versus time is plotted in Figure 107.
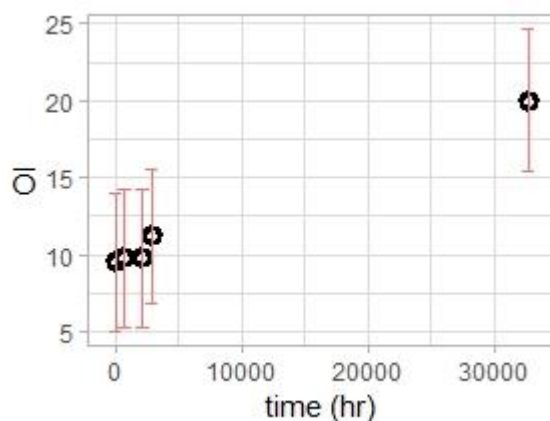
Figure 107- OI values versus time in XLPE-Com aging at 90 °C, error bars represent SE

From our FTIR-ATR results on aged specimens of XLPE-Com at 90 °C, we concluded that oxidation is the most important degradation reaction. Therefore, in the rest of our FTIR-ATR interpretations on XLPE specimens, we focus on the carbonyl peak intensity changes from 1650 cm^{-1} to 1750 cm^{-1} and OI values which are the area under the carbonyl peaks from 1650 cm^{-1} to 1750 cm^{-1}.

Figure 108-FTIR spectrum of XLPE-Com insulation after one month at 120°C

Figure 109- enlarged scale of FTIR spectrum in the oxidation region of XLPE-Com insulation after one month at 120°C

In Figure 108 and Figure 109, FTIR-ATR spectrum of XLPE-Com insulation and enlarged scale of FTIR spectrum in the oxidation region of XLPE-Com insulation after one month at 120°C are shown. The OI was calculated to be 9.5 which did not change with respect to that in un-aged specimen.

Figure 110- FTIR spectrum of XLPE-Com insulation after three months at 120°C

Figure 111- enlarged scale of FTIR spectrum in the oxidation region of XLPE-Com insulation after three months at 120°C

In Figure 110 and Figure 111, FTIR-ATR spectrum of XLPE-Com insulation and enlarged scale of FTIR spectrum in the oxidation region of XLPE-Com insulation after three months at 120°C are shown. The OI was calculated to be 9.5 which did not change with respect to that in one-month aged and un-aged specimen.
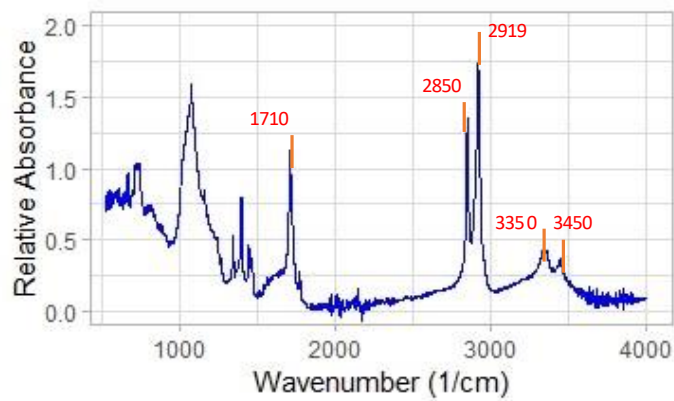
Figure 112- FTIR spectrum of XLPE-Com insulation after four months at 120°C

Figure 113- enlarged scale of FTIR spectrum in the oxidation region of XLPE-Com insulation after four months at 120°C

In Figure 112 and Figure 113, FTIR-ATR spectrum of XLPE-Com insulation and enlarged scale of FTIR spectrum in the oxidation region of XLPE-Com insulation after four months at 120°C are shown. The OI was calculated to be 14 which shows the progress of oxidation reactions after four months of aging at 120 °C.

Figure 114- FTIR spectrum of XLPE-Com insulation after five months at 120°C

Figure 115- enlarged scale of FTIR spectrum in the oxidation region of XLPE-Com insulation after five months at 120°C

In Figure 114 and Figure 115, FTIR-ATR spectrum of XLPE-Com insulation and enlarged scale of FTIR spectrum in the oxidation region of XLPE-Com insulation after five months at 120°C are shown. The OI was calculated to be 17 which shows the progress of oxidation reactions after five months of aging at 120 °C comparing to that after four months. The OI values change versus time at 120 °C is shown in Figure 116.
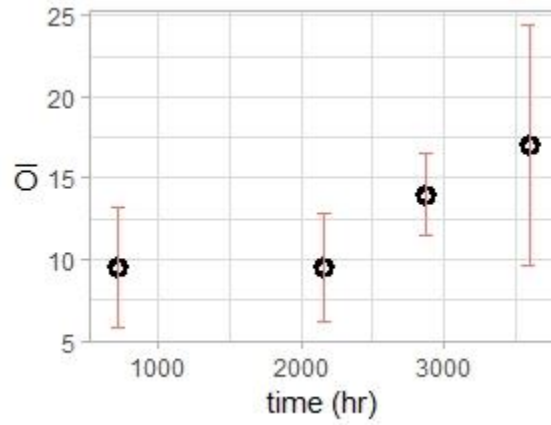
*Figure 116- OI versus time in XLPE-Com aging at 120 °C, error bars represent SE*

Figure 117- FTIR spectrum of XLPE-Com insulation after two weeks at 140°C

124

Figure 118- enlarged scale of FTIR spectrum in the oxidation region of XLPE-Com insulation after two weeks at 140°C

In Figure 117 and Figure 118, FTIR-ATR spectrum of XLPE-Com insulation and enlarged scale of FTIR spectrum in the oxidation region of XLPE-Com insulation after two weeks at 140°C are shown. The OI was calculated to be 11.25 which shows the progress of oxidation reactions after two weeks of aging at 140 °C comparing to that in un-aged specimen.
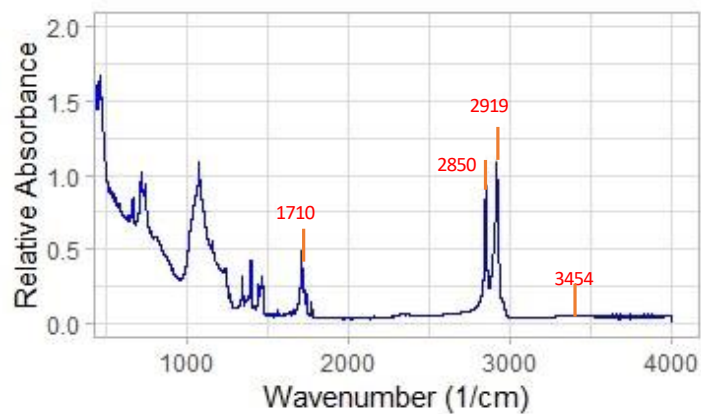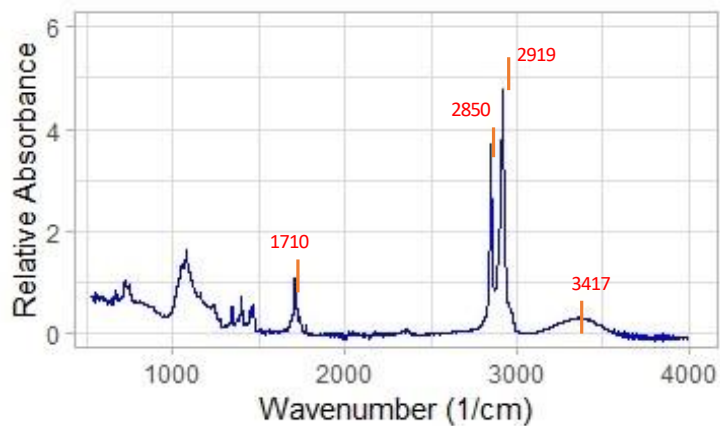
Figure 119- FTIR spectrum of XLPE-Com insulation after three weeks at 140°C
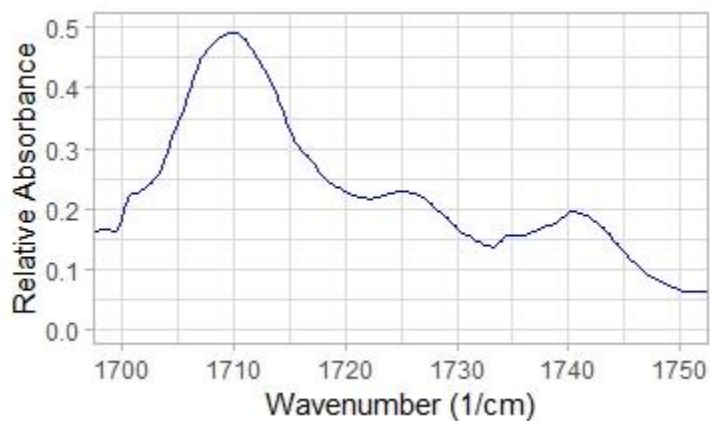

Figure 120- enlarged scale of FTIR spectrum in the oxidation region of XLPE-Com insulation after three weeks at 140°C

In Figure 119 and Figure 120, the FTIR-ATR spectrum of XLPE-Com insulation and

enlarged scale of FTIR spectrum in the oxidation region of XLPE-Com insulation after

three weeks at 140°C are shown. The OI was calculated to be 12.5 which shows the

progress of oxidation reactions after three weeks of aging at 140 °C comparing to that
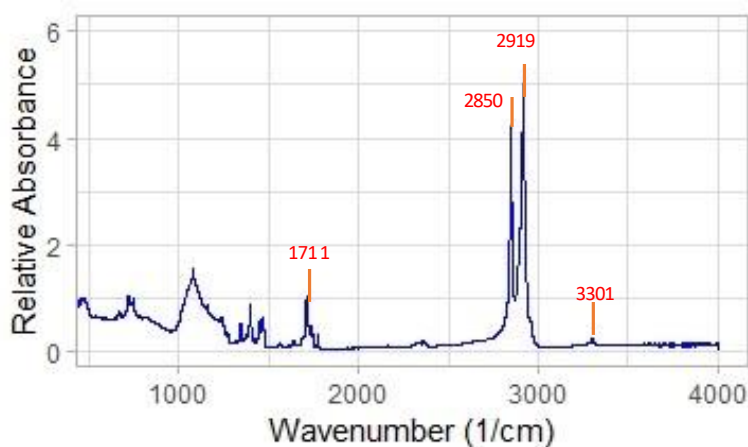
in the aged specimen after two weeks.

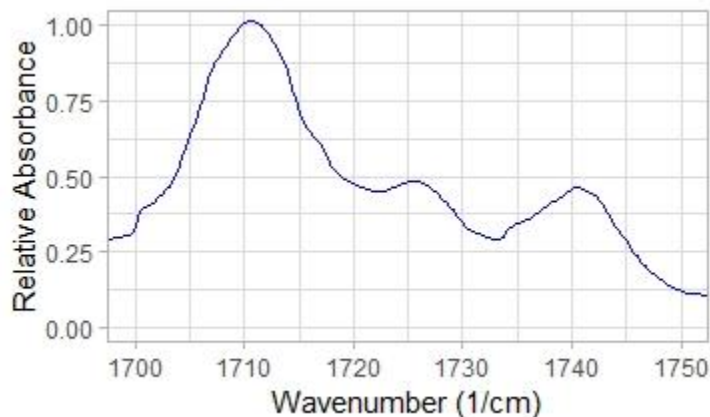*Figure 121- FTIR spectrum of XLPE-Com insulation after four weeks at 140°C*

Figure 122- enlarged scale of FTIR spectrum in the oxidation region of XLPE-Com insulation after four weeks at 140°C

In Figure 121 and Figure 122, the FTIR-ATR spectrum of XLPE-Com insulation and enlarged scale of FTIR spectrum in the oxidation region of XLPE-Com insulation after four weeks at 140°C are shown. The OI was calculated to be 27.5 which shows the significant progress of oxidation reactions after four weeks of aging at 140 °C comparing to that in the aged specimen after three weeks. Figure 123 shows the plot of OI values versus time aged at 140 °C.
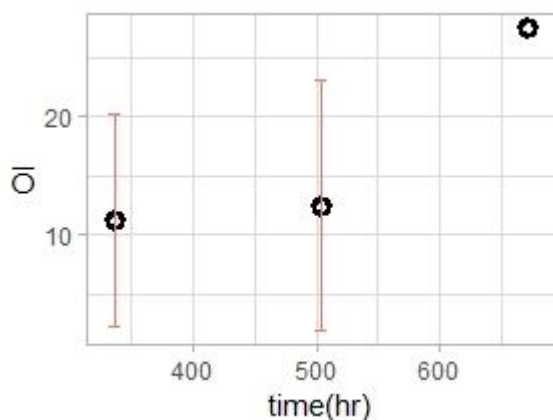
Figure 123- OI versus time in XLPE-Com aging at 140 °C, error bars represent SE

The OI values versus time at different temperatures are reported in Table 5.

Table 5- OI values of XLPE-Com insulations aged at time and different temperatures

Aging time (hr)	Aging Temperature (°C)	OI
0	90	9.5
720	90	9.75
2160	90	9.75
2880	90	11.2
32760	90	20
720	120	9.5
2160	120	9.5
2880	120	14
3600	120	17
336	140	11.25
504	140	12.5
672	140	27.5

The OI versus time in XLPE-Com aged at 90 °C, 120 °C and 140 °C is shown in Figure 124.
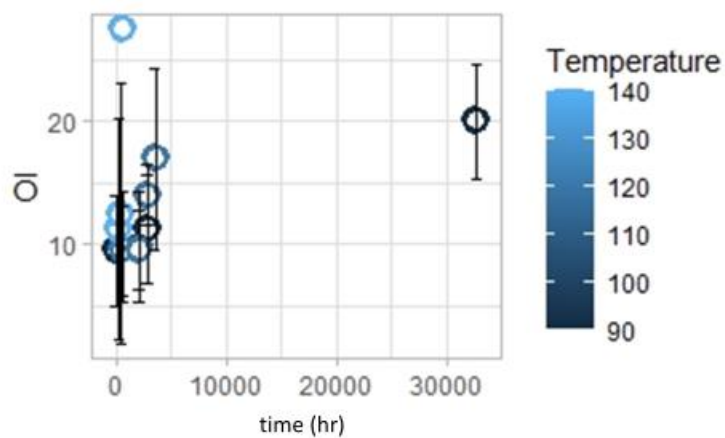
Figure 124- OI versus time in XLPE-Com aged at 90 °C, 120 °C and 140 °C, error bars represent SE

The Time-temperature superposed OI values at the reference temperature of 90 °C is

shown in Figure 125.

Figure 125- Time-temperature superposed OI values at the reference temperature of 90 °C, error bars represent SE

The activation energy of 48.56 kJ/mol with SE of 0.741is calculated from the slope of

the Arrhenius plot in Figure 126.
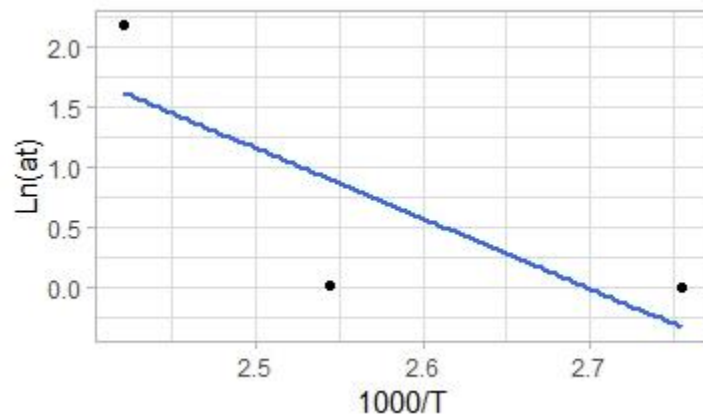
Figure 126- Shift factor versus temperature in Arrhenius plot of XLPE-Com

4.3.2.2 FTIR-ATR results on XLPE-NU

In this section the results of FTIR-ATR on XLPE-NU cables aged at 90°C and 120 °C will be discussed.

In   Figure 127 and Figure 128, FTIR-ATR spectrum of un-aged XLPE-NU insulation and enlarged scale of FTIR spectrum in the oxidation region of un-aged XLPE-NU are shown. The spectra show that the un-aged specimen was not oxidized over the manufacturing process.
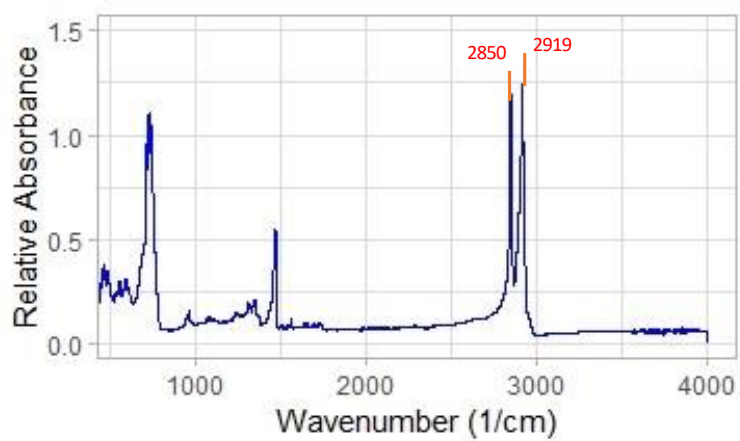
Figure 127- FTIR spectrum of un-aged XLPE-NU
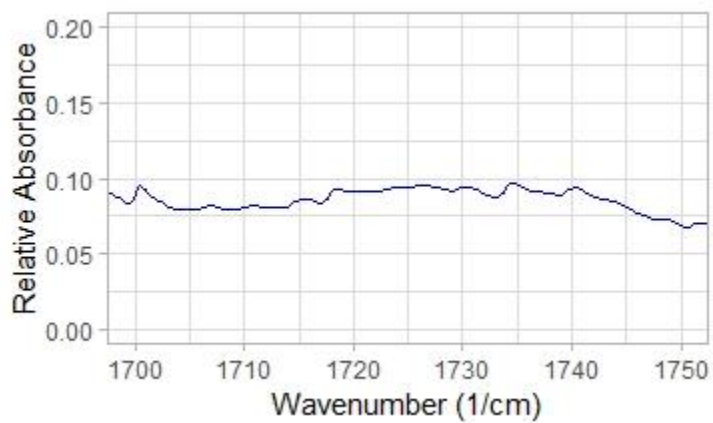
Figure 128- enlarged scale of FTIR spectrum in the oxidation region of un-aged XLPE-NU.
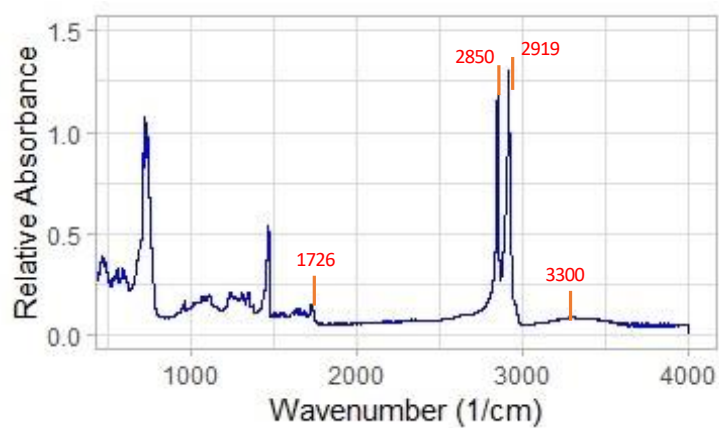
Figure 129- FTIR spectrum of XLPE-NU insulation after one month at 90°C
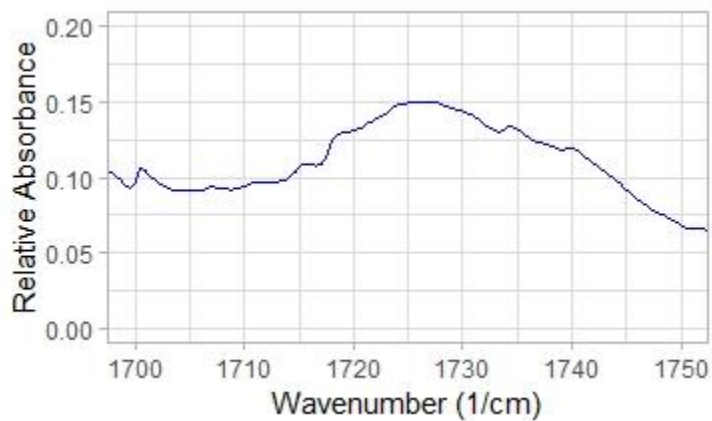
Figure 130- enlarged scale of FTIR spectrum in the oxidation region of XLPE-NU insulation after one month at 90°C

In Figure 129 and Figure 130, FTIR-ATR spectrum of XLPE-NU insulation and enlarged scale of FTIR spectrum in the oxidation region of XLPE-NU insulation after

one month at 90°C are shown. The OI was calculated to be 1.5 which changed slightly
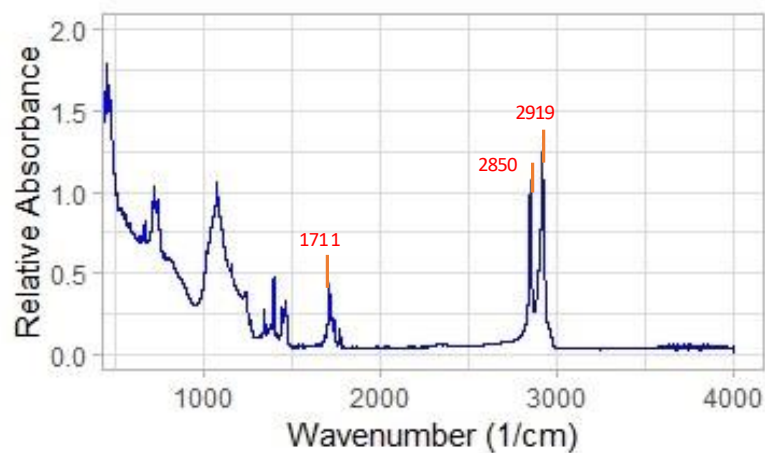
with respect to that in the un-aged specimen.
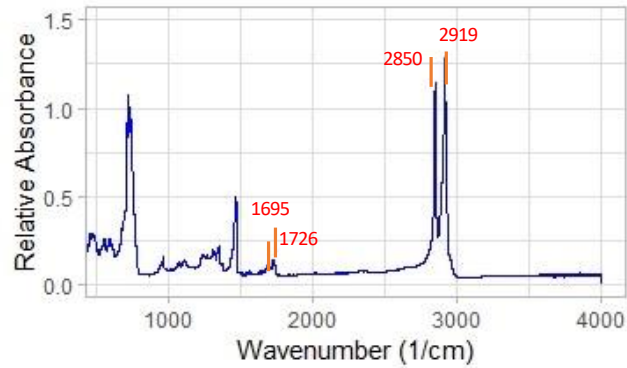
Figure 131- FTIR spectrum of XLPE-NU insulation after three months at 90°C
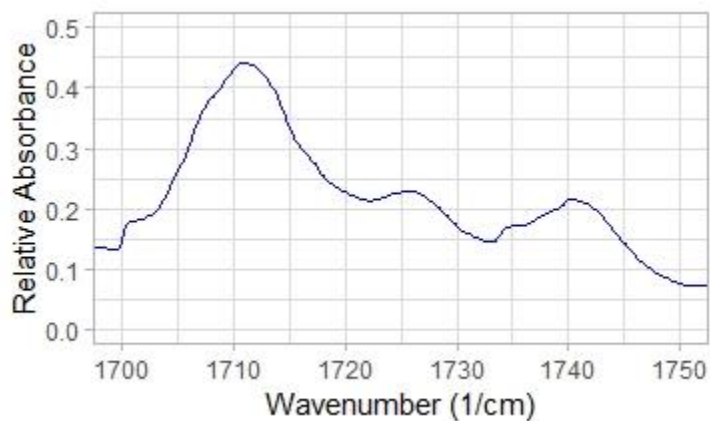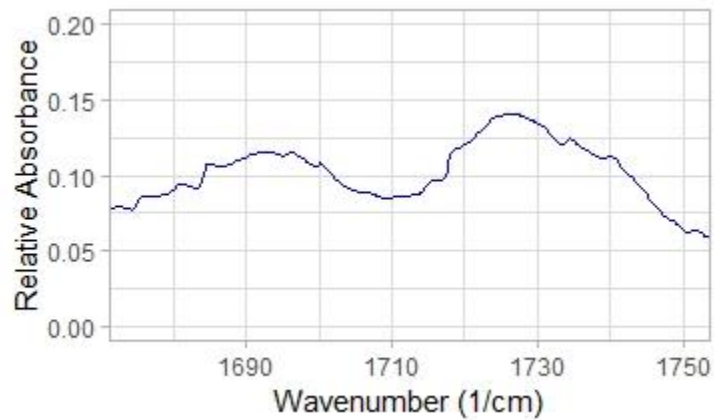

Figure 132- enlarged scale of FTIR spectrum in the oxidation region of XLPE-NU insulation after three months at 90°C

In Figure 131 and Figure 132, FTIR-ATR spectrum of XLPE-NU insulation and enlarged scale of FTIR spectrum in the oxidation region of XLPE-NU insulation after three months at 90°C are shown. The OI was calculated to be 3.75 which shows the slight progress of oxidation reactions after one months of aging at 90 °C.
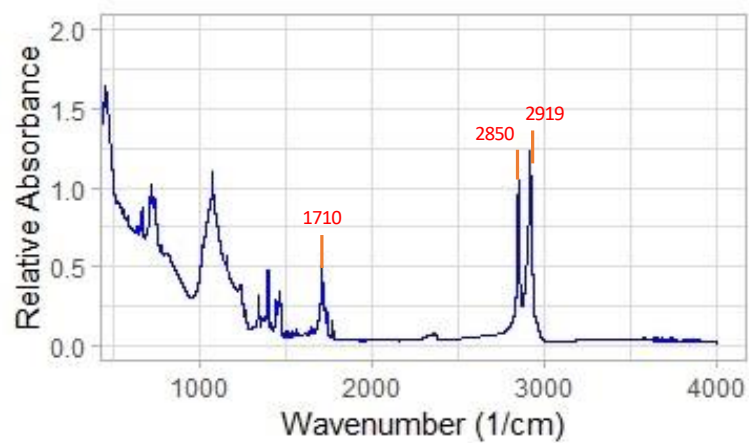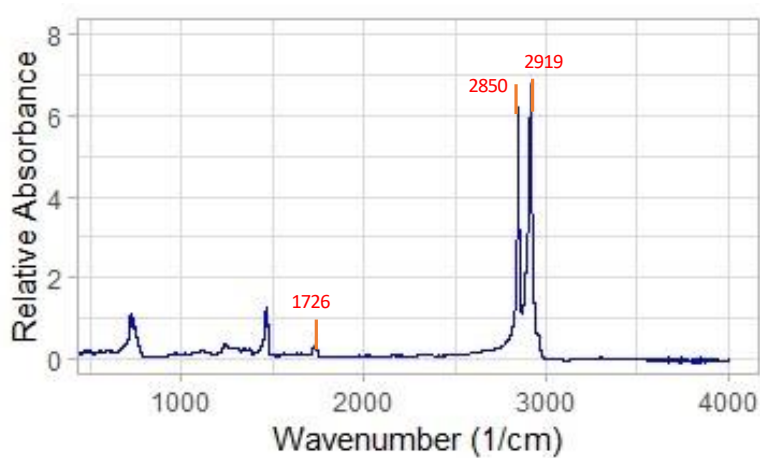

Figure 133- FTIR spectrum of XLPE-NU insulation after four months at 90°C
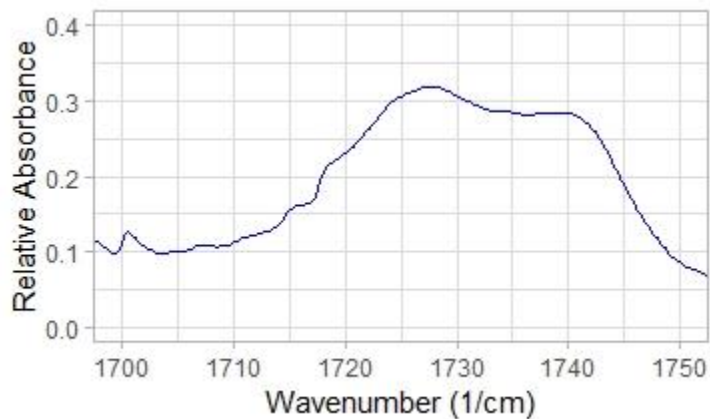
Figure 134- enlarged scale of FTIR spectrum in the oxidation region of XLPE-NU insulation after four months at 90°C

In Figure 133 and Figure 134, FTIR-ATR spectrum of XLPE-NU insulation and enlarged scale of FTIR spectrum in the oxidation region of XLPE-NU insulation after four months at 90°C are shown. The OI was calculated to be 5.25 which shows higher progress of oxidation reactions after four months of aging at 90 °C.
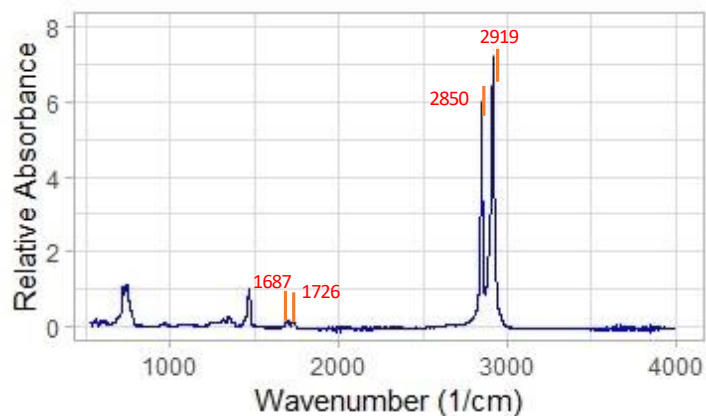
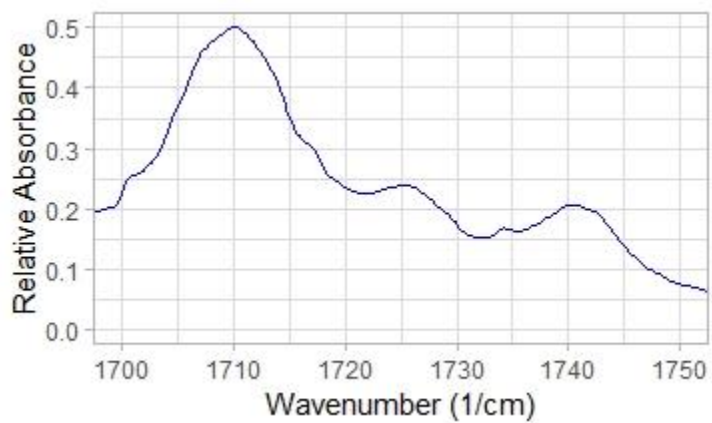*Figure 135- FTIR spectrum of XLPE-NU insulation after 3 years and 9 months at 90°C*

136
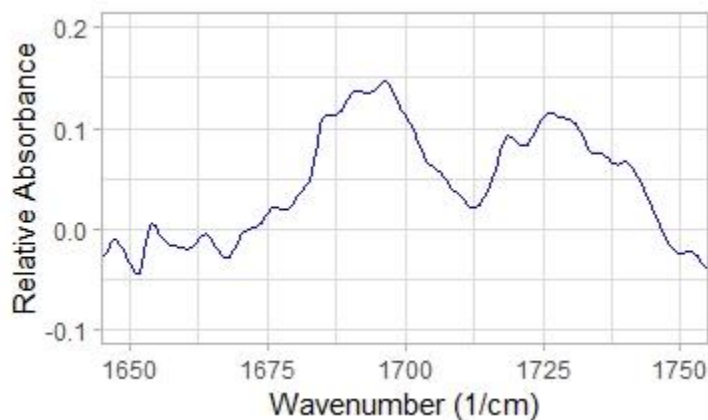
Figure 136- enlarged scale of FTIR spectrum in the oxidation region of XLPE-NU insulation after 3 years and 9 months at 90°C

In Figure 135 and Figure 136, FTIR-ATR spectrum of XLPE-NU insulation and enlarged scale of FTIR spectrum in the oxidation region of XLPE-NU insulation after 3 years and 9 months at 90°C are shown. The OI was calculated to be 9.68 which shows higher progress of oxidation reactions. Figure 137 shows the plot of OI values versus time at 90° C.
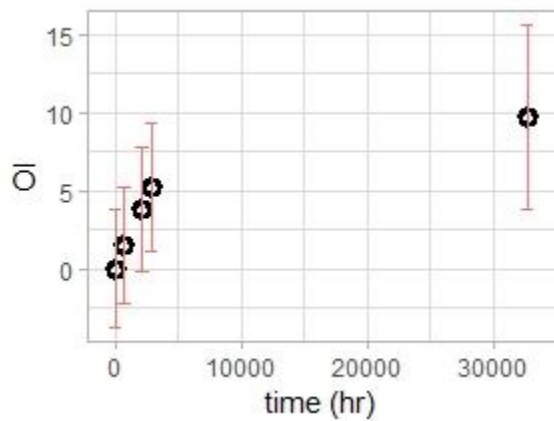
*Figure 137- OI versus time in XLPE-NU aging at 90 °C , error bars represent SE*
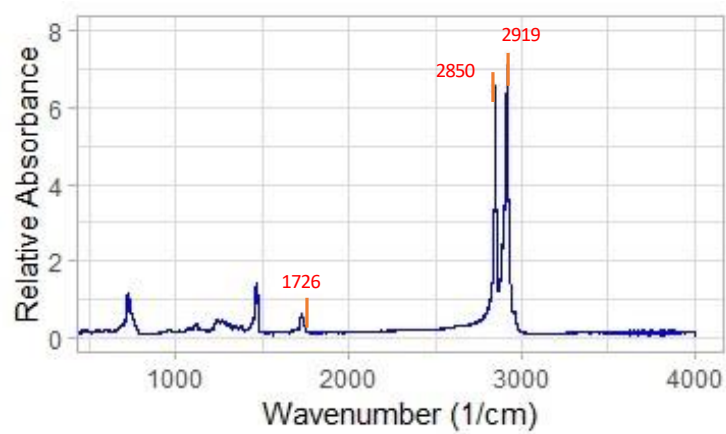
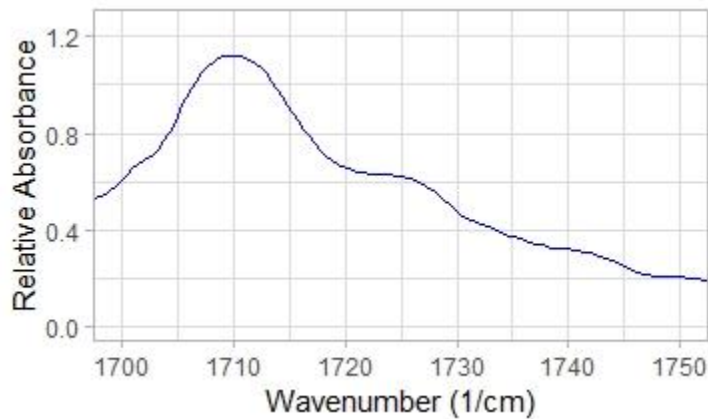*Figure 138- FTIR spectrum of XLPE-NU insulation after two months at 120°C*

138
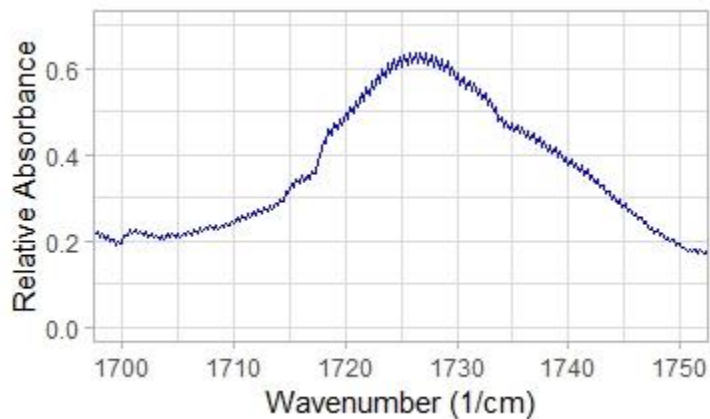
Figure 139- enlarged scale of FTIR spectrum in the oxidation region of XLPE-NU insulation after two months at 120°C

In Figure 138 and Figure 139, FTIR-ATR spectrum of XLPE-NU insulation and enlarged scale of FTIR spectrum in the oxidation region of XLPE-NU insulation two months at 120°C are shown. The OI was calculated to be 9 which shows higher progress of oxidation reactions comparing to that in the un-aged specimen.
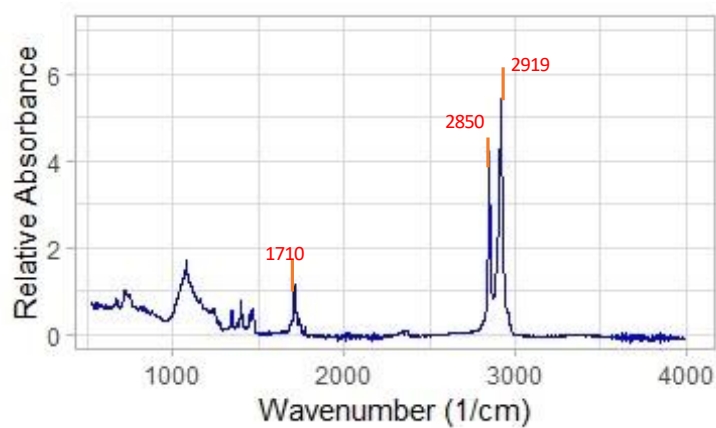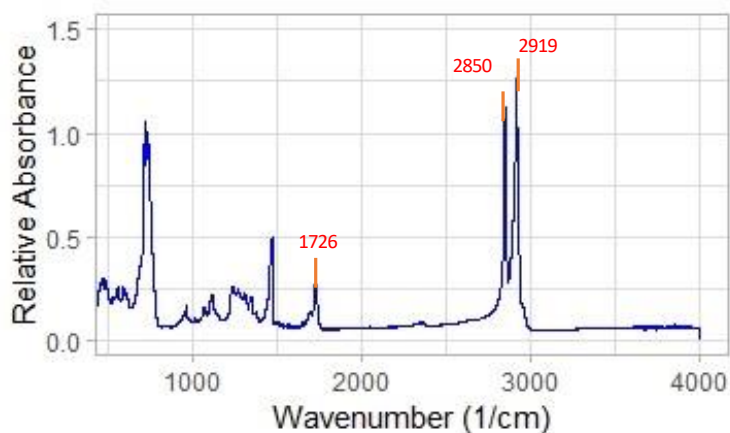

Figure 140- FTIR spectrum of XLPE-NU insulation after three months at 120°C
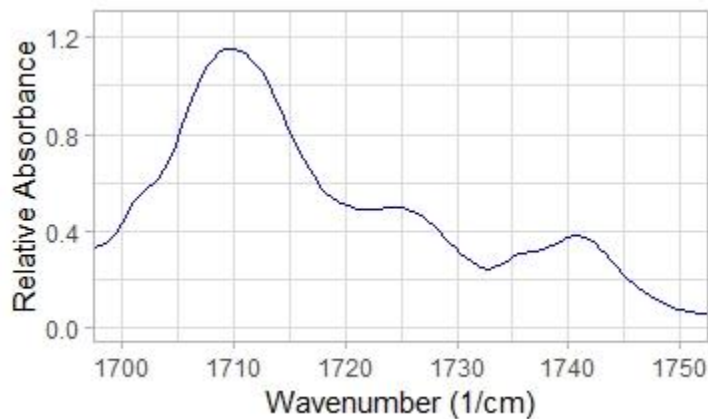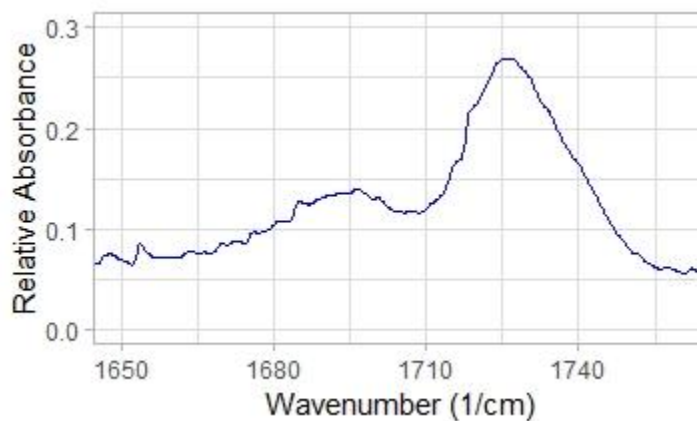
Figure 141- enlarged scale of FTIR spectrum in the oxidation region of XLPE-NU insulation after three months at 120°C

In Figure 140 and Figure 141, FTIR-ATR spectrum of XLPE-NU insulation and enlarged scale of FTIR spectrum in the oxidation region of XLPE-NU insulation three months at 120°C are shown. The OI was calculated to be 9 which did not change in oxidation reactions comparing to that in the two-months-aged specimen.
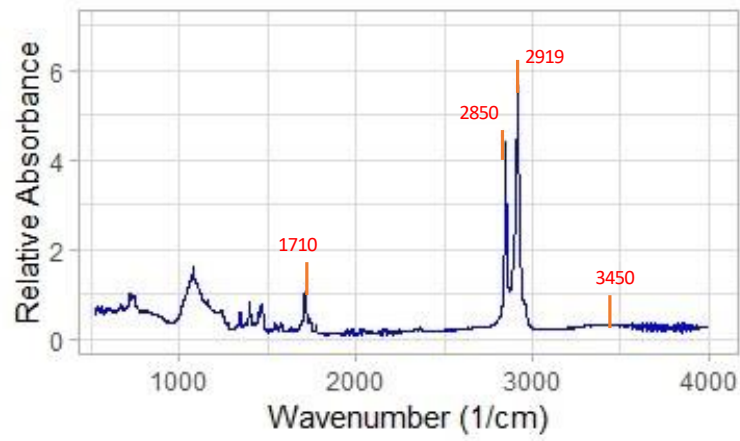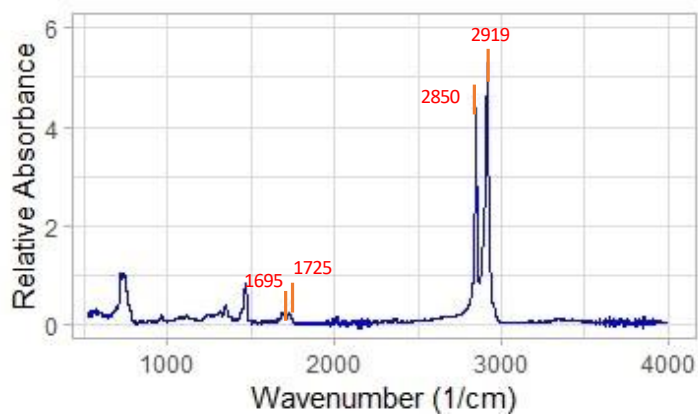
Figure 142- FTIR spectrum of XLPE-NU insulation after four months at 120°C
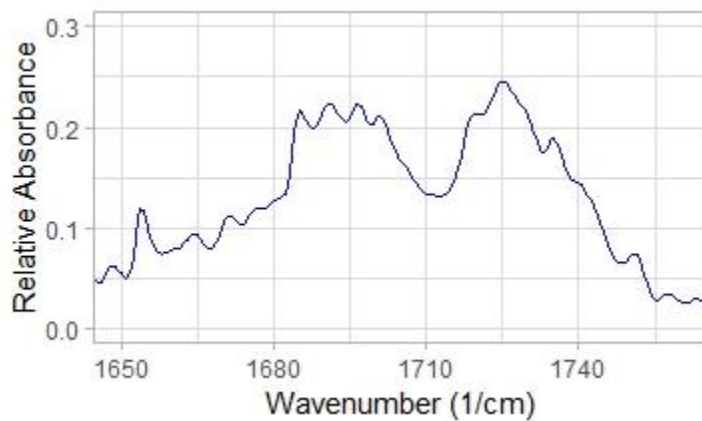
Figure 143- enlarged scale of FTIR spectrum in the oxidation region of XLPE-NU insulation after four months at 120°C

In Figure 142 and Figure 143, FTIR-ATR spectrum of XLPE-NU insulation and enlarged scale of FTIR spectrum in the oxidation region of XLPE-NU insulation four months at 120°C are shown. The OI was calculated to be 16.5 which showed a

significant change in the oxidation reactions progress comparing to that in the previous

aged specimens.
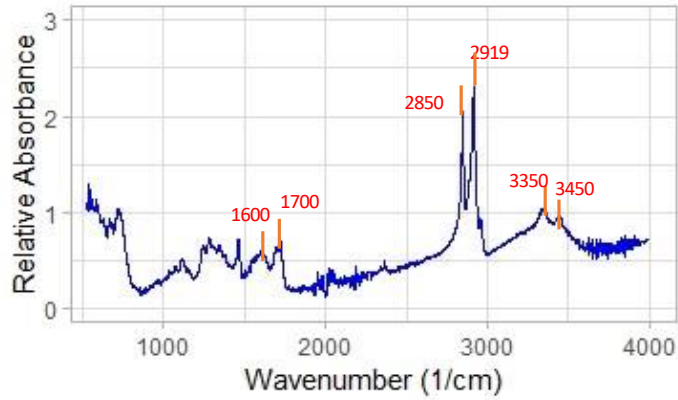
Figure 144- FTIR spectrum of XLPE-NU insulation after five months at 120°C
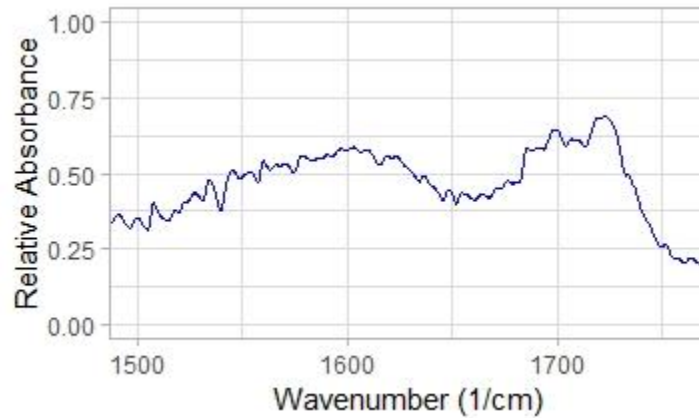
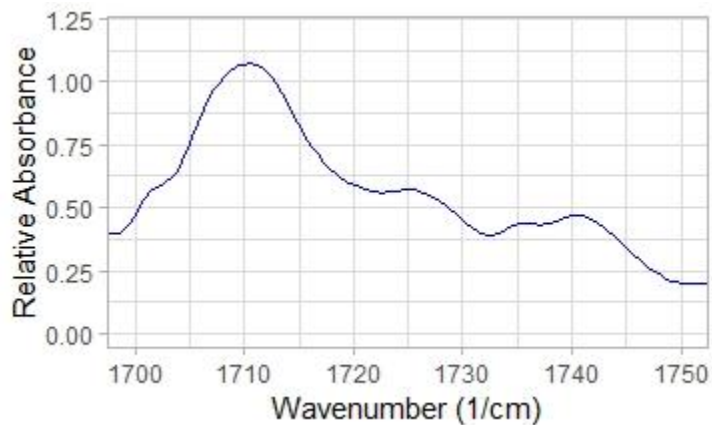*Figure 145- enlarged scale of FTIR spectrum in the oxidation region of XLPE-NU insulation after five months at 120°C*

142

In Figure 144 and Figure 145, FTIR-ATR spectrum of XLPE-NU insulation and enlarged scale of FTIR spectrum in the oxidation region of XLPE-NU insulation five months at 120°C are shown. The OI was calculated to be 25 which showed the oxidation reactions progress highly proceeded comparing to all the earlier extracted aged specimens. Figure 146 shows the OI values plotted versus aging time at 120 °C.
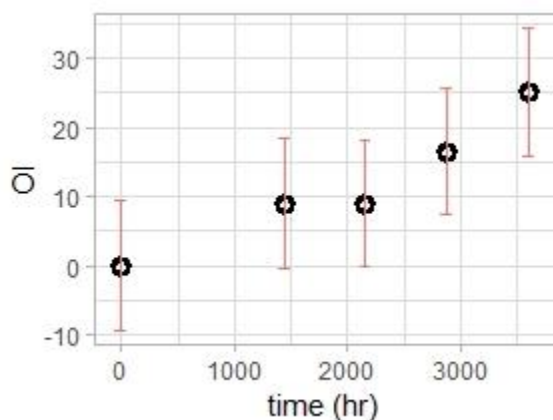
*Figure 146- OI values versus aging time at 120 °C, error bars represent SE*

143
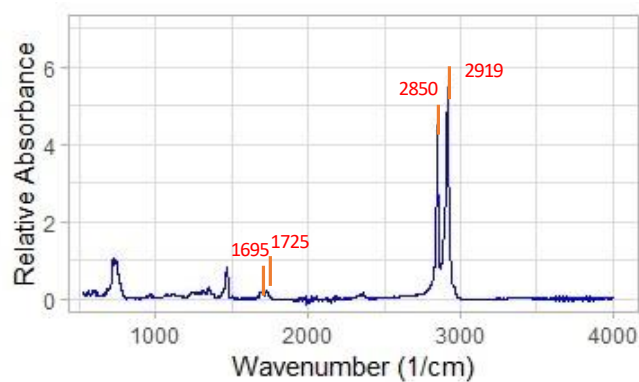
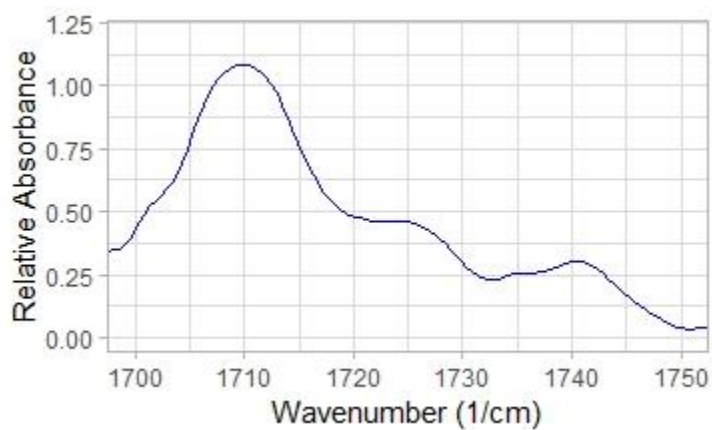*Figure 147- FTIR spectrum of XLPE-NU insulation after two weeks at 140°C*
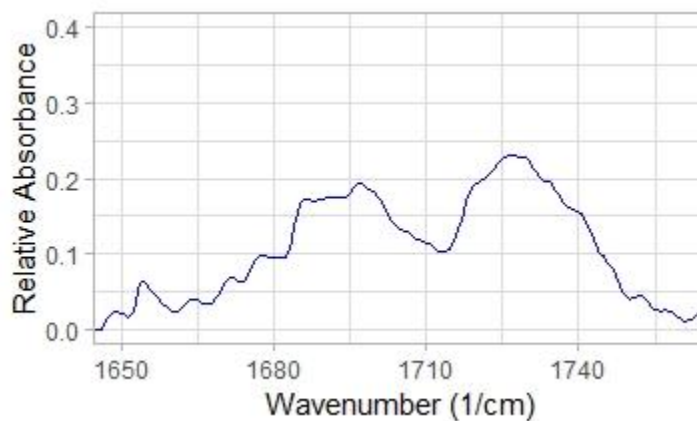
Figure 148- enlarged scale of FTIR spectrum in the oxidation region of XLPE-NU insulation after two weeks at 140°C

In Figure 147 and Figure 148, the FTIR-ATR spectrum of XLPE-NU insulation and

enlarged scale of FTIR spectrum in the oxidation region of XLPE-NU insulation after

144

two weeks at 140°C are shown. The OI was calculated to be 12.75 which showed the

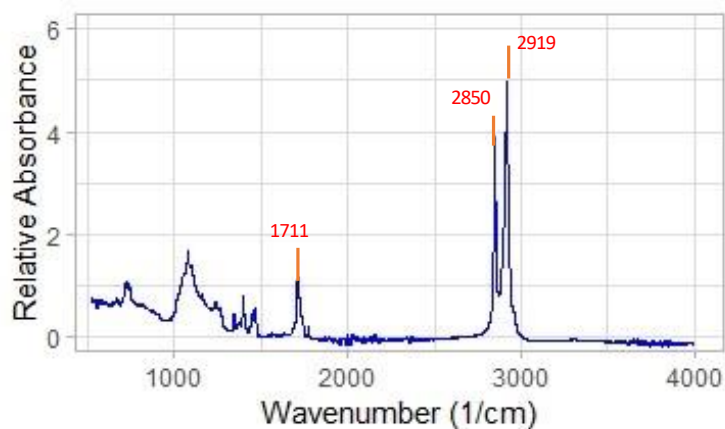oxidation reactions progress comparing un-aged specimens.
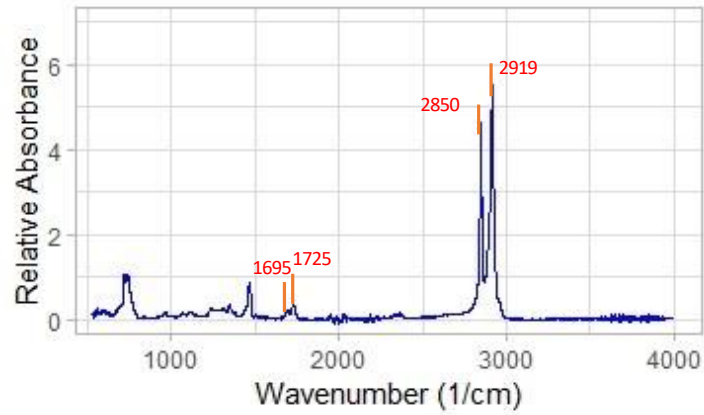
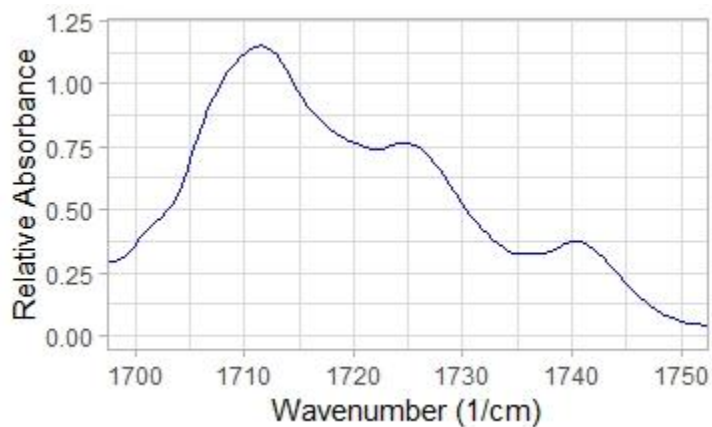*Figure 149- FTIR spectrum of XLPE-NU insulation after three weeks at 140°C*
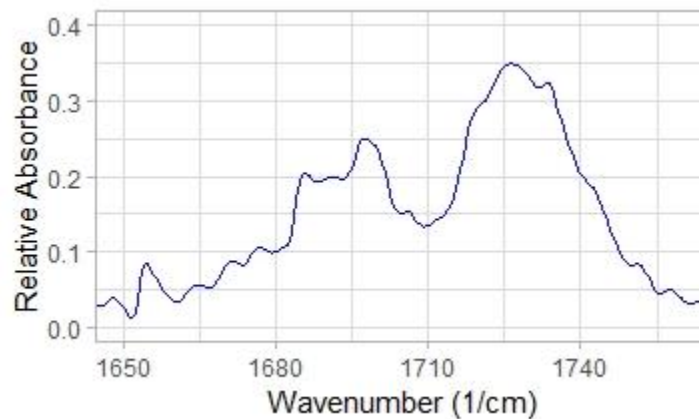
Figure 150- enlarged scale of FTIR spectrum in the oxidation region of XLPE-NU insulation after three weeks at 140°C

In Figure 149 and Figure 150, the FTIR-ATR spectrum of XLPE-NU insulation and enlarged scale of FTIR spectrum in the oxidation region of XLPE-NU insulation after three weeks at 140°C are shown. The OI was calculated to be 17.25 which showed higher progress in the oxidation reactions comparing to two-weeks-aged specimens.
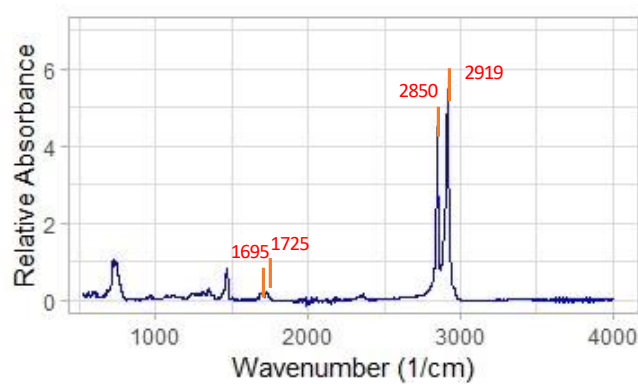
Figure 151- FTIR spectrum of XLPE-NU insulation after four weeks at 140°C
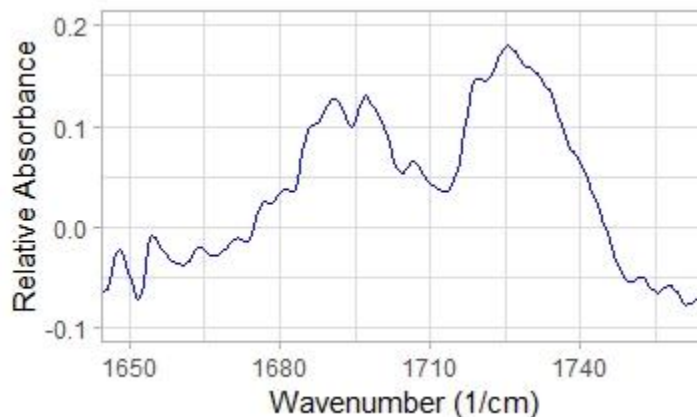
Figure 152- enlarged scale of FTIR spectrum in the oxidation region of XLPE-NU insulation after four weeks at 140°C

In Figure 151 and Figure 152, the FTIR-ATR spectrum of XLPE-NU insulation and enlarged scale of FTIR spectrum in the oxidation region of XLPE-NU insulation after four weeks at 140°C are shown. The OI was calculated to be 18 which showed slightly higher progress in the oxidation reactions comparing to three-weeks-aged specimens.

Figure 153 shows the OI values plotted versus aging time at 140 °C.
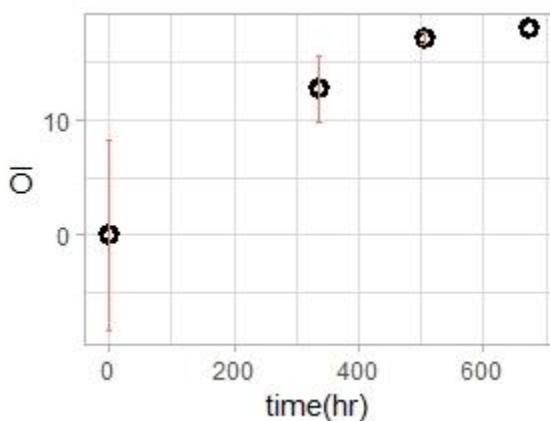
Figure 153- OI values versus aging time at 140 °C, error bars represent SE

147

The OI values of XLPE-NU insulations aged at different time and temperatures are reported in Table 6.

Table 6-OI values of XLPE-NU insulations aged at different time and temperatures

Aging time (hr)	Aging Temperature (°C)	OI
0	90	0
720	90	1.5
2160	90	3.75
2880	90	5.25
32760	90	9.68
0	120	0
1440	120	9
2160	120	9
2880	120	16.5
3600	120	25
0	0	0
12.75	336	140
17.25	504	140
18	672	140

The OI values versus time in XLPE-NU aged at 90 °C, 120 °C and 140 °C are shown in Figure 154.

The Time-temperature superposed OI values at the reference temperature of 90 °C is shown in Figure 155.
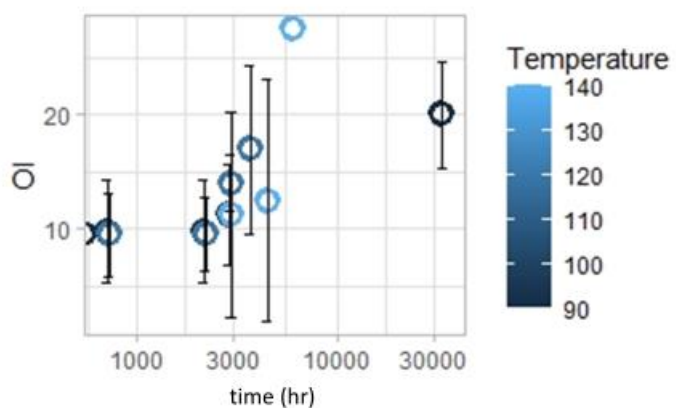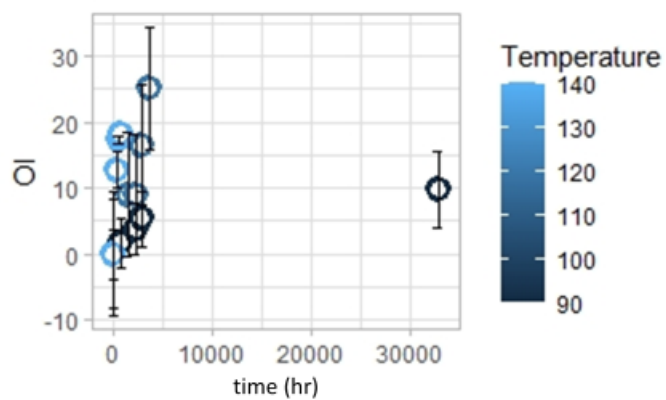
Figure 154- OI versus time in XLPE-NU aged at 90 °C, 120 °C and 140 °C, error bars represent SE

.
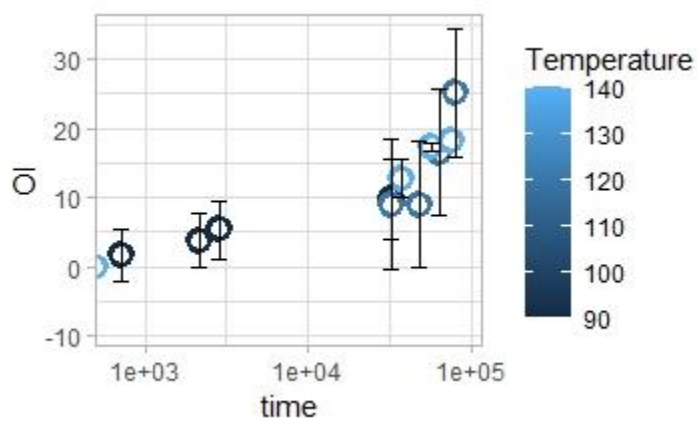
Figure 155- Time-temperature superposed OI values at the reference temperature of 90 °C, error bars represent SE
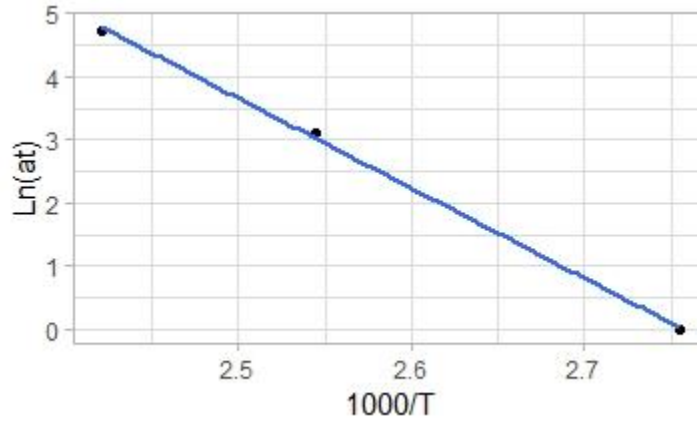
Figure 156- Shift factor versus temperature in Arrhenius plot of XLPE-NU

The activation energy of 118.27 kJ/mol with SE of 0.44 is calculated from the slope of the Arrhenius plot in Figure 156.

4.3.3 ESR results

In this section, ESR spectroscopy results on XLPE cable insulations will be explained. Over the 50 years of the advent of ESR spectroscopy, a very limited number of research have been done on ESR spectroscopy analysis of cable insulations. In fact, these investigations briefly mentioned the existence of peroxyl radicals associated with the ESR spectra and did not employed ESR spectra changes at different aging conditions for the insulation aging investigation. [78], [79],[80] and [81]

To our knowledge, this is the first time, a thorough investigation on ESR spectra analysis on aged XLPE cable insulations has been done. It should be noted that the ESR spectra were recorded after four years of aging of XLPE cable insulations, with an exception for that recorded on 45 months of aging XLPE cable insulations after three months, which evidences the stability of the studied free radicals. [82]

150

4.3.3.1 ESR results on XLPE-NU

The ESR results on XLPE-NU specimens of unaged and aged for 1 month, 4 months and 45 months at 90 °C are illustrated in Figure 157.
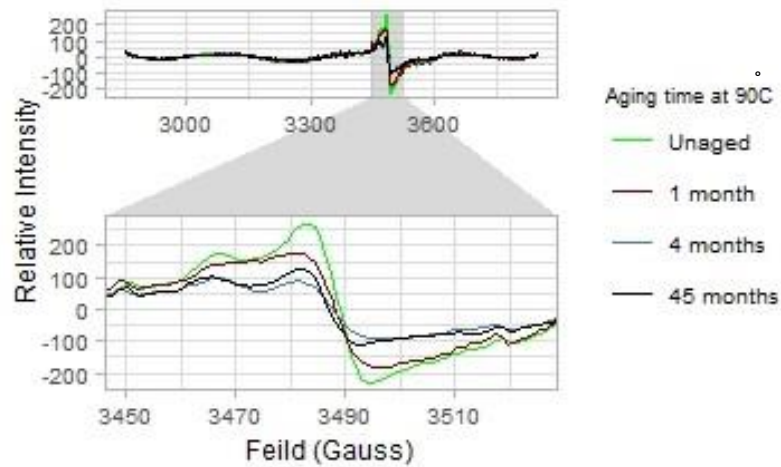
Figure 157-The ESR spectra on XLPE-NU specimens of unaged and aged at 90 °C for 1 month, 4 months and 45 months.

As it is seen in Figure 157, the presence of a singlet in all the ESR spectra represents the existence of free radicals.[82] The highest peak amplitude belongs to the unaged specimen which is attributed to the presence of free radicals over the manufacturing process. [75] However, after one month of aging the amplitude is reduced which is due to the progression of crosslinking reactions. [28]

As it is shown, the peak amplitude of samples aged from one month to four months of aging at 90 °C decreases and remained almost the same in samples aged for 45 months.

It is attributed to the peroxyl radical consumption in the crosslinking reactions after 4 months to 45 months of aging. [82]

The ESR spectra on XLPE-NU specimens of unaged and aged for 3 months, 4 months and 5 months at 120 °C are illustrated in Figure 158.
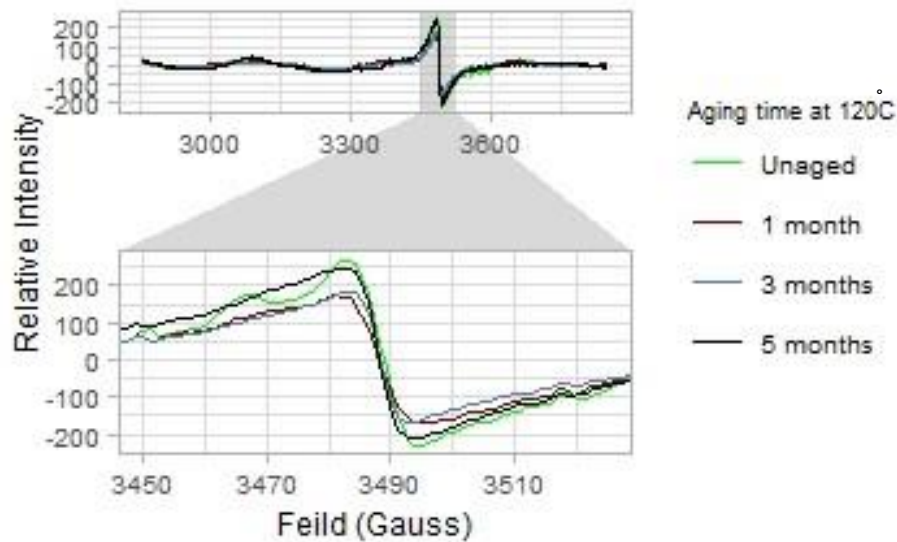
Figure 158--The ESR spectra on XLPE-NU specimens of unaged and aged at 120 °C for 3 months, 4 months and 5 months.

As it is seen in Figure 158, the presence of a singlet on all the ESR spectra evidences the existence of peroxy radicals. [82]

The peak corresponding to the unaged specimen is due to the presence of peroxyl radicals which were formed over the manufacturing process. [75] However, after three months of aging the amplitude is reduced which is due to the progression of crosslinking reactions. [28], [64]

A sudden remarkable increase in the peak amplitude of specimens aged for 5 months is observed which may be due to the oxidation of lower molecular weight species formed by the fragmentation of polymeric chains after four months of aging at 120 °C. [28]

Figure 159 shows the ESR spectra on XLPE-NU specimens of unaged and aged at 140 °C for 2 weeks, 3 weeks and 4weeks.

As it is seen in Figure 159, the presence of a singlet on all the ESR spectra evidences the existence of polyenyl radicals and a small contribution of peroxyl radicals. [82]

The peak corresponding to the unaged specimen is due to the presence of peroxyl radicals which were formed over the manufacturing process. [75] After 2 weeks of aging the amplitude is reduced which is due to the progression of crosslinking reactions. [28], [64]

A sudden remarkable increase in the peak amplitude of specimens aged for 3 weeks is observed which may be due to the oxidation of lower molecular weight species formed by the fragmentation of polymeric chains after 3 weeks of aging at 140 °C. [28]
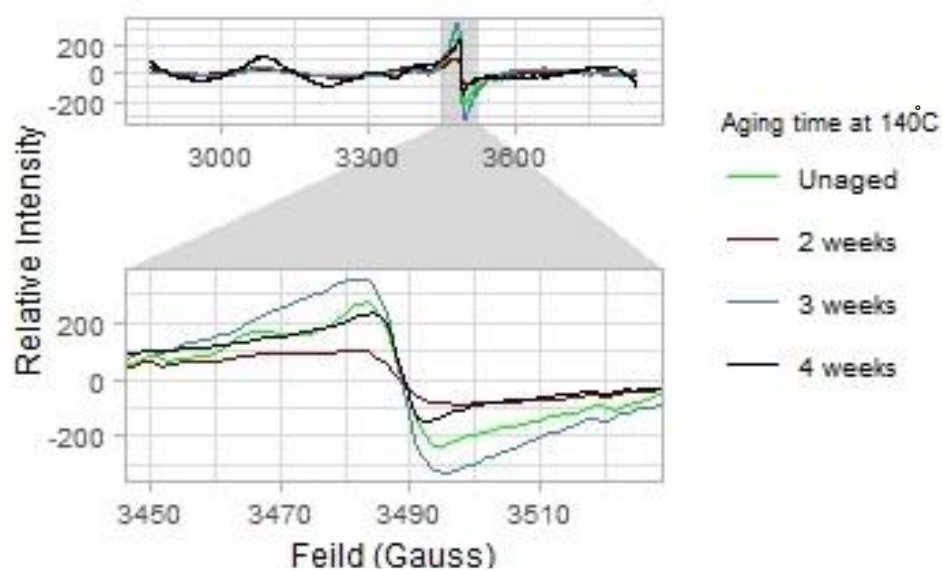
Figure 159- The ESR spectra on XLPE-NU specimens of unaged and aged at 140

°C for 2 weeks, 3 weeks and 4weeks.

The reduction of the peak amplitude after 4 weeks of aging is due to the progression of

the crosslinking reactions.

4.3.3.2 ESR results on XLPE-Com

The ESR results on XLPE-Com specimens aged for unaged and aged for 1 month, 4

months and 45 months at 90 °C are illustrated in Figure 160.
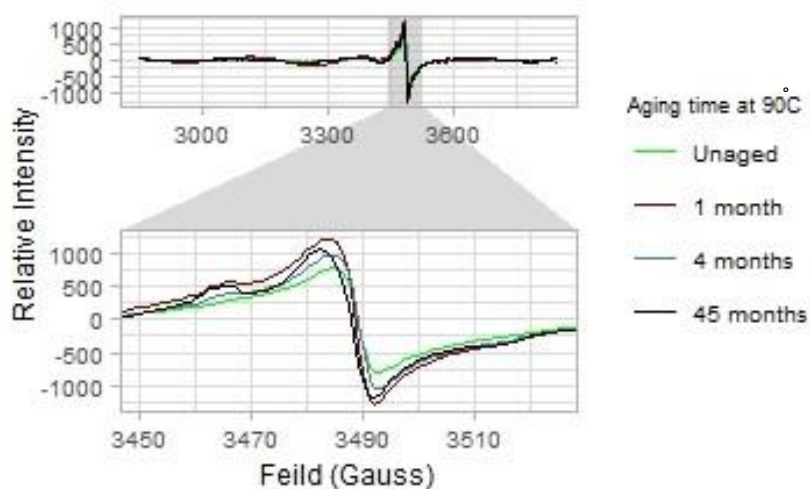
Figure 160-The ESR spectra on XLPE-Com specimens of unaged and aged at 90 °C for 1 month, 4 months and 45 months.

As it is seen in Figure 160, the presence of a singlet in all the ESR spectra represents the existence of peroxyl radicals. [82] The lowest peak amplitude belongs to the unaged specimen which is attributed to the presence of peroxyl radicals over the manufacturing process. [75] After one month of aging the amplitude increased which may be due to the oxidation of lower molecular weight species formed by the fragmentation of polymeric chains after one month of aging at 90 °C. [28]

As it is shown, the peak amplitude associated to one-month aged samples decreased to that corresponding to four months of aging at 90 °C and then kept constant after 45 months which is due to the progression of crosslinking reactions. [28], [64]

The ESR spectra on XLPE-Com specimens of unaged and aged for 3 months, 4 months and 5 months at 120 °C are illustrated in Figure 161.

155
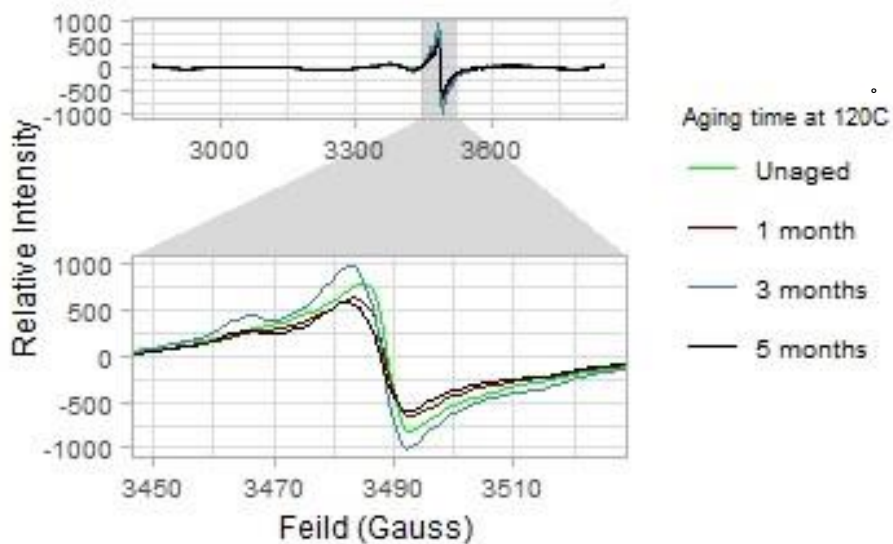
Figure 161-The ESR spectra on XLPE-Com specimens of unaged and aged at 120 °C for 1 month, 3 months and 5 months.

As it is seen in Figure 161, the presence of a singlet on all the ESR spectra evidences the existence of free radicals. [82]

The peak corresponding to the unaged specimen is assigned to free radicals which were formed over the manufacturing process. [75] After one month of aging the amplitude is reduced which is due to the progression of crosslinking reactions. [28], [64]

A remarkable increase in the peak amplitude of specimens aged for 3 months is observed which may be due to the oxidation of lower molecular weight species formed by the fragmentation of polymeric chains after four months of aging at 120 °C. [28]

The peak amplitude reduction after 5 months of aging is due to the progression of crosslinking reactions, and other reactions which involve the self-termination of free radicals. [28], [64]

Figure 162 shows the ESR spectra on XLPE-Com specimens of unaged and aged at 140 °C for 1 week, 2 weeks and 3 weeks.

As it is seen in Figure 162, the presence of a singlet on all the ESR spectra evidences the existence of polyenyl radicals, with a small contribution, if any, from peroxyl radicals. [82], [30]

The peak corresponding to the unaged specimen is due to the presence of peroxyl radicals which were formed over the manufacturing process. [75] After one week of aging the amplitude is increased and kept almost constant after two weeks of aging which is due to the progression of oxidation reactions leading to the production of free radicals. [28], [64]

The peak amplitude reduction after three weeks of aging is due to the progression of crosslinking reactions. [28], [64]
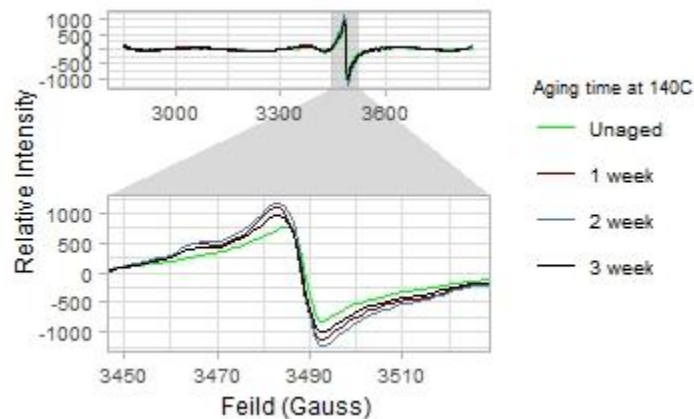
Figure 162- The ESR spectra on XLPE-Com specimens of unaged and aged at 140 °C for 1 week, 2 weeks and 3 weeks.

Chapter 5:

Activation Energy of EAB Modeling Based on CM Parameters

5.1 Introduction

The results of the experiments will be discussed in this chapter. The activation energy corresponding to CM parameters and EAB data of XLPE and EPR cables based on the experimental results in this thesis and C-PAD database will be reported. The activation energy calculated based on experimental results performed in this thesis has been explained in Chapter 4. The method of calculating activation energy based on C-PAD data for several CM parameters are reported in Appendix.

5.2 Activation Energy Calculations based on C-PAD database

Activation energy calculations corresponding to EAB and a few CM parameters, based on the datapoints extracted from C-PAD database will be shown and explained in the following. The diffusion limited oxidation, DLO, was considered in the calculations by eliminating those data which did not give the best superposition.[60]

5.2.1 Activation energy corresponding to EAB

In this section, the results of EAB measurements of EPR cables, C-12 manufactured by Anaconda, from C-PAD database will be discussed. As seen in Figure 163, EAB versus time plots are shown at 100.9 °C, 150 °C, 170 °C temperatures. Using time-temperature superposition method, the plots at 150 °C and 170 °C were shifted to the reference temperature, 100.9 °C. The results are shown in Figure 164. As seen, the three plots are nicely superposed at the reference temperature.
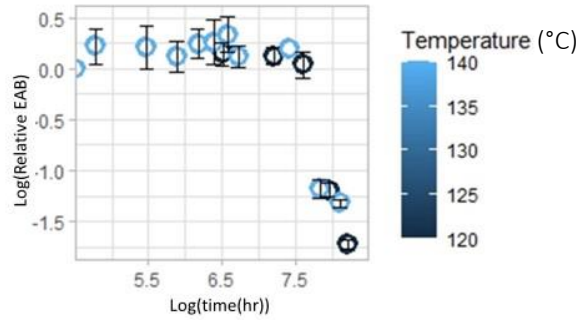
Figure 163- EAB-time plots at different indicated temperatures for EPR cables, manufactured by Anaconda company, error bars represent SD

It is very important to note that the nice superposition of the plots occurred while there is a broad range of temperature difference in the plots. This can be assuring that the accelerated assumption is valid in this material [59].
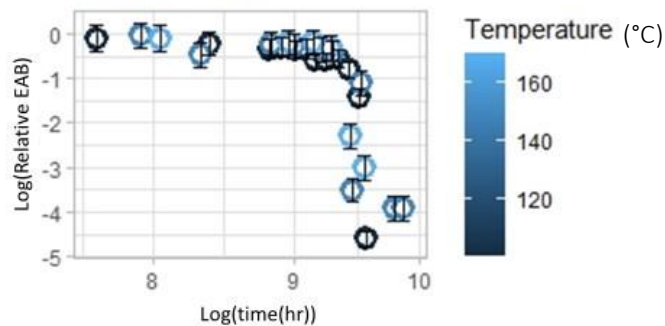
The shift factors corresponding to different temperatures are given in the Table 7.

Table 7-Shift factors for the thermally aged EPR cable

Temperature (°C)	a_T	$Ln(a_T)$
100.9	1	0
150	57.11	4.04
170	195.3	5.26

In the next step, the activation energy will be calculated from the slope of the shift
factor versus temperature. The Arrhenius plot of shift factor versus temperature is
shown in Figure 165. The linearity of the plot evidenced the Arrhenius behavior of the
material.
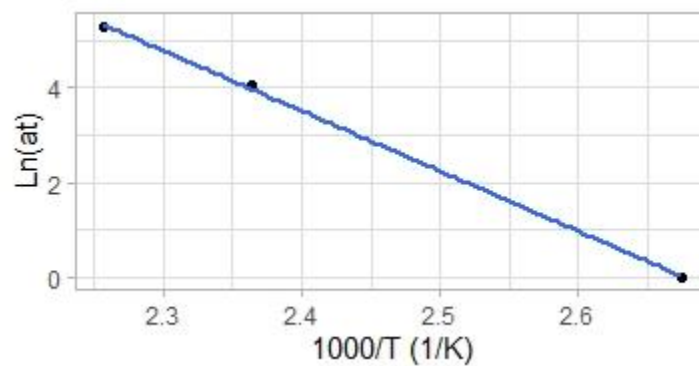
Figure 165- Shift factor versus temperature in the Arrhenius plot

Activation energy was calculated according to equation (2.14) to be 105.79 kJ/mol with SE of 0.3074.

5.2.2 Activation energy corresponding to Modulus

In this section, the results of modulus measurements of EPR cables, C-12 manufactured by Anaconda, from C-PAD database will be discussed. As seen in Figure 166, modulus versus time plots is shown at 110 °C, 125 °C, 140 °C temperatures. Using time-temperature superposition method, the plots at 125 °C and 140 °C were shifted to the reference temperature, 110 °C. The results are shown in Figure 167. As seen, the three plots are nicely superposed at the reference temperature.
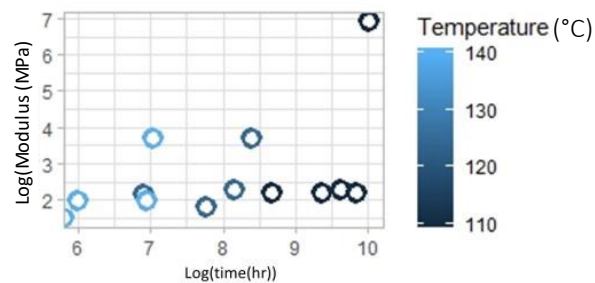
Figure 166- Modulus-time plots at different indicated temperatures for EPR cables, manufactured by Anaconda company
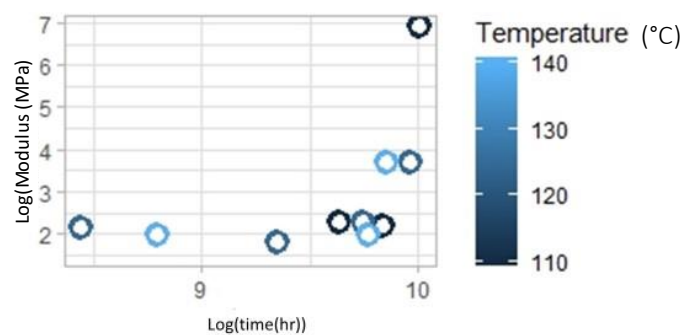
Figure 167- Time-temperature superposed modulus results at the reference temperature of 110 °C.

The shift factors corresponding to different temperatures are given in the Table 8.

Table 8- Shift factors for the thermally aged EPR cable

Temperature (°C)	a_T	$Ln(a_T)$
110	1	0
125	4.82	1.58
140	16.44	2.8

In the next step, the activation energy will be calculated from the slope of the shift factor versus temperature. The Arrhenius plot of shift factor versus temperature is shown in Figure 168. The linearity of the plot evidenced the Arrhenius behavior of the material.
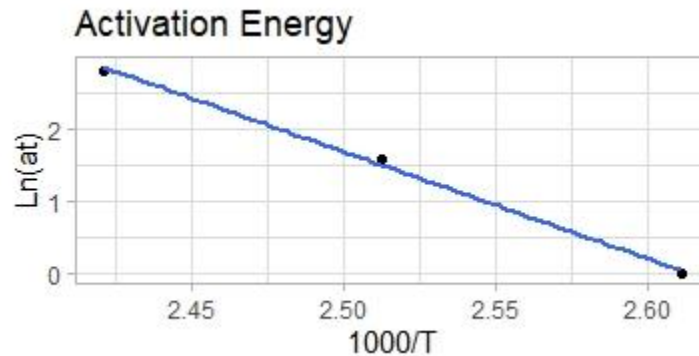
Figure 168- Shift factor versus temperature in the Arrhenius plot

Activation energy was calculated according to equation (2.14) to be 122.8 kJ/mol with SE of 0.7312.

5.2.3 Activation energy corresponding to density

In this section, the results of density measurements of EPR cables , C-12 manufactured by Anaconda, from C-PAD database will be discussed. As seen in Figure 169, modulus versus time plots is shown at 110 °C, 125 °C, 140 °C temperatures. Using time-temperature superposition method, the plots at 125 °C and 140 °C were shifted to the

reference temperature, 110 °C. The results are shown in Figure 170. As seen, the three

plots are nicely superposed at the reference temperature.
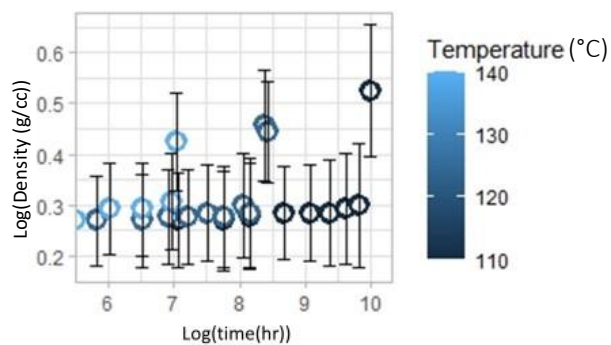
Figure 169- Density-time plots at different indicated temperatures for EPR cables, manufactured by Anaconda company, error bars represent SD
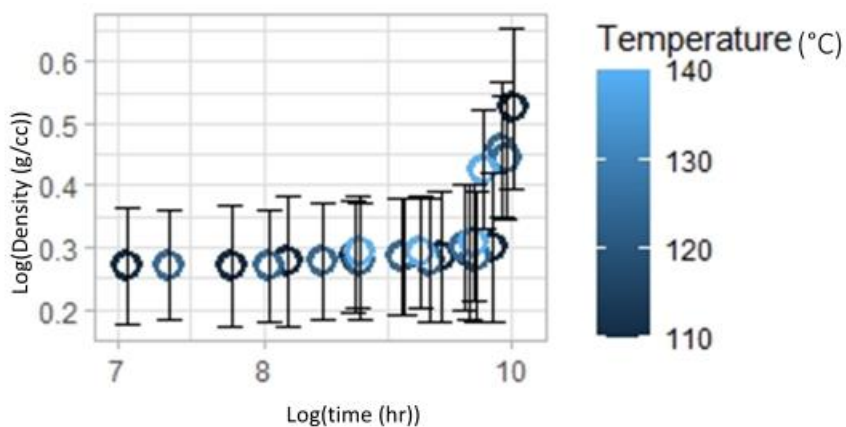
Figure 170- Time-temperature superposed density results at the reference temperature of 110 °C, error bars represent SD

The shift factors corresponding to different temperatures are given in the Table 9.

Table 9- Shift factors for the thermally aged EPR cable

Temperature (°C)	a_T	$Ln(a_T)$
110	1	0
125	4.58	1.52
140	14.53	2.7

In the next step, the activation energy will be calculated from the slope of the shift factor versus temperature. The Arrhenius plot of shift factor versus temperature is shown in Figure 171. The linearity of the plot evidenced the Arrhenius behavior of the material.
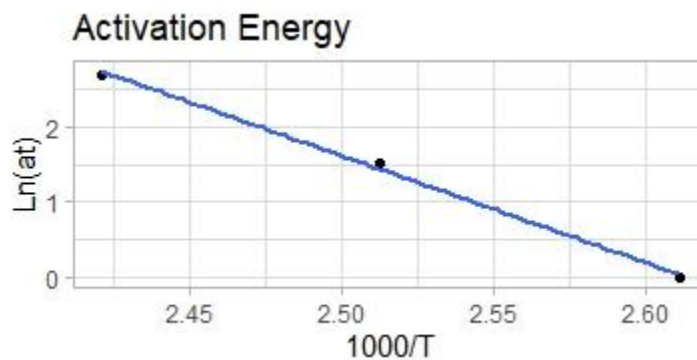
Figure 171- Shift factor versus temperature in the Arrhenius plot

Activation energy was calculated according to equation (2.14) to be 118.58 kJ/mol with SE of 0.724.

5.2.4 Activation energy corresponding to Modulus

In this section, the results of modulus measurements of EPR cables, ZO cables manufactured by Okonite, from C-PAD database will be discussed. The damage was chosen as modulus value equal to 4 MPa.

The DED data along with dose-rate and temperature are shown in Table 10

Table 10- DED Table

Dose-Rate	DED	Temperature
(Gy/h)	(Gy)	(°C)
0.0013	10.3	57.2

0.0058	216.0	42.8
0.0108	403.0	49.4
0.0126	732.0	46.1
0.0021	141.0	67.2

The DED data versus dose-rate at different temperatures are shown in Figure 172.
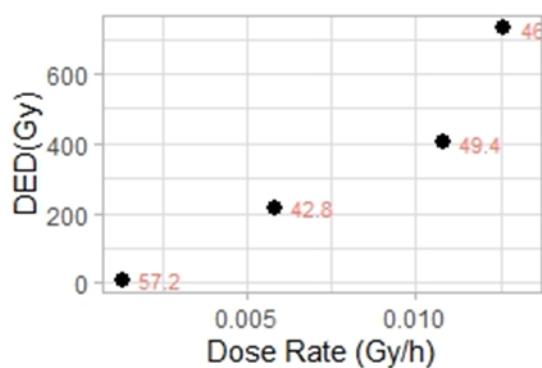
Figure 172-DED data versus dose rate at indicated temperatures

The next step is to iterate activation energy to shift the data to the reference temperature which is 45°C with the best superposed results [60]. The activation energy with the best superposed results will be picked as the activation energy corresponding to modulus.

The best superposed fit is demonstrated in Figure 173. The activation energy was found to be 33 kJ/mol with SE of 0.634.

5.2.5 Activation energy corresponding to density

In this section, the results of modulus measurements of EPR cables, ZO cables manufactured by Okonite, from C-PAD database will be discussed. The damage was chosen as density value equal to 1.28 g/cc.

The DED data along with dose-rate and temperature are shown in Table 11.

Table 11- DED Table

Dose-Rate (Gy/h)	DED (Gy)	Temperature (°C)
10^4	50000	132.0
10^4	50000	132.0
10^4	250000	132.0
10^4	250000	132.0
8.49×10^{-2}	679.0	53.3

1.30×10^{-3}	10.3	57.2
7.10×10^{-3}	62.1	39.4
1.69×10^{-2}	149.0	47.8
3.86×10^{-2}	452.0	54.4
3.00×10^{-4}	5.0	41.1
3.00×10^{-4}	4.3	47.2
4.10×10^{-3}	84.2	30.0
4.10×10^{-3}	84.2	30.0
2.00×10^{-3}	40.8	37.8
4.20×10^{-3}	124.0	45.6
5.40×10^{-3}	161.0	42.2
8.10×10^{-3}	242.0	50.6
1.27×10^{-2}	384.0	40.0
1.84×10^{-2}	637.0	30.0
1.16×10^{-2}	403.0	48.3

The DED data versus dose-rate at different temperatures are shown in Figure 174.
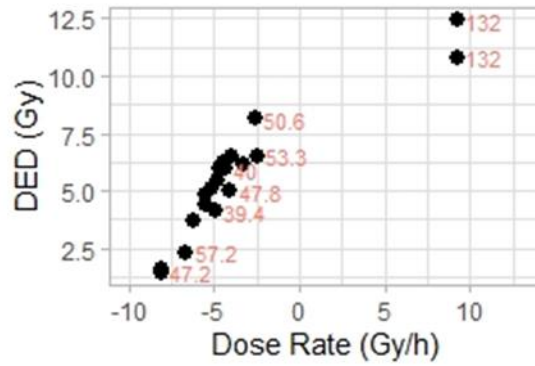
Figure 174- DED data versus dose rate at indicated temperatures

The next step is to iterate activation energy to shift the data to the reference temperature which is 45°C with the best superposed results [60]. The activation energy with the best superposed results will be picked as the activation energy corresponding to density.
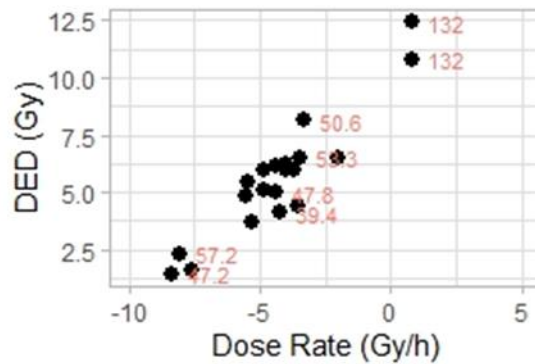
Figure 175- Superposed DED versus dose-rate plot

The best superposed fit is demonstrated in Figure 175. The activation energy was found to be 103 kJ/mol with the SE of 0.584.

5.2.7 Activation energy corresponding to EAB

171

In this section, the results of EAB measurements of XLPE cables, ZR cables manufactured by Rockbestos company, from C-PAD database will be discussed. The damage was chosen as relative EAB equal to 0.88.

The DED data along with dose-rate and temperature are shown in Table 12.

Table 12- DED Table

Dose-Rate (Gy/h)	DED (Gy)	Temperature (°C)
0.0071	243	42.2
0.0238	1110	45.6
0.0249	827	54.4
0.0386	452	54.4
0.0386	452	54.4
0.0578	2510	48.3
0.0869	1460	46.1

The DED data versus dose-rate at different temperatures are shown in Figure 176.
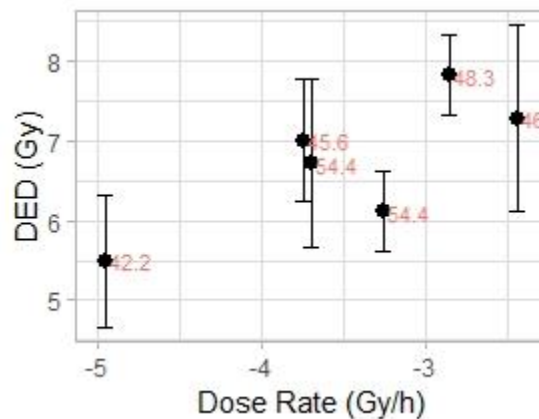
Figure 176- DED data versus dose rate at indicated temperatures, error bars represent SD

The next step is to iterate activation energy to shift the data to the reference temperature which is 45°C with the best superposed results [60]. The activation energy with the best superposed results will be picked as the activation energy corresponding to EAB.

Figure 177-Superposed DED versus dose-rate plot, error bars represent SD

The best superposed fit is demonstrated in Figure 177. The activation energy was found to be 50 kJ/mol with the SE of 0.85.

173

5.2.8 Activation energy corresponding to modulus

In this section, the results of modulus measurements of XLPE cables, ZR cables manufactured by Rockbestos company, from C-PAD database will be discussed. The damage was chosen as modulus value between 800 and 1200 MPa.

The DED data along with dose-rate and temperature are shown in Table 13.

Table 13-DED Table

Dose-Rate	DED	Temperature
(Gy/h)	(Gy)	(°C)
0.0069	399	43.3
0.0126	732	46.1
0.0234	1020	53.9
0.0283	1550	57.2
0.0363	2000	45.6
0.0578	2510	48.3
0.0722	3480	50.6
0.0826	5520	48.3

The DED data versus dose-rate at different temperatures are shown in Figure 178.

Figure 178-DED data versus dose rate at indicated temperatures

The next step is to iterate activation energy to shift the data to the reference temperature which is 45°C with the best superposed results [60]. The activation energy with the best superposed results will be picked as the activation energy corresponding to modulus.

Figure 179-Superposed DED versus dose-rate plot, error bars represent SD

The best superposed fit is demonstrated in Figure 179. The activation energy was found to be 26 kJ/mol with SE of 0.653. Because the dataset was not in the range of expected

values of activation energy, they were not included in the table for coefficient calculations.

5.2.9 Activation energy corresponding to EAB

In this section, the results of EAB measurements of EPR cables, ZO cables manufactured by Okonite, from C-PAD database will be discussed. The damage was chosen as relative EAB equal to 0.64.

The DED data along with dose-rate and temperature are shown in Table 14.

Table 14- DED Table

Dose-Rate (Gy/h)	DED (Gy)	Temperature (°C)
10^4	25000	132
10^4	25000	132
10^4	50000	132
1.3×10^{-3}	10.3	57.2
1.4×10^{-2}	655	58.3
3.45×10^{-2}	1640	32.2
3.63×10^{-2}	2000	45.6
6.90×10^{-3}	399	43.3
8.26×10^{-2}	5220	48.3

The DED data versus dose-rate at different temperatures are shown in Figure 180.
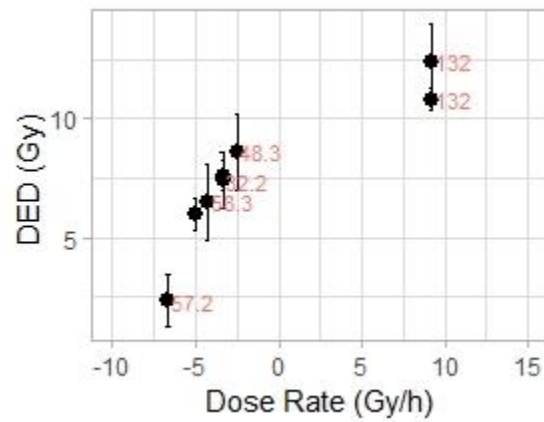
Figure 180- DED data versus dose rate at indicated temperatures, error bars represent SD

The next step is to iterate activation energy to shift the data to the reference temperature which is 45°C with the best superposed results [60]. The activation energy with the best superposed results will be picked as the activation energy corresponding to EAB.
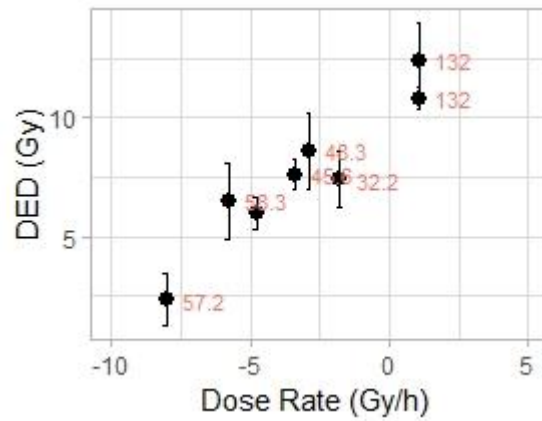
Figure 181- Superposed DED versus dose-rate plot, error bars represent SD

The best superposed fit is demonstrated in Figure 181. The activation energy was found to be 100 kJ/mol with SE of 0.712.

5.3 Summary of the results

The results of activation energies of aged XLPE and EPR cables calculated based on C-PAD database and experimental results in this thesis conducted in the UMD lab are summarized in Table 15.

178

Table 15- Activation energy results calculated based on C-PAD data and experimental results in the UMD lab

Source	material	manufacturer	cable code	Ea EAB (kJ/mol)	Ea Density (kJ/mol)	Ea Indenter Modulus (kJ/mol)	Ea Gel% (kJ/mol)	Ea SAB (kJ/mol)	Ea Water Uptake (kJ/mol)	Ea OI (kJ/mol)
CPAD	EPR	Eaton		121.9	124.1	114.2	143.5	95.01	-	-
CPAD	EPR	Anaconda	12	105.77	118.57	104.08	129	-	152.97	-
CPAD	EPR	Dawyler	2	106.3	-	119.65	-	-	-	-
CPAD	EPR	Kerite		117	105	134	-	115	-	-
CPAD	EPR	Okonite	18	50.28	54.36	78.97	-	-	-	-
CPAD	EPR	Okonite	ZO	100	103	33	-	93	-	-
CPAD	EPR	Sumuel Moore	A	125	42	173	-	138	-	-
CPAD	EPR	General Cable		95.5	138	87.5	-	95.5	-	-
CPAD	EPR	BIW	ZB	92	118	-	-	96	-	-
CPAD	FR-EPR	Anaconda	C	191	106	72	-	190	-	-
CPAD	FR-EPR	Kerite	D	130	130	130	-	141	-	-
CPAD	XLPE	Rockbestos	PAP86RB229	111	-	108	-	-	-	-
CPAD	XLPE	GE	C-1	87	-	-	-	73	-	-
UMD	XLPE	RSCC	NU	63.5	-	-	-	-	-	118.27

Lab									

5.4 Model Derivation

The new model was derived based on the theory explained in section 2.7 of this thesis. As it was described, the coefficients of the model are obtained by normalizing the calculated activation energy of each CM parameter's changes with the activation energy of EAB changes.

Ea $_{EAB}$ will be modeled with N number of CM parameters in equation (5.1).

$$Ea_{EAB} = {}^1\!/\!_N \sum_{i=1}^{N} \alpha_i \left(Ea_{CM_i}\right) \tag{5.1}$$

In equation (5.1), Ea_{EAB} is the activation energy corresponding to EAB, N is the number of CM parameters, α_i is the coefficient corresponding to the ith CM parameter, Ea_{CM_i} is the activation energy corresponding to the ith CM parameter.

Based on the described data in this thesis, there were 6 number of CM parameters. The coefficients of the model are shown in Table 16.

Table 16- Model Coefficients

CM parameter	Coefficient
Density	1.12
Indenter Modulus	1.06
Gel%	1.2
SAB	0.9
Water-Uptake	0.68
OI	1.85

5.5 Model Validation

In this section, the CM parameters of aged cables will be extracted from the published data and the activation energy corresponding to EAB and CM parameters will be calculated. Then, the modeled activation energy corresponding to EAB will be compared with that corresponding to EAB extracted from experimental data.

5.5.1.1 Calculation of Activation Energy from the dataset published by C. Silva et.al. [6]

The dataset published by C. Silva et.al. were used to determine Activation energy corresponding to indenter modulus, density and EAB extracted from experimental data. [6]

- Activation energy corresponding to Density
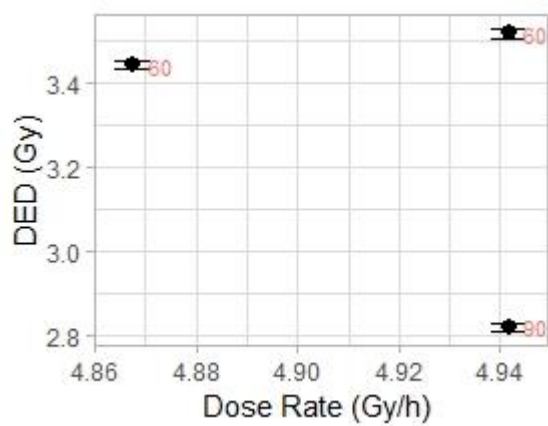
Figure 182- DED data versus dose rate at indicated temperatures
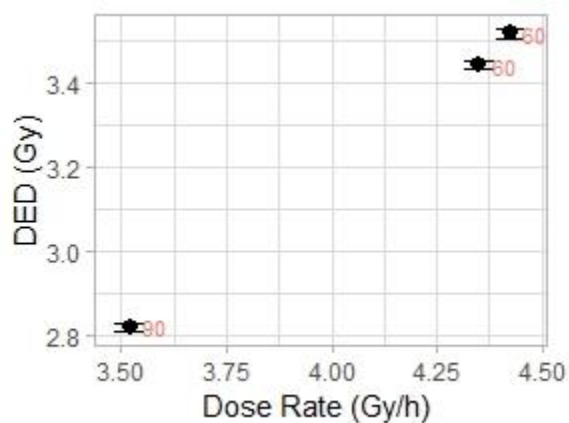
Figure 183- Superposed DED versus dose-rate plot

The activation energy corresponding to density was calculated to be 135.744 kJ/mol

with SE of 0.748.

- Activation energy corresponding to Indenter Modulus
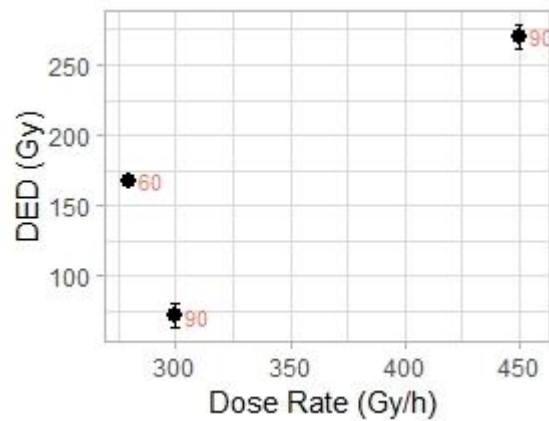
Figure 184- DED data versus dose rate at indicated temperatures
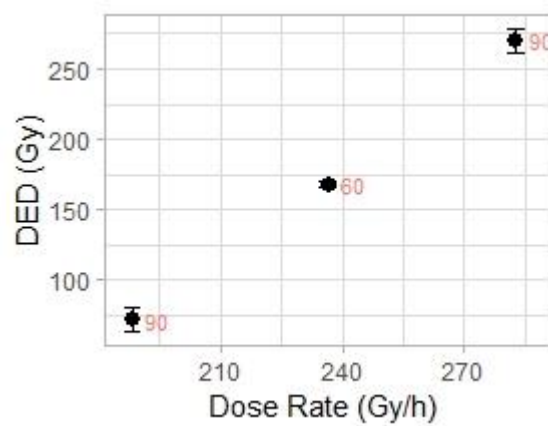
Figure 185- Superposed DED versus dose-rate plot

The activation energy corresponding to indenter modulus was calculated to be 41.976 kJ/mol with SE of 0.458.

- Activation energy corresponding to EAB
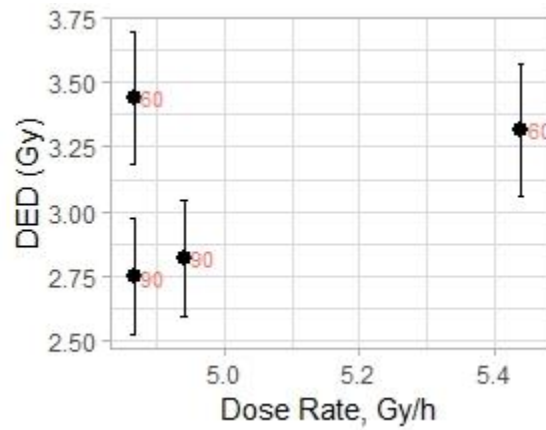
Figure 186- DED data versus dose rate at indicated temperatures
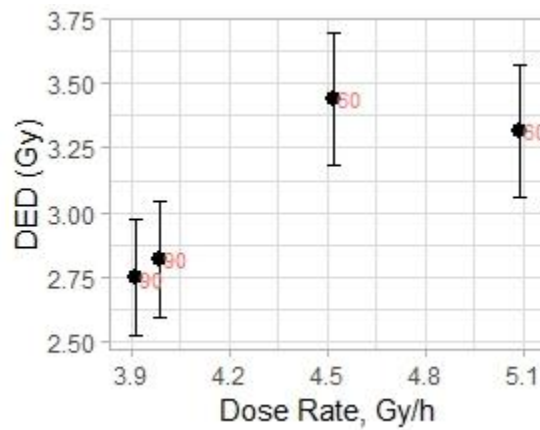
Figure 187- Superposed DED versus dose-rate plot

The activation energy corresponding to EAB was calculated to be 81.2 kJ/mol with SE of 0.738.

184

5.5.1.2 Calculation of Activation Energy from the Model

The estimated activation energy corresponding to EAB derived from the model, according to the equation (5.2), is 88.9 kJ/mol, which is a close estimation the actual activation energy corresponding to EAB.

$$Ea_{EAB} = {}^{1}\!/_{2}\ (1.12(Ea_{Density}) + 1.06(Ea_{Indenter\ Modulus})) \qquad (5.2)$$

5.5.2.1 Calculation of Activation Energy from the dataset published by Y. Kusama [84]

The dataset published by Y. Kusama et.al. was used to determine activation energy corresponding to SAB and EAB extracted from experimental data. [84]

- Activation energy corresponding to SAB
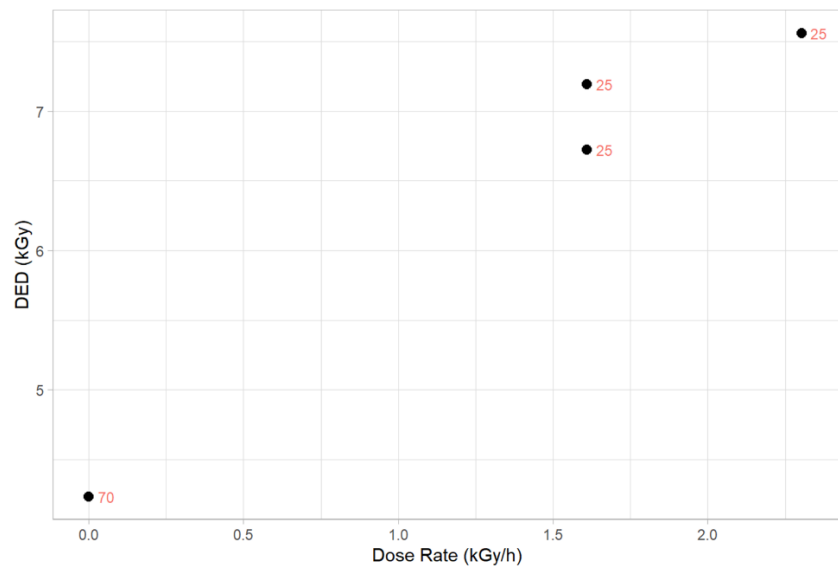
Figure 188- DED data versus dose rate at indicated temperatures
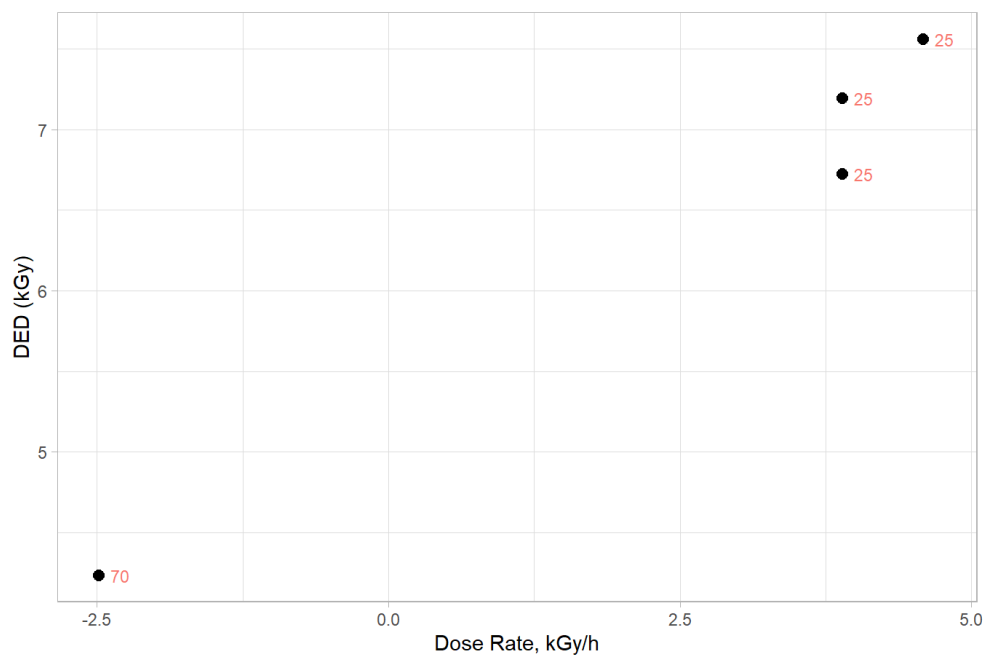
Figure 189- Superposed DED versus dose-rate plot

186

The activation energy corresponding to SAB was calculated to be 90 kJ/mol with SE

of 0.37.

- Activation energy corresponding to EAB
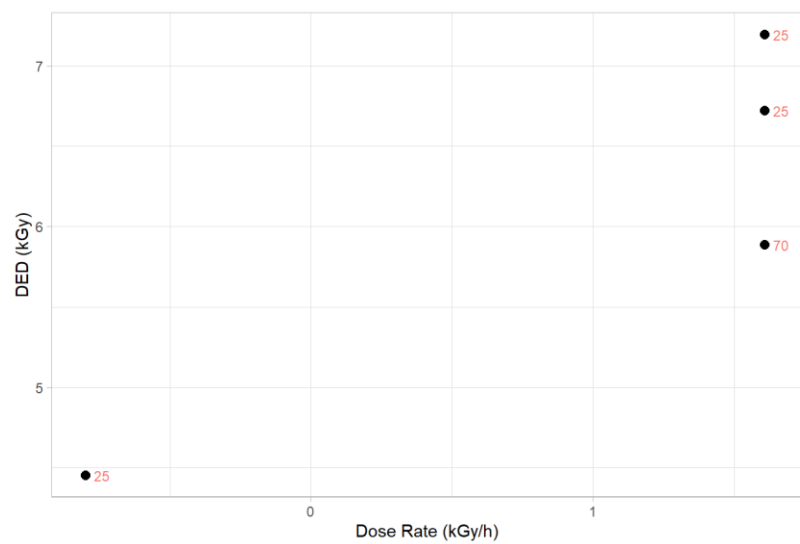
Figure 190- DED data versus dose rate at indicated temperatures
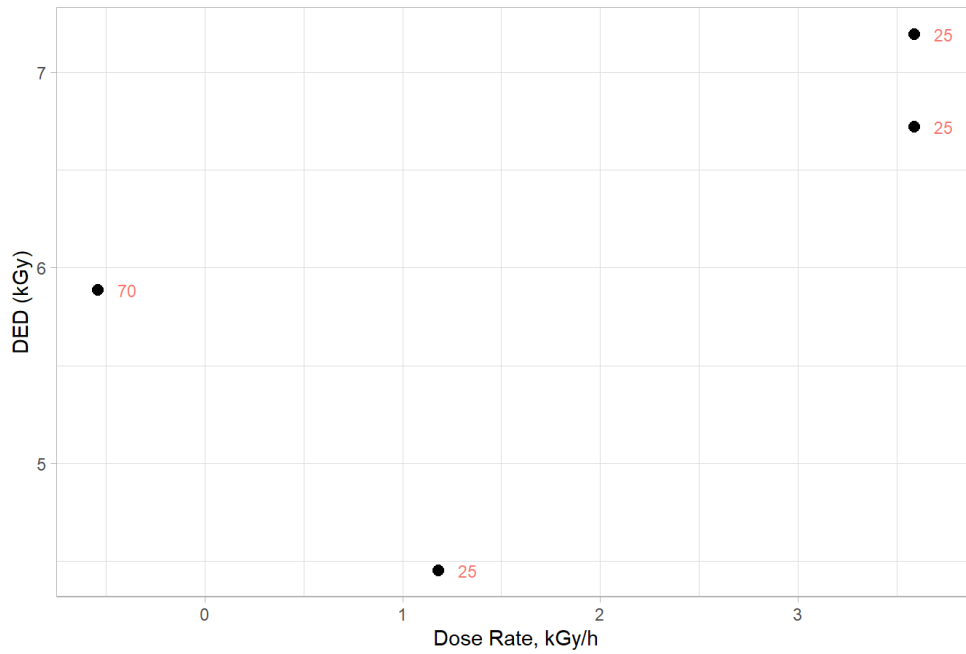
Figure 191- Superposed DED versus dose-rate plot

The activation energy corresponding to EAB was calculated to be 78.2 kJ/mol with standard error of 0.86.

5.5.2.2 Calculation of Activation Energy from the Model

The estimated activation energy corresponding to EAB derived from the model, according to the equation (5.3), is 81 kJ/mol, which is a close estimation the actual activation energy corresponding to EAB.

$$Ea_{EAB} = 0.9(Ea_{SAB}) \qquad\qquad (5.3)$$

188

Chapter 6:

Conclusion, Contribution to Science and suggestions for Future Work

6.1 Conclusion

The purpose of this dissertation was to correlate the activation energy of the degradation reaction measured by EAB changes to the activation energy corresponding to materials' property. Therefore, it is possible to estimate EAB values from the substitution of the correlated activation energy of the non-destructive condition monitoring parameters with that of EAB in the developed equations. [7],[8] and [9] The new model developed in this dissertation was validated by dataset of density, indenter modulus and EAB of aged XLPE insulation cables published by C. Silva. [6]

6.1.1 This dissertation model theory

The model of this PhD dissertation is based on the correlation of activation energies corresponding to physical property changes and that of EAB. The correlation is based on Dakin's theory which stated that the activation energy of chemical reactions is correlated with that of physical properties.[53]

It can be concluded that the activation energy of NDE-CM parameters' changes is equal to the activation energy of EAB changes. However, the equality has not always been observed due to the experimental conditions and the accuracy of calculation methods. A coefficient multiplication to each activation energy of NDE-CM parameters' changes can make them equal to the activation energy of EAB changes. This coefficient is obtained by the average of normalizing activation energy of each NDE-CM parameter's changes with the activation energy of EAB changes.

Therefore, it is possible to find a mathematical relationship between activation energy of EAB variations and that of other physical properties.

The practical use of this finding is to substitute the correlated activation energy in any of EAB models to estimate EAB based on variation of CM parameters.

6.1.2 Coefficients corresponding to CM parameters of the developed model in this dissertation

The coefficients corresponding to each CM parameter was obtained by normalizing the activation energy corresponding to the CM parameter to that of EAB.

- Coefficient corresponding to OI

    The dataset corresponding to OI parameter was obtained from FTIR experiments and tensile tests in the UMD labs.

    The FTIR experimental results showed that the oxidation of EPR cables had little oxidation. To verify it, the ESR experiments were done which agreed with the FTIR results. The FTIR experimental results showed that XLPE insulation cables were oxidized, and it was possible to calculate OI. To verify it, the ESR experiments were done which agreed with the FTIR results. The activation energy corresponding to OI, obtained from FTIR experiments, and EAB, obtained from tensile tests, of XLPE cables were calculated. The coefficient corresponding to OI is listed in Table 16 by normalizing the activation energy corresponding to OI to that of EAB.

- Coefficient corresponding to Density

    The dataset corresponding to Density parameter was obtained from CPAD database.

The activation energy corresponding to density and EAB of the cables were calculated. The coefficient corresponding to density is listed in Table 16 by normalizing the activation energy corresponding to density to that of EAB.

- Coefficient corresponding to Indenter Modulus

  The dataset corresponding to Indenter Modulus parameter was obtained from CPAD database.

  The activation energy corresponding to indenter modulus and EAB of the cables were calculated. The coefficient corresponding to indenter modulus is listed in Table 16 by normalizing the activation energy corresponding to indenter modulus to that of EAB.

- Coefficient corresponding to Indenter Modulus

  The dataset corresponding to Indenter Modulus parameter was obtained from CPAD database.

  The activation energy corresponding to indenter modulus and EAB of the cables were calculated. The coefficient corresponding to indenter modulus is listed in Table 16 by normalizing the activation energy corresponding to indenter modulus to that of EAB.

- Coefficient corresponding to Gel%

  The dataset corresponding to gel% parameter was obtained from CPAD database.

  The activation energy corresponding to gel% and EAB of the cables were calculated. The coefficient corresponding to gel% is listed in Table 16 by

normalizing the activation energy corresponding to indenter modulus to that of EAB.

- Coefficient corresponding to Water-Uptake

  The dataset corresponding to water-uptake parameter was obtained from CPAD database.

  The activation energy corresponding to water-uptake and EAB of the cables were calculated. The coefficient corresponding to water-uptake is listed in Table 16 by normalizing the activation energy corresponding to water-uptake to that of EAB.

- Coefficient corresponding to Strength At Break, SAB

  The dataset corresponding to SAB parameter was obtained from CPAD database.

  The activation energy corresponding to SAB and EAB of the cables were calculated. The coefficient corresponding to SAB is listed in Table 16 by normalizing the activation energy corresponding to SAB to that of EAB.

6.1.3 Model derivation

Ea $_{EAB}$ will be modeled with N number of CM parameters according to equation (5.1).

6.1.4 Model validation

The validity of the model was evaluated by dataset published by C. Silva et.al. [6]

The modeled Ea $_{EAB}$ agreed with the Ea $_{EAB}$ of the experimental data.

6.2 Contributions to Science

This dissertation created a scientific approach to estimate EAB values by extending Dakin's theory to other physical properties. [53]

A mathematical relationship between activation energy of EAB variations and that of other physical properties established a scientific method to have a better understanding of activation energy variations among physical and chemical properties of insulation cables.

There has been a lot of efforts to model EAB with the activation energy corresponding to EAB as well as estimate the EAB values based on CM parameter values. However, a gap of a scientific approach to bridge these two regions has always been observed in the cable insulation field. The impact of this research is to estimate EAB values in any of EAB models based on activation energy corresponding to EAB developed so far with the variations of CM parameters.

Besides, employing both the FTIR and ESR spectroscopy techniques provided a strong investigation technique on studying oxidation reactions on both XLPE and EPR cable insulations which it was combined with tensile tests to measure the macroscopic changes.

Other important issue is that the presence of the relative stable polyenyl radicals in all aged insulators. This work provided ESR results, which show the presence of the polyenyl radicals.

194

This dissertation model is not only based on the experimental results which have been done at the UMD labs, but also involves the datasets of the C-PAD database which was built by the contribution of several global nuclear power plants.

6.3 Future Work Suggestions

The focus of future experiments should be on obtaining datasets of CM parameters of aged cable insulations under at least three temperature and radiation conditions extracted at different time intervals. The increase in the number of activation energies corresponding to each CM parameter will enhance the statistical significance of coefficients of the new model in this dissertation. Besides, the number of CM parameters should increase. OI is one of the NDE-CM parameters that is rarely used while it can give a lot of information about the oxidation degradation reaction in the cable. The employment of cables from different manufacturers aged at least at three different temperatures can enhance the statistical significance of the coefficients.

The employment of ESR spectroscopy can enhance the confidence in OI measurements by FTIR spectroscopy technique. The existence and stability of free radicals can be determined by ESR spectroscopy which has been rarely used. The employment of ESR in the insulation field can also improve the understanding of the mechanism of degradation reactions due to the capability of the spectrometer to follow the free radicals which are responsible for the degradation reactions.

References

[1]   "Initial Acceptance Criteria Concepts and Data for Assessing Longevity of
        Low-Voltage Cable Insulations and Jackets. EPRI, Palo Alto, CA, and U.S.
        Department of Energy, Washington, DC: 2005. 1008211. 11."

[2]   N. Bowler and S. Liu, "Aging Mechanisms and Monitoring of Cable
        Polymers," *Progn. Heal. Manag. Soc.*, pp. 1–12, 2015.

[3]   J. V. Gasa, Z. Liu, and M. T. Shaw, "Relationship between density and
        elongation-at-break of naturally and artificially aged cable materials used in
        nuclear power plants," *Polym. Degrad. Stab.*, vol. 87, no. 1, pp. 77–85, 2005.

[4]   K. Anandakumaran, "Aging and condition monitoring studies of composite
        insulation cables used in nuclear power plants," *IEEE Trans. Dielectr. Electr.
        Insul.*, vol. 14, no. 1, pp. 227–237, 2007.

[5]   J. Gillen, K. T.; Clough, R. L.; Wise, "Prediction of Elastomer Lifetimes from
        Accelerated Thermal-Aging Experiments," *Adv Chem Ser*, vol. 249, no. I, pp.
        557–575, 1996.

[6]   C. C. De Silva, S. P. Beckman, S. Liu, and N. Bowler, "Principal component
        analysis (PCA) as a statistical tool for identifying key indicators of nuclear
        power plant cable insulation degradation," *Miner. Met. Mater. Ser.*, pp. 1227–
        1239, 2019.

[7]   Y.-S. Chang and A. Mosleh, "Probabilistic Degradation Models for Cable
        Insulation in Nuclear Power Plants," in *American Nuclear Society Meeting*,
        2017.

[8]   A. J. Buslik, L. Chu, M. Subudhi, and J. Lehner, "NUREG/CR-68699,BNL-

NUREG-73676-2005"A Reliability Physics Model for Aging of Cable Insulation Materials ",” U.S. Nuclear Regulatory Commission, Office of Nuclear Regulatory Research Washington, DC 20555-0001, 2005.

[9]   Y. Kemari, A. Mekhaldi, M. Teguar, and G. Teyssedre, “Nonlinear Regression Modeling to Predict Thermal Endurance of XLPE Material under Thermal Aging,” in *IEEE 2nd International Conference on Dielectrics (ICD)*, 2018.

[10]   T. Yamamoto and T. Minakawa, “JNES-SS-0903,"The Final Report of The project of ‘Assessment of Cable Aging for Nuclear Power Plants’",Japan Nuclear Energy Safety Organization (JNES), Tokyo, Japan,” 2009.

[11]   F. Guérout, A. Blouin, L. Cissé, and R. Boor, “Development of Non-Destructive Condition Monitoring Techniques,” in *Proceedings of the 8th International Conference on CANDU Maintenance*, 2008.

[12]   L. Verardi, “Ph.D. Thesis,"Aging of Nuclear Power Plant Cables: in search of non-destructive diagnostic quantities", Department of Elect. and Inform. Eng. , Univ. Bologna,” 2013.

[13]   P. LIndsay, S. Benson, and R. Black, “RCM Report, ‘Ageing Management of Cable in Nuclear Generating Stations’,The Canadian Nuclear Safety Commission, Canada,” 2012.

[14]   “IAEA, Nuclear Energy Series NO.NP-T-3.6, ASSESSING AND MANAGING CABLE AGEING IN NUCLEAR POWER PLANTS,” 2012.

[15]   M. C. Celina, K. T. Gillen, and E. R. Li, “SANDIA REPORT, ‘Nuclear power plant cable materials - review of qualification and currently available aging data for margin assessments in cable’, SAND2013-2388,” 2013.

[16] B. Bernstein and W. A.Thue, "Historical perpective of electrical cables," in *Electrical Power Engineering*, 2nd ed., W. A.Thue, Ed. New York: Marcel Dekker, INC, 2005, pp. 1–9.

[17] C. Landinger, "Basic Dielectric Theory of Cable," in *Electrical Power Engineering*, 2nd ed., W. A.Thue, Ed. New York: Marcel Dekker, INC, 2005.

[18] R. Bartnikas, "Characteristics of cable materials," *Power Commun. Cables Theory Appl.*, pp. 76–170, 2003.

[19] C. Landinger, "Conductors," 2nd ed., W. A.Thue, Ed. New York: Marcel Dekker, INC, 2005.

[20] Nexan, ""6-36kV Medium Voltage Underground Power Cablese ", [Brochure]. Retrieved from https://www.powerandcables.com/wp-content/uploads/2016/12/Nexans-6-33kV-Medium-High-Voltage-Underground-Power-Cables.pdf."

[21] M. Subudhi, "Literature Review of Environmental Qualification of Safety-Related Electric Cable, NUREG/CR-6384 BNL-NUREG-52480 Vol.1," Washington, DC 20555-0001, 1996.

[22] B. S. Bernstein, "Electrical Insulation Materials," in *Electrical Power Engineering*, 2nd ed., W. A.Thue, Ed. .

[23] J. Brown *et al.*, "SANDIA REPORT 'Submerged Medium Voltage Cable Systems at Nuclear Power Plants : A Review of Research Efforts Relevant to Aging Mechanisms and Condition Monitoring,'" 2015.

[24] C. Landinger, "Sheath, Jackets, and Armors," in *Electrical Power Engineering*, 2nd ed., W. A.Thue, Ed. New York: Marcel Dekker, INC, 2005.

[25] D. Tommasin, *Dielectric insulation and high-voltage issues. CAS 2009 - CERN Accelerator School: Magnets Retrieved from https://arxiv.org/abs/1104.0802*. 2009, pp. 335–355.

[26] Greg Stone, "Partial Discharges in Electrical Insulation," *Am. Soc. Nav. Eng. - J.*, vol. 52, no. 2–4, pp. 184–187, 1940.

[27] S. M. Tamboli, S. T. Mhaske, and D. D. Kale, "Crosslinked polyethylene," *Indian J. Chem. Technol.*, vol. 11, no. 6, pp. 853–864, 2004.

[28] F.Tudos and M.Iring, "THERMAL OXIDATION OF POLYETHYLENE AND polypropylene:Effects of Chemical structure and reaction conditions on the oxidation process," *prog.poly.sci*, vol. 15, pp. 217–262, 1990.

[29] L. Chen *et al.*, "Experimental and modeling approaches for the formation of hydroperoxide during the auto-oxidation of polymers: Thermal-oxidative degradation of polyethylene oxide," *Chem. Phys. Lett.*, vol. 657, pp. 83–89, 2016.

[30] A. L. Forster, Z. Tsinas, and M. Al-Sheikhly, "Effect of irradiation and detection of long-lived polyenyl radicals in highly crystalline ultra-high molar mass polyethylene (UHMMPE) fibers," *Polymers*, vol. 11, no. 5. 2019.

[31] Z. Tsinas, "TOWARDS AN UNDERSTANDING OF THE DEGRADATION MECHANISMS OF UHMWPE-BASED SOFT BALLISTIC INSERTS," University of Maryland, 2016.

[32] A. L. Forster *et al.*, "Long-term stability of UHMWPE fibers," *Polym. Degrad. Stab.*, vol. 114, pp. 45–51, 2015.

[33] T. M. Alam *et al.*, "γ-irradiation of ultrahigh-molecular-weight polyethylene:

Electron paramagnetic resonance and nuclear magnetic resonance spectroscopy and imaging studies of the mechanism of subsurface oxidation," *J. Polym. Sci. Part A Polym. Chem.*, vol. 42, no. 23, pp. 5929–5941, 2004.

[34] M. Giurginca, L. Popa, and T. Zaharescu, "Thermo-oxidative degradation and radio-processing of ethylene vinyl acetate elastomers," *Polym. Degrad. Stab.*, vol. 82, no. 3, pp. 463–466, 2003.

[35] IAEA NUCLEAR ENERGY SERIES, "Assessing and Managing Cable Ageing in Nuclear Power Plants, No. NP-T-3.6," vienna, 2012.

[36] W. Callister, *Materials science and engineering : an introduction , 7th ed, New York, John Wiley & Sons*. 2007.

[37] J. Coble *et al.*, "A Review of Prognostics and Health Management Applications in Nuclear Power Plants," *Int. J. Progn. Heal. Manag.*, vol. 6, p. 16, 2015.

[38] H. M. Hashemian, B. Mcconkey, G. Harmon, and C. Sexton, "Methods for testing nuclear power plant cables," *IEEE Instrum. Meas. Mag.*, vol. 16, no. 5, pp. 31–36, 2013.

[39] K. Simmons *et al.*, "PNNL-22812"Determining Remaining Useful Life of Aging Cables in Nuclear Power Plants – Interim Study FY13, Pacific Northwest National Laboratory Richland, Washington 99352," 2013.

[40] R. J. York, J. B. Ulrich, G. Murphy, D. G. Prather, R. York, and R. Benson, "'Mitigation of aging in low voltage power cables in nuclear power plants' (2015). University of Tennessee Honors Thesis Projects. http://trace.tennessee.edu/utk_chanhonoproj/1879," 2015.

[41]   A. Shimada, M. Sugimoto, H. Kudoh, K. Tamura, and T. Seguchi, "Degradation distribution in insulation materials of cables by accelerated thermal and radiation ageing," *IEEE Trans. Dielectr. Electr. Insul.*, vol. 20, no. 6, pp. 2107–2116, 2013.

[42]   K. T. Gillen and R. Bernstein, "SANDIA REPORT"Review of Nuclear Power Plant Safety Cable Aging Studies with Recommendations for Improved Approaches and for Future Work",SAND 2010-7266 Unlimited Release Printed November 2010," 2010.

[43]   M. Celina, K. T. Gillen, and R. A. Assink, "Accelerated aging and lifetime prediction: Review of non-Arrhenius behaviour due to two competing processes," *Polym. Degrad. Stab.*, vol. 90, no. 3, pp. 395–404, 2005.

[44]   S. Hvidsten, P. Werelius, and J. Christensen, "Evaluation of on-site dielectric response methods for nondestructive testing of water treed MV XLPE cables," in *CIRED. 16th International Conference and Exhibition on Electricity Distribution (IEE Conf. Publ No. 482), 1, 5 pp*, 2001.

[45]   R. Papazyan, R. Eriksson, H. Edin, and H. Flodqvist, "Detection and localisation of water treeing for condition based replacement of medium voltage cables," in *CIRED2005 ,8TH INTERNATIONAL CONFERENCE ON ELECTRICITY DISTRIBUTION, TURIN, 6-9 JUNE*, 2005.

[46]   F. Liu, X. Huang, J. Wang, and P. Jiang, "Insulation ageing diagnosis of XLPE power cables under service conditions," in *Proceedings of 2012 IEEE International Conference on Condition Monitoring and Diagnosis, CMD 2012*, 2012, no. September, pp. 647–650.

[47]   Y. T. Hsu, K. S. Chang-Liao, T. K. Wang, and C. T. Kuo, "Monitoring the moisture-related degradation of ethylene propylene rubber cable by electrical and SEM methods," *Polym. Degrad. Stab.*, vol. 91, no. 10, pp. 2357–2364, 2006.

[48]   W. J. Chatterton, "A green method for cable diagnostics coupled with selective cable restoration - Re-use instead of replace," in *2010 IEEE PES Transmission and Distribution Conference and Exposition: Smart Solutions for a Changing World*, 2010, pp. 1–4.

[49]   B. Shumaker, J. B. Ledlow, R. D. O. Hagan, D. E. Mccarter, and H. M. Hashemian, "Remaining Useful Life Estimation of Electric Cables in Nuclear Power Plants," *Chem. Eng. Trans.*, vol. 33, pp. 877–882, 2013.

[50]   M. Celina, J. M. Skutnik Elliott, S. T. Winters, R. A. Assink, and L. M. Minier, "Correlation of antioxidant depletion and mechanical performance during thermal degradation of an HTPB elastomer," *Polym. Degrad. Stab.*, vol. 91, no. 8, pp. 1870–1879, 2006.

[51]   K. T. Gillen and M. Celina, "SANDIA REPORT,Sand 2000-1199J,"The Wear-out Approach for Predicting the Remaining Lifetime of Materials"Sandia National Laboratories, Albuquerque," 2000.

[52]   J. Brown *et al.*, "Sandia Report"Submerged Medium Voltage Cable Systems at Nuclear Power Plants : A Review of Research Efforts Relevant to Aging Mechanisms and Condition Monitoring", SAND 2015-#### Unlimited Release Printed March 2015," Albuquerque, New Mexico 87185 and Livermore, California 94550, 2015.

[53]   T. W. Dakin, "Electrical Insulation Deterioration Treated as a Chemical Rate Phenomenon," *Trans. Am. Inst. Electr. Eng.*, vol. 67, pp. 113–122, 1948.

[54]   L. J. Berberich and T. W. Dakin, "Guiding Principles in the Thermal Evaluation of Electrical Insulation," *Trans. Am. Inst. Electr. Eng. Part III Power Appar. Syst.*, 1956.

[55]   G. Mazzanti and G. C. Montanari, "A comparison between XLPE and EPR as insulating materials for HV cables," *IEEE Trans. Power Deliv.*, vol. 12, no. 1, pp. 15–26, 1997.

[56]   P. Cygan and J. R. Laghari, "Models for Insulation Aging under Electrical and Thermal Multistress," *IEEE Trans. Electr. Insul.*, vol. 25, no. 5, pp. 923–934, 1990.

[57]   G. C. Montanari, G. Mazzanti, and L. Simoni, "Progress in electrothermal life modeling of electrical insulation during the last decades," *IEEE Trans. Dielectr. Electr. Insul.*, vol. 9, no. 5, pp. 730–745, 2002.

[58]   A. Tobolsky, *properties and structure of polymers*. New York: John Wiley, 1960.

[59]   K. T. Gillen, R. A. Assink, and R. Bernstein, "SANDIA REPORT"Final Report on Aging and Condition Monitoring of Low-Voltage Cable Materials", SAND2005-7331 Unlimited Release Printed November 2005," 2005.

[60]   K. T. Gillen and R. L. Clough, "Time-temperature-dose rate superposition: A methodology for extrapolating accelerated radiation aging data to low dose rate conditions," *Polym. Degrad. Stab.*, vol. 24, no. 2, pp. 137–168, 1989.

[61]   Y.S.Chang and A.Mosleh, "physics-based model of the degradation of cable

insulation subject to radiation and heat," in *IEEE Conference on Electrical Insulation and Dielectric Phenomenon*, 2017, pp. 145–148.

[62] Y. Chang, Y. Zhang, and A. Mosleh, "Predictive Model on the Reliability of the Insulation Made from Special Heat-Resistant Polyvinyl Chloride," in *Probabilistic Safety Assessment and Management PSAM*, 2018, no. September.

[63] "'Test Sample Cutters', Retrieved from Https://industrialphysics.com/product/test-sample-cutters/," 2021. .

[64] K. Anandakumaran, "Assessment of oxidative thermal degradation of crosslinked polyethylene and ethylene propylene rubber cable insulation," *Polym. Eng. Sci.*, vol. 32, 1992.

[65] R. T. Weber, J. Jiang, and D. P. Barr, "'EMX USER'S Manual',Bruker Instruments, Inc.Billerica, MA USA," 1998. .

[66] R. T. Weber, "'Xenon User's Guide',Bruker BioSpin Corporation Billerica, MA USA," 2011.

[67] K. T. Gillen, M. Celina, and R. L. Clough, "Density measurements as a condition monitoring approach for following the aging of nuclear power plant cable materials," *Radiat. Phys. Chem.*, vol. 56, no. 4, pp. 429–447, 1999.

[68] T. Seguchi, K. Tamura, T. Ohshima, A. Shimada, and H. Kudoh, "Degradation mechanisms of cable insulation materials during radiation-thermal ageing in radiation environment," *Radiat. Phys. Chem.*, vol. 80, no. 2, pp. 268–273, 2011.

[69] L. Shuaishuai, "Composition identification, aging mechanisms and nondestructive aging indicator of commercial filled cross-linked polyethylene

(XLPE) cable insulation materials," pp. 75–91, 2017.

[70] C. Blivet, J. F. Larché, Y. Israëli, P. O. Bussière, and J. L. Gardette, "Thermal oxidation of cross-linked PE and EPR used as insulation materials: Multi-scale correlation over a wide range of temperatures," *Polym. Test.*, vol. 93, no. July 2020, 2021.

[71] P. Pourmand, "PhD thesis 'Long-term performance of polymeric materials in nuclear power plants' Univ. KTH. Stockholm, Sweden," 2017.

[72] B. Han *et al.*, "Study on the structure and dielectric properties of zeolite/LDPE nanocomposite under thermal aging," *Polymers (Basel).*, vol. 12, no. 9, pp. 1– 12, 2020.

[73] L. Boukezzi, A. Boubakeur, C. Laurent, and M. Lallouani, "Observations on structural changes under thermal ageing of cross-linked polyethylene used as power cables insulation," *Iran. Polym. J. (English Ed.*, vol. 17, no. 8, pp. 611– 624, 2008.

[74] A. Levet, J. Colombani, and L. Duponchel, "Studying radiolytic ageing of nuclear power plant electric cables with FTIR spectroscopy," *Talanta*, vol. 172, no. May, pp. 139–146, 2017.

[75] W. A.Thue, *Electrical Power Cable Engineering*. .

[76] L. Cao, A. Zanwar, and S. Grzybowski, "Electrical aging phenomena of medium voltage EPR cable energized by ac voltage with switching impulses superimposed," *2011 IEEE Electr. Sh. Technol. Symp. ESTS 2011*, pp. 353– 356, 2011.

[77] B. Fayolle, X. Colin, L. Audouin, and J. Verdu, "Mechanism of degradation

induced embrittlement in polyethylene," *Polym. Degrad. Stab.*, vol. 92, no. 2, pp. 231–238, 2007.

[78] A. M. Nobrega, M. L. B. Martinez, and A. A. A. De Queiroz, "Investigation and analysis of electrical aging of XLPE insulation for medium voltage covered conductors manufactured in Brazil," *IEEE Trans. Dielectr. Electr. Insul.*, vol. 20, no. 2, pp. 628–640, 2013.

[79] M. A. Morsy and M. H. Shwehdi, "Electron spin resonance spectral study of PVC and XLPE insulation materials and their life time analysis," *Spectrochim. Acta - Part A Mol. Biomol. Spectrosc.*, vol. 63, no. 3, pp. 624–630, 2006.

[80] H. J. Hee, C. Hoon, L. Y. Ki, and K. C. Soon, "ESR spectrum of cables in nuclear power plant," in *Transactions of the Korean Nuclear Society Autumn Meeting,Gyeongju, Korea*, 2006, pp. 2–3.

[81] M. A. Morsy, M. H. Shwehdi, and A. M. Abu-Gurain, "Novel exploration of cable insulation materials using electron spin resonance spectroscopy," *Conf. Electr. Insul. Dielectr. Phenom. (CEIDP), Annu. Rep.*, pp. 108–111, 2003.

[82] B. Rånby and J. F. Rabek, *"ESR Spectroscopy in Polymer Research" Berlin Heidelberg New York,Springer-Verlag*. 1977.

[83] M. J. Kasser, "THE PHOTOCHEMISTRY OF POLYENYL RADICALS AND ITS APPLICATION TO UHMWPE FOR USE IN REPLACEMENT JOINTS," University of Maryland.

[84] W. K. Y. Kusama, S.Okada, M. ITOH, T. Yagi, M.Yoshikawa, K.Yoshida, S. Machi, N. Tamura, "EFFECT OF OXYGEN IN THE SIMULATED LOCA ENVIRONMENTS ON THE DEGRADATION OF OF CABLE

INSULATING MATERIALS," in *Radiation Damage to Organic Materials in Nuclear Reactors and Radiation Environments*, 1989, no. July 1989, pp. 17–20.